Development and Characterization of a Dual Neutron and Gamma Detector

By

Abuzar Fariad

A Thesis Submitted in Partial Fulfillment

Of the Requirements for the Degree of

Master of Applied Science

In

Nuclear Engineering

Faculty of Energy Systems and Nuclear Science

University of Ontario Institute of Technology

August, 2011

ABSTRACT

A dual neutron and gamma detection system has been developed for online measurements. The system consists of a single crystal mounted on a photomultiplier tube to detect simultaneously gamma radiation as well as thermal neutrons. A compact data acquisition system has been used for neutron and gamma discrimination. The system has been tested with different gamma energies and with an Am-Be neutron source at the University of Ontario Institute of Technology neutron facility. This thesis presents the characteristics of the developed detector, and experimental data carried out in different experiments in different fields.

ACKNOWLEDGEMENTS

First and foremost I owe my gratitude to God, The Almighty, who has made all things possible.

I am indebted to my family but especially to my mother and father, Zainab and Said Alam Fariad, for their continued support throughout my life and particularly during the course of my studies.

Last but not least, I appreciate the effort Dr. Machrafi, whose encouragement and guidance steered me in the right direction and enabled me to develop understanding of the subject.

TABLE OF CONTENTS

LIST OF FIGURES

LIST OF TABLES

NOMENCLATURE

ADC	Analog to Digital Converter
Bq	Disintegrations per second
c	Speed of light, *m/s*
Ci	3.7E10 disintegrations per second
C_f	*Feedback capacitor, farads*
D	*Diffusion coefficient*
DAQ	*Data Acquisition System*
$\frac{dL}{dE}$	*Light output per unit energy loss, photon/MeV*
$\frac{dE}{dx}$	Stopping power, *MeV*/cm
E_b	Binding energy, *MeV*
E_o	Energy of particle, *MeV*
eV	Electron Volt
H_o	Centroid of peak, Channel #
hv	Energy of photon, Joules
I_o	Intensity of the original beam, %
$m_o c^2$	Rest mass energy of particle, *MeV*
MCA	Multi Channel Analyzer
Q	Deposited charge, Coulombs
$R_f C_f$	Time constant for detector, seconds
R	Resolution of detector, %
R_f	Feedback Resistor, Ω
w_r	Radiation Weighting factor

Greek Letters

α	Alpha- Particle
β	Beta ray
γ	Gamma ray
$\sum$	Macroscopic cross section, cm^{-1}
σ	Microscopic cross section, barn
ε	Luminescent efficiency, %
Φ	Flux, $\#/cm^2 s$
θ	Angle of Scatter, degrees
λ	Half-Life, time
τ	Fermi Age, mm^2

Subscripts

a	absorption
s	scattering
n	neutron
e	electron
i	inelastic
f	fission

INTRODUCTION

Neutron research goes as far back as 1930's, when scientists discovered that when a beam of alpha-particles (α) interacted with beryllium, there was a highly energetic radiation that was emitted. At first glance it was thought to be gamma radiation (γ). Both radiation were highly penetrating into matter, and were non responsive to electromagnetic fields, therefore neutral. The difference emerged in the interactions with electron rich material. γ-rays produced what is known as photoelectric effect, however with the unknown radiation this phenomenon was not observed. Subsequently, Irene Curie devised an experiment to create a beam of the unknown radiation and bombard a proton rich target material, such as paraffin. The reaction caused protons to be knocked out of the material which were then detected by a Geiger counter. In 1932 James Chadwick proposed that the unknown radiation was none other but the neutron. Using kinematics and conservation of momentum equations it was determined that the mass of the neutron was approximately equal to the mass of a proton. The adoption of the neutron paved the way for current theories of nuclear structure.

Detection of neutrons is based on measuring the energy deposits of the secondary charged particles as a product of neutron interaction. Neutrons can have a wide range of energies, thus the detection methods which are used are different for slow (low energy) and fast (higher energy) neutrons. Detectors designed to detect neutrons below energies of 0.5eV are called thermal neutron detectors.

Various kinds of detectors have been used to measure thermal neutrons including proportional counters and scintillation detectors. These detectors have different performances for slow neutrons

and preference is traditionally given to detectors which have higher neutron detection efficiency combined with their γ-ray discrimination capabilities which is one of the most important aspects of neutron detection.

Thermal neutron proportional counters are usually constructed by encasing a gas whose absorption cross section is high for thermal region of neutrons into a cylindrical geometry. Gas filled neutron detectors which operate in proportional region usually contain BF_3 gas or ^3He gas. BF_3 proportional counter is a type of detector that consists of a substance gas Boron Tri-fluoride. Due to its high concentration of ^{10}B (96%) (Knoll, 1989), it acts both as target and neutron converter. It is one of the most common types of slow neutron detectors as its efficiency is around 91% for thermal neutrons with energies close to 0.025 eV (for 30 cm tube length and pressure of 600 torr). Unfortunately for energies above 100 eV the efficiency decreases to 3.8 % (Knoll, 1989). The BF_3 tube must be constructed with quite large dimensions so that all the reactions occur at a far distance from the detector's wall. The product of the neutron interaction with ^{10}B releases α-particle and Lithium particles (^7Li). The $^{10}B(n, \alpha)^7Li$ has a relatively high Q-value, which is the energy release of the reaction, making it a good sensor medium for gamma ray and neutron detection. Following the reaction both particles will move in opposite directions. If the reaction products are slowed down in the detectors sensitive volume, they deposit their full energy. However if one or both of them reach the detector wall, only a part of their energy is deposited in the sensitive volume while the rest is deposited in the wall material 'wall effect'. Therefore the energy deposited will not reflect the full energies of the charged particles. Thus, in order to obtain a spectrum with the most efficient full energy deposition the size and design of the BF_3 volume should be appropriate.

Helium based detectors such as ^{3}He proportional counters are favorable thermal neutron detectors due to their higher value for the thermal neutron cross-section (5330 barns). ^{3}He can be used instead of the BF_3 (3840 barns) detector for slow neutron observation. In order to overcome the drawbacks faced by the wall effect, the detector's dimensions have to be larger, or the pressure of the ^{3}He gas could be increased, which would decrease the distance of travel that the emitted charged particles (^{3}He and protons) within the tube. This is a key point for detectors employing BF_3 because they cannot be operated at pressures higher than 0.5-1.0 atm due to the "poor" gas performance at higher pressures (Knoll, 1989). Aside from a high cross section for thermal neutrons and other properties mentioned above, ^{3}He is also non-toxic. These properties have made the isotope the ideal candidate for neutron detection from a strictly scientific perspective.

Following the recent terrorist attacks of September 11, 2001, the United Stated federal government deployed neutron detectors across its borders. The detectors were mainly ^{3}He based and used for prevention of smuggled radioactive material across its borders. The sudden deployment of helium based detectors created a sharp demand for ^{3}He isotope and thus caused the beginning of the decline of the stockpiles of ^{3}He. By 2010 the stockpiles of ^{3}He were reduced to 50000 liters from 235000 liters in 2001 (D.A Shea, 2010).

Shortage of ^{3}He supply can be a serious issue for neutron detection applications. In order to offset the demand, detection techniques based on alternative sensors must be developed. Industry standards have been developed and it requires alternative radiation detectors to be cost efficient, rugged, safe, and reliable (D.A Shea, 2010).

Perhaps one of the most widely used areas for detection includes radiation surveying. The need to detect radiological hazards efficiently has become a necessity. Areas which are common to radiation are subjected to mixed radiation fields, such as γ-ray, and neutron radiation. Some detection methods show promising results for γ-ray sensitivity but lack neutron detection capability. A combination of γ-ray and neutron detection within a single instrument will reduce the survey times, and the complexities involved with using separate neutron and γ- detectors. The following will examine the past alternatives to neutron detection, and investigate new scintillating crystals which are showing promising results.

Combinations of different inorganic scintillation detectors can also be used for thermal neutron detection based on different nuclear reactions. A combination of inorganic elements of low atomic number would cause these detectors to become inefficient in detecting γ-ray and very efficient for thermal neutron detection (van Eijk et al., 2004). LiF/ZnS:Ag has recently received some attention in its ability to have good neutron and gamma discrimination (Brookheaven National Lab, 1998). They are most frequently used for thermal neutron detection but the other detectors are also in the experimental stages and show great promise in the field of thermal neutron detection (van Eijk et al., 2004). ^{6}Li and ^{10}B based scintillators receive more attention than the gadolinium (Gd) detectors because Gd detector has very low efficiency and lacks good discrimination capabilities. On the other hand, Ce-doped scintillators are considered to have potential for fast response and good light yield (Czirr, 1998).

^{6}LidepGd ($^{11}BO_3$)$_3$: Ce doped scintillator is a detector that contains a combination of interesting materials with useful properties. The use of ^{6}Li offers a high signal response and the compound can be quite efficient where light transport is concerned due to its low refraction index of 1.66. A thin layer of scintillation allows this detector to cover a large area (Czirr, 1998). Another scintillation detector with good pulse shape discrimination, developed very recently, is the Cs_6LiYCl_6:Ce (A. Bessiere, 2003). This sensor has advantages of being Ce-doped material but has the drawback that the material is hygroscopic and also because neutrons are absorbed both by Cs and Cl (A. Bessiere, 2003).

For first responders, and radiation protection programs, it is desirable to have a detector with the ability to dually detect neutrons and γ radiation. Gaseous detectors in use nowadays are not suitable for dual γ-neutron detection and are limited by packaging options. Moreover as the need for ^{3}He, which is utilized frequently in gaseous neutron detectors, is outpacing production due to the increased demand. An alternative can be the use of lithium iodide doped with europium, LiI(Eu), scintillators not only for slow neutron detection but also for γ-radiation spectroscopy. It exhibits similar properties in chemical composition to NaI (Sodium Iodide) and therefore has a high light output (around 35%). Moreover, ^{6}Li has a large Q-value 4.78 *MeV* which plays an important role in γ-ray discrimination and does not exhibit significant wall effect because the distances the particles travel are very short in the LiI(Eu) crystal. Some of the drawbacks are due to the fact that the LiI(Eu) crystal is hygroscopic and therefore it must be sealed in a canning material for its protection. In this regard, LiI(Eu) and is attractive candidate due to its detection efficiency as well as to its proprieties of distinguishing between the neutron and γ-radiation.

Objectives:

The objective of this thesis is to investigate the possibility of developing a handheld scintillating detector based on LiI(Eu) with the ability to simultaneously detect neutrons and γ radiation in mixed fields using single crystal and evaluate its performance.

The thesis consists of an introduction, three chapters, conclusion and ends with a list of references, and appendices. Chapter 1 includes a background of the importance of neutrons as fundamental particles in fundamental and applied research. It discusses the complexities of neutron field and its large energy span and contains further detail on the neutron and γ-ray sources that were used in order to carry out the experiments. A General description of interactions of neutron and γ-ray with matter and a short review of currently available detectors are also given in the chapter.

Chapter 2 outlines the detector development, methodology and describes the pulse formation by the each radiation type. Chapter 3 is a description of the data acquisition system used in the experiments. Chapter 4 presents the results of measurements and discusses the obtained findings. This chapter also includes the detector characteristics such as resolution and its ability of dual detection of neutron and γ radiation. A discussion of detector calibration will be included with different source will be also discussed.

Finally the thesis concludes with a discussion of the main findings and is followed with a list of references and appendices.

Chapter 1

Background on Neutron and Gamma Radiation

1.1. Complexity of Mixed Neutron and Gamma Fields

Working environments where radiation protection is of concern may be constantly bathed in radiation which comes from a variety of natural and artificial sources. These sources include cosmic rays, natural radioactive isotopes, medical diagnostics, and radioactive sources used in the industry. Of the various types of radiation, the most penetrating of them include neutrons and γ-rays. Neutron radiation is often accompanied with γ radiation in mixed fields. For example, an environment containing an encapsulated Americium Beryllium (Am-Be) neutron source, releases various photon energies due to alpha induced nuclear excitation which prompts γ-rays to be released as the nucleus is rearranged during the de-excitation process. The de-excitation mechanism described above is typical for most nuclear reactions involving neutron emission. Therefore γ-ray emission is characteristic of neutron emission. Fission reactions such as those found in nuclear reactors, cause the atom to split into fragments, subsequently releasing neutrons along with γ-rays. Research reactors and isotope producing reactors often involve high neutron flux and a wide range of γ radiation. Such as in the process of Californium (^{252}Cf) production, the Plutonium isotope (^{242}Pu) is irradiated with a high neutron flux of about 10^{15}n/cm^{2}s and is finally converted into ^{252}Cf with several neutron absorptions and beta decays which is accompanied with γ radiation.

Neutrons exhibit energies that are low, intermediate, and high depending on the source. Neutron sources found in research facilities often produce neutron energies of tens of *keV* up to several *MeV*. Fission reactors often contain moderators in order to slow down neutrons to energies of 1/40 eV or 2200*m/s*, where the cross sections of the target are high enough to allow nuclear reactions to occur. Neutrons emitted from fission reactions are sometimes partially moderated and they are known as epithermal neutrons with energies of 0.1 *keV* to 10 *keV*. Fusion induced neutrons which involve deuterium-deuterium or deuterium-tritium (D-T) reactions are released with 2.45 and 14 *MeV*, respectively and are generally used in neutron generators. Lastly, secondary particles released from particle accelerators or from the atmosphere from cosmic rays may be high-energy neutrons which have energies of 10 *MeV* to hundreds of *MeV*.

In terms of radiation protection, biological effects which are caused by radiation are a strong function of the type of radiation and its energy. Therefore each radiation type is assigned a radiation weighting factor (w_r) as can be seen in the table 1. Biological damage occurs with increasing ionizing effects of a particle.

Table 1: Radiation types and weighting factors (Leo, 1994)

Radiation type and energy	Radiation weighting factor, w_R
Photons, all energies	1
Electrons and muons, all energies*	1
Neutrons	
<10 k*eV*	5
10 k*eV* to 100 k*eV*	10
>100 k*eV* to 2 *MeV*	20
> 2 *MeV* to 20 *MeV*	10
> 20 *MeV*	5
Protons, other than recoil protons, energy > 2 *MeV*,	5
α–particles, fission fragments, heavy nuclei	20
*Excluding Auger electrons emitted from nuclei bound to DNA	

An individual may be subjected to different types of ionizing radiation as shown above. Ionization radiation poses serious risk to personal health if adequate safeguards are not present. Therefore, personal dosimeters are worn by individuals to record personal dose equivalent and survey instruments are used to monitor radiation fields in real-time. The purpose of the information from the survey meter is to designate areas in terms of allowed occupancy and investigate radiation levels in the area prior to and during work. Often radiation detection devices are suited for specific types of radiation i.e. specific to neutrons or specific to γ-rays. Moreover, only a limited number of devices can be used to detect the full range of neutron energies. In addition to such limitations, there are also issues when employing these devices in workplaces with the surrounding conditions of noise, temperature, humidity etc… which cause less reliable measurements compared to measurements taken in an ideal laboratory setting.

1.2. Gamma-Ray Interactions with Matter

Similar to the nature of energy levels in the electron shells, the nucleus also contains discrete energy levels. Nuclear transitions between these energy levels results in the emission of electromagnetic radiation known as gamma rays (γ-ray). Transitions amongst the energy levels can be made if the correct amount of energy is released or absorbed; i.e. energies are equal to the difference between energy levels of the participating nuclear levels. Quanta of energy, also called photons which are emitted are categorized by their origin. Bremsstrahlung radiation is caused by the deceleration of a charged particle typically due to an electron being deflected by atomic nucleus where the loss of energy is converted into photons. Characteristic X-rays are emitted as a result of transitions in bound electrons between shells K, L, M. Most γ-ray emissions are a result of Beta decay (β) as shown in the decay scheme of ^{60}Co below.

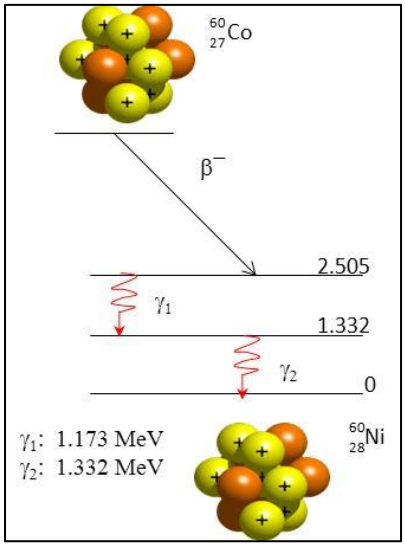

Figure 1: Decay Scheme for ^{60}Co

In this process, ^{60}Co decays through β^- with a 5.26 year half-life thereby forming an excited state of Nickel (Ni). The emission of β^- occurs when the nucleus has excess neutron (neutron rich element), and a neutron will transform into a proton and electron, thereby emitting the electron (e-) and antineutrino (υ) in the following the decay scheme:

$$_{A}^{Z}X \rightarrow {}_{A+1}^{Z}Y + e^{-} + \upsilon \quad (1)$$

Equation 1 shows the emission of e^- from the parent atom (X), which causes a daughter atom (Y) to have an excess of one proton, therefore an increase of positive charge (A). The atomic mass number (Z) remains the same. The γ-ray photon energies are equal to the difference between the initial and final nuclear energy states within ^{60}Ni. After β^- decay, the ^{60}Ni nucleus is in an excited state of 2.505 *MeV*. In order for ^{60}Ni to de-excite and become a stable ^{60}Ni isotope,γ_1 (1.173 *MeV*) and γ_2 (1.332 *MeV*) are released. Interactions of γ-ray in matter occur in many different ways. Fano has systematically categorized the interaction of γ-rays in the following manner:

Table 2: Possible gamma ray interaction modes (Fano,1953)

Kinds of interaction	Effects of interaction
1. Interaction with atomic electrons	(a) Complete absorption
2. Interaction with nucleons	(b) Elastic scattering (coherent)
3. Interaction with the electric field surrounding nuclei or electrons	(c) Inelastic scattering (incoherent)
4. Interaction with the meson field surrounding nucleons	

There are 12 combinations of interaction modes, by combining columns 1 and 2, however many are do not occur frequently and some have never been observed. All but three of the twelve

processes from above are explainable by the Compton effect, photoelectric effect, and pair production. Therefore these processes are considered as the three major interaction types of γ-ray interactions. All of these processes lead to a partial or complete energy transfer to the electron energy. Unlike charged particles γ-ray photons either deposits their energy completely and disappears or scatter through a significant angle. Moreover, the transfer of energy is sudden, in contrast to the behavior of charged particles as they gradually lose their energy, until slowing down and finally losing all of their energy to the surrounding absorber atom at the end of their path length, and is known as the Bragg Peak and discussed in section 2.1.

In 1887 Hertz discovered that photons of visible light would liberate electrons from a metal surface. Photoelectric absorption is the basis for the observed phenomena. When γ-rays transfer all their energy to a bound electron it ceases to exist, and it is known as photoelectric absorption which is shown below in Figure 2. Some of the energy from the γ-ray is used to overcome the binding energy of the electron and the remainder is given off as kinetic energy to the electron. In order to maintain conservation of momentum, a small fraction of the energy is transferred to the recoil energy of the atom. Tightly bound electrons have the greatest probability of absorbing the incident photon. Therefore the majority of interactions occur in the K-shell as long as the incident photon has energy greater than the binding energy of the K-shell. The presence of a target atom is essential for photoelectric absorption to occur therefore it is known to be an interaction that involves a photon and the atom cloud from which an electron is emitted (usually K or L shell) with the energy that is equal to Ee and is shown in the equation below:

$$\boldsymbol{E_e = h\nu - E_b} \tag{2}$$

Where, E_b is the binding energy of the electron shell

$h\nu$ is the energy of the incident photon.

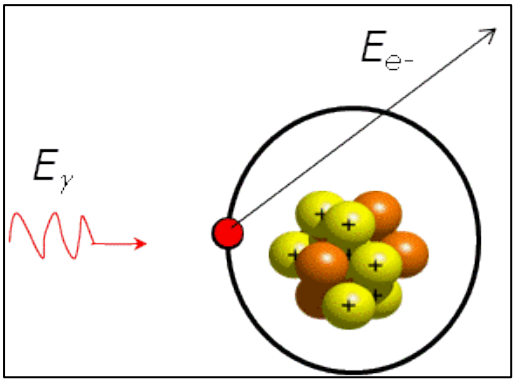

Figure 2: Schematic of photoelectric absorption process

Compton scattering is an interaction between the incident γ-ray and the electrons in the atoms of the target material. This mode of interaction is the most dominant for typical energy levels for γ-ray sources. The interaction involves the least tightly bound electrons in the outermost electron shell. Because the binding energy is very low it is usually not considered to affect the energy of the recoil electron. The incoming γ-ray photon transfers some of its energy to an electron assumed to have energy equal to its rest mass, and continues through a deflection by an angle θ. The photon and recoil electron travel in different directions as shown below (Figure 3).

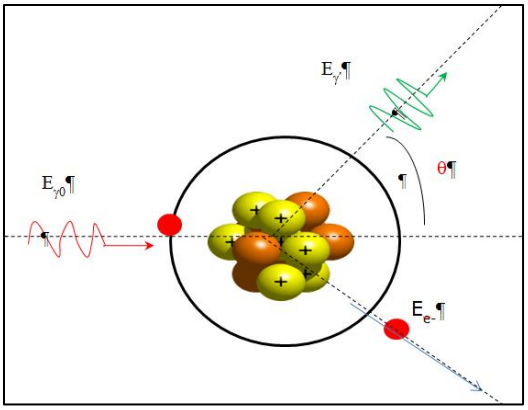

Figure 3: Schematic of Compton scattering of incident photon

$$\mathbf{E_e = E_{\gamma o} - E_{\gamma'}} \tag{3}$$

Where E_e is the energy of the recoil electron.

E_γ' is the energy of the scattered photon.

Since all the angles of interaction are possible, the energy that is transferred to the electron can vary from zero to nearly as much as the incident γ-ray photon energy. The energy of the scattered γ-ray is given by equation 4.

$$\mathbf{E_\gamma{}' = \frac{E_{\gamma 0}}{[1+\frac{E_{\gamma 0}}{m_o c^2}(1-\cos\theta)]}} \tag{4}$$

Where $m_o c^2$: the mass of electron $\simeq$ 511 keV

θ: The angle between scattered photon and incident photon

For a head on collision, the photon is scattered by 180^{o} and is left with the minimum energy also given by equation below.

$$\mathbf{E_{\gamma}{}'_{(min)}} = \frac{\mathbf{E_{\gamma 0}}}{\mathbf{1+\frac{2E_{\gamma 0}}{m_o c^2}}} \tag{5}$$

For very small angles ($\theta \simeq 0$) of photon scattering, the recoil electron carries away very little energy and the scattered photon is left with energy nearly the incident photon energy. The energy of the scattered electron is from zero to a max energy known as the Compton edge and is given by equation below:

$$\boldsymbol{E_{e(max)} = E_{\gamma 0} - \frac{E_{\gamma 0}}{1+\frac{2E_{\gamma 0}}{m_o c^2}}} \tag{6}$$

The energy of various Compton edges as a function of the electron's incident energy deposition as shown below (Figure 4).

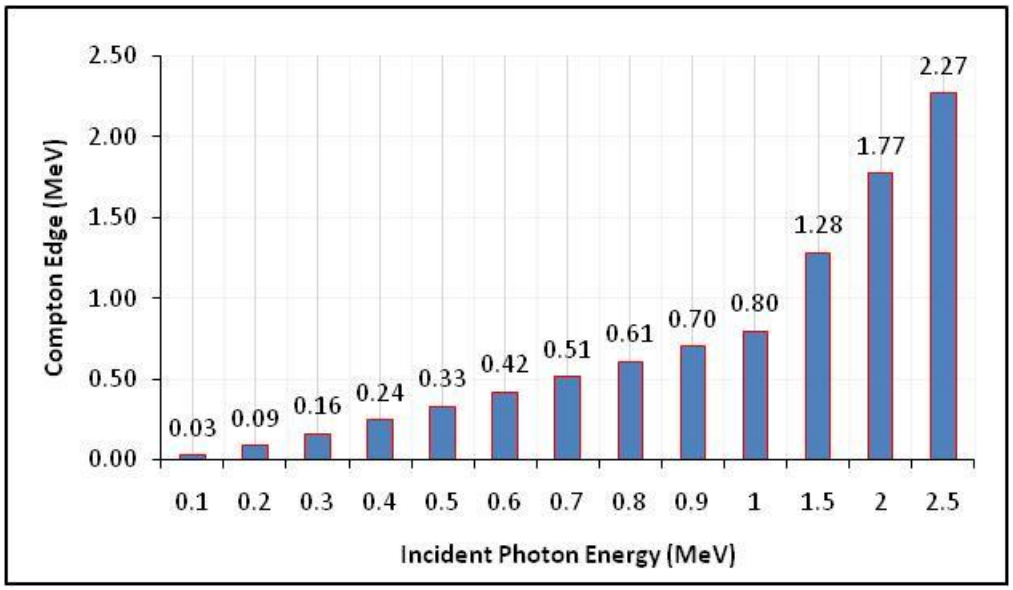

Figure 4: Energy of various compton edges as a function of incident photon energies

An incident γ-ray with minimum energy of 1.022 *MeV* can create an electron-positron pair in the nucleus when it is subjected to a strong nuclear field and within the vicinity of the nucleus. The atom receives a small amount of recoil energy but the remainder of the energy is transferred to the electron positron pair. If the γ-ray has energy beyond 1.022 *MeV* the excess energy is shared amongst the electron-positron pair. The electron and positron are emitted from the atom and lose their kinetic energy within the absorber, until the positron combines with an electron by releasing two oppositely charged 0.511 *MeV* γ-rays as shown below (Figure 5).

.

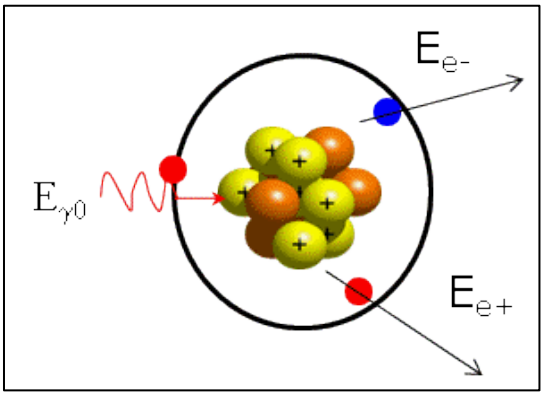

Figure 5: Schematic of pair production process

The relative importance for the three major γ-ray interactions, which were described above, along with various materials of different atomic number are shown below in Figure 6..

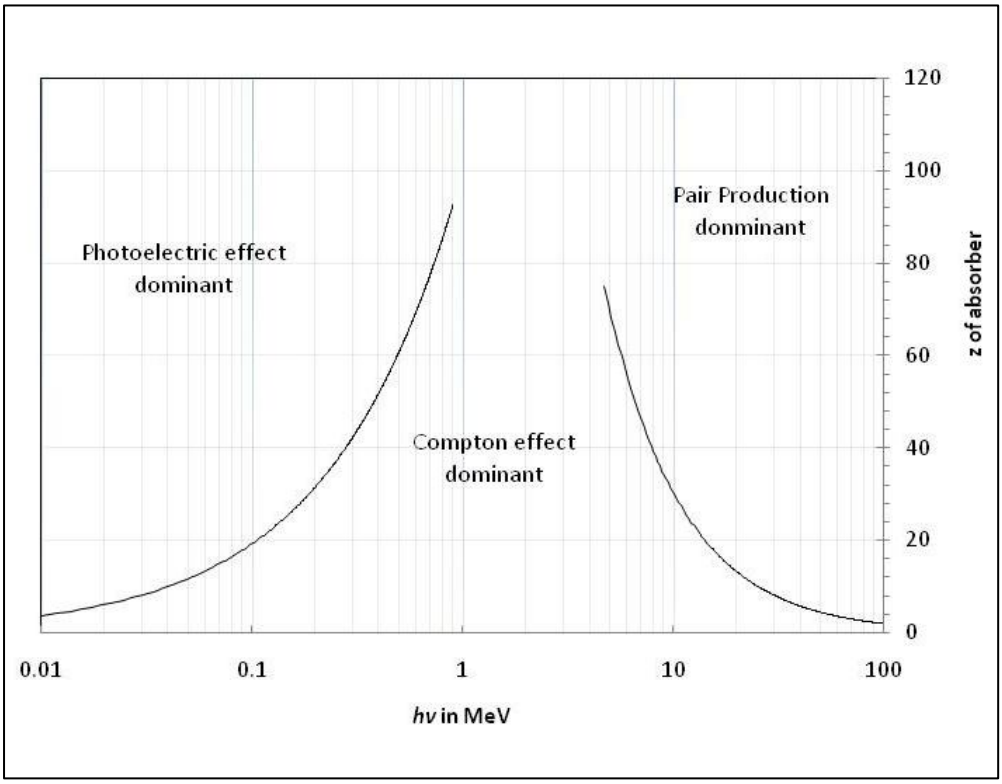

Figure 6: Relative importance of the three major types of gamma ray interaction (Evans, 1955)

1.3. Neutron Interactions with Matter

Interactions of neutrons with matter depend primarily on their energies, which range from eV to tens of *MeV*. The neutron is uncharged and borrows its name from the fact that it is a neutral particle. Due to the uncharged characteristic of the neutron, it will travel in matter and not interact with electrons. However the neutron may interact with the nuclei of these atoms. Nuclear force which allows these interactions to occur is very short ranged, approximately 10^{-13} cm (Leo,1994), therefore the neutron needs to be very close to the nuclei in order for the event to occur. Since the size of the nucleus is relatively small, compared to the size of the atom as a whole, a neutron will travel significant distances with very low probabilities of interaction.

The microscopic cross section explains the probability of an interaction between a neutron and a nucleus. Take for instance a beam of mono energetic neutrons that is travelling towards a thin target. At the other end of the target it will be observed that neutrons may be scattered at in different directions and have changed in energy, while some of the neutrons continue with the same energy and direction as before, and other neutrons do not pass through the target at all. These interactions are known as scattering, no interaction, and absorption, respectively. The ratio between the interacting neutrons in each event to the number of neutrons in the initial beam is the probability of interaction. The cross section of each incident is based on this ratio. For example, the probability of neutron absorption is the ratio of the number of absorbed neutrons in the target to the number of neutrons originally in the incident beam. Therefore the absorption cross section is the ratio between the probabilities of neutron absorption to the number of target atoms per unit area. Another way to conceptualize the microscopic cross section is by considering the probability that a neutron strikes a material of cross sectional area A, which contains N number of nuclei, and

each nucleus having a cross section of σ. The total maximum area that an approaching neutron could interact with the material would be the sum of the target nuclei multiplied by their respective cross section, $N\sigma$, i.e. the target area. Therefore when considering the atom as a whole, the probability of interaction of the neutron is the ratio between the target area and the cross sectional area of the material or $N\sigma/A$ (Rinard, 1991). Neutron cross sections are measured in barns, which is $10^{-24}cm^2$. Each type of neutron interaction is denoted by its partial cross section. For example inelastic scattering, by the inelastic cross-section, σ_i, radiative capture, by capture cross section, σ_γ, fission, by the fission cross section, σ_f, etc… When all the possible interactions are considered, their cross sections are summed, and it is referred to as the total cross section, σ_t.

Another concept worth mentioning is the macroscopic cross section which is defined by considering an incident parallel beam of neutrons onto a thick target with several atomic layers. The beam will interact with each layer within the target using concepts found in microscopic cross section. The macroscopic cross section is considered when dealing with the material rather than pure nuclides. After integrating through the layers of the target until you find a depth (x), the intensity of the uncollided beam is calculated by equation 7 and can be shown in Figure 7.

$$\boldsymbol{I(x) = I_o e^{(-N\sigma_t x)}} \tag{7}$$

Where I_o is the intensity of the original beam, N is the atomic density and σ_t is the total cross section.

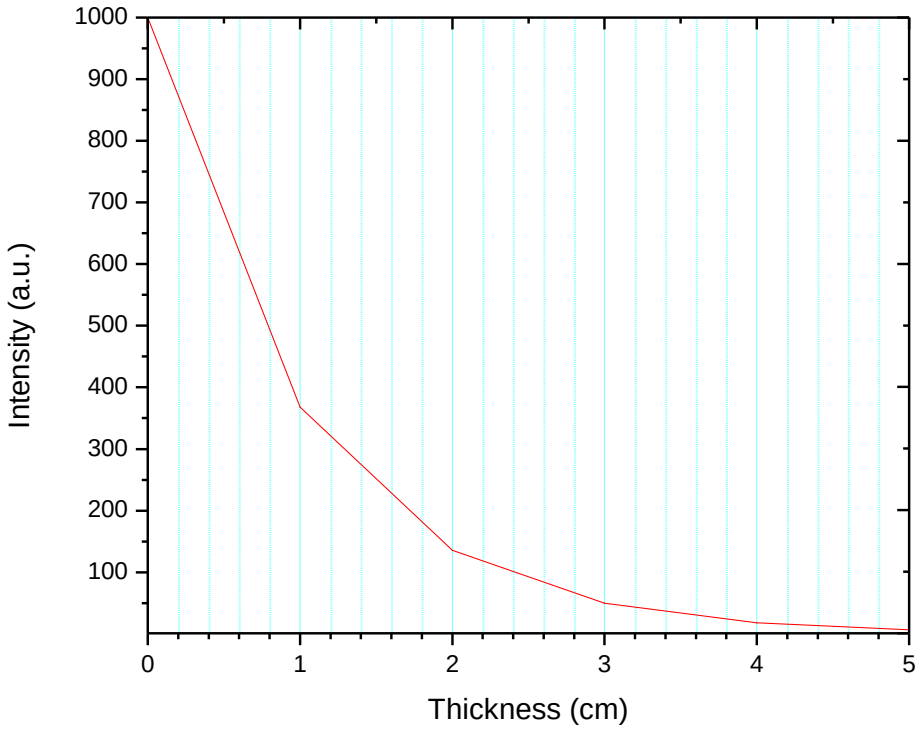

Figure 7: Intensity of uncollided neutron beam through thickness of material

The total macroscopic cross section shown below has dimensions of cm^{-1}.

$$\sum_t = N\sigma_t \tag{8}$$

"If only a particular type of interaction is of interest a macroscopic cross section for it alone can be defined using its microscopic cross section in place of the total cross section." (Rinard, 1991). Therefore in this context, we are discussing mainly microscopic cross sections. Microscopic cross sections are dependent on neutron energies as shown below (Figure 8). This is reasonable because the classical expression for energy of a particle ($E=mv^2/2$) is proportional to its velocity. For instance as the velocity of a neutron is decreased, it has more chance for interaction with the target

material, whereas a neutron with higher velocity will have less time for interaction with the target material and cause the particle to pass through without interacting thereby decreasing its probability of interaction

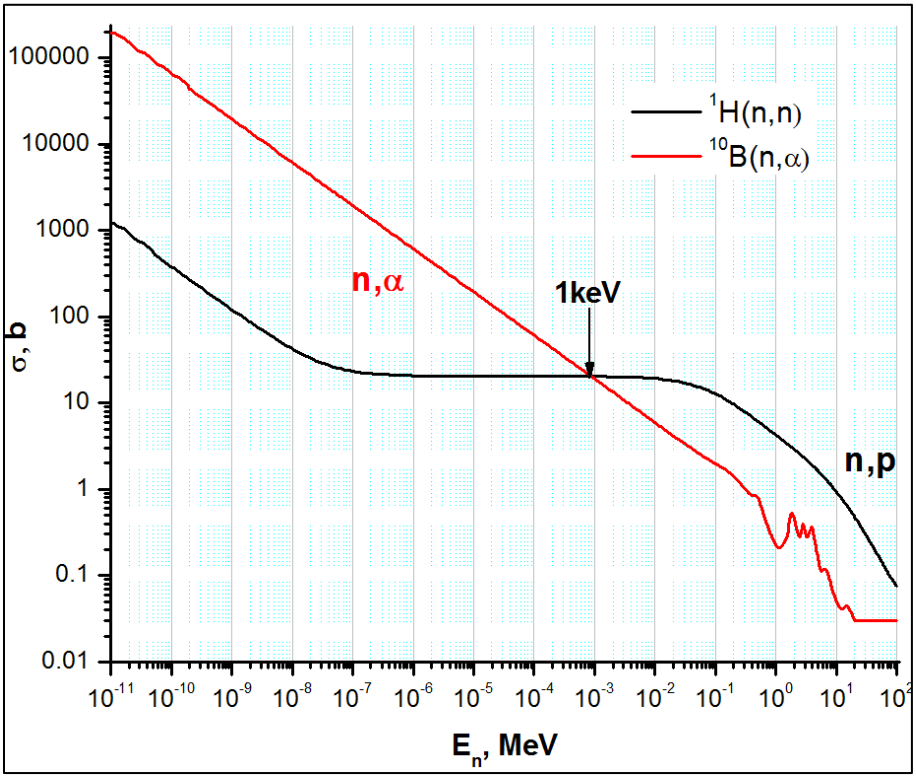

Figure 8: Neutron reaction for *(n,n)* and *(n,α)* on hydrogen and boron as function of neutron energy

For example a 1 *MeV* neutron with the speed of 1.383 x 10^7 *m/s*, crosses a 15 cm thin target in 11*ns*. A thermalized neutron with energy of 1/40 *eV* and velocity of 2187 *m/s* will cross the same target material in 70*μs* (Rinard, 1991). It is evident that reducing the energy to the thermal region is beneficial due to the increased number of interactions. In the following, neutron thermalization will be discussed.

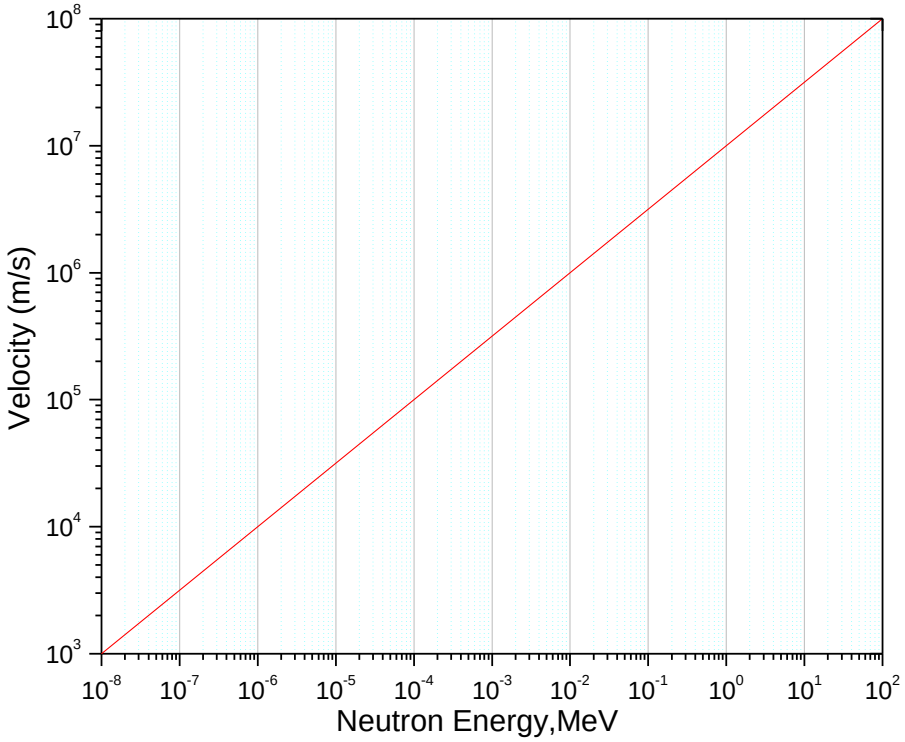

Figure 9: Relationship between neutron energy and velocity

At energies below 1 *MeV*, the total cross section remains to have a 1/*v* (where v is the velocity) trend for the lower energy neutrons, such that the microscopic cross section is inversely proportional to the velocity of the neutron. At energies usually above 1 *MeV*, the general trend of 1/*v* is changed by large peaks that occur in between which are known as resonance peaks as shown in Figure 10.

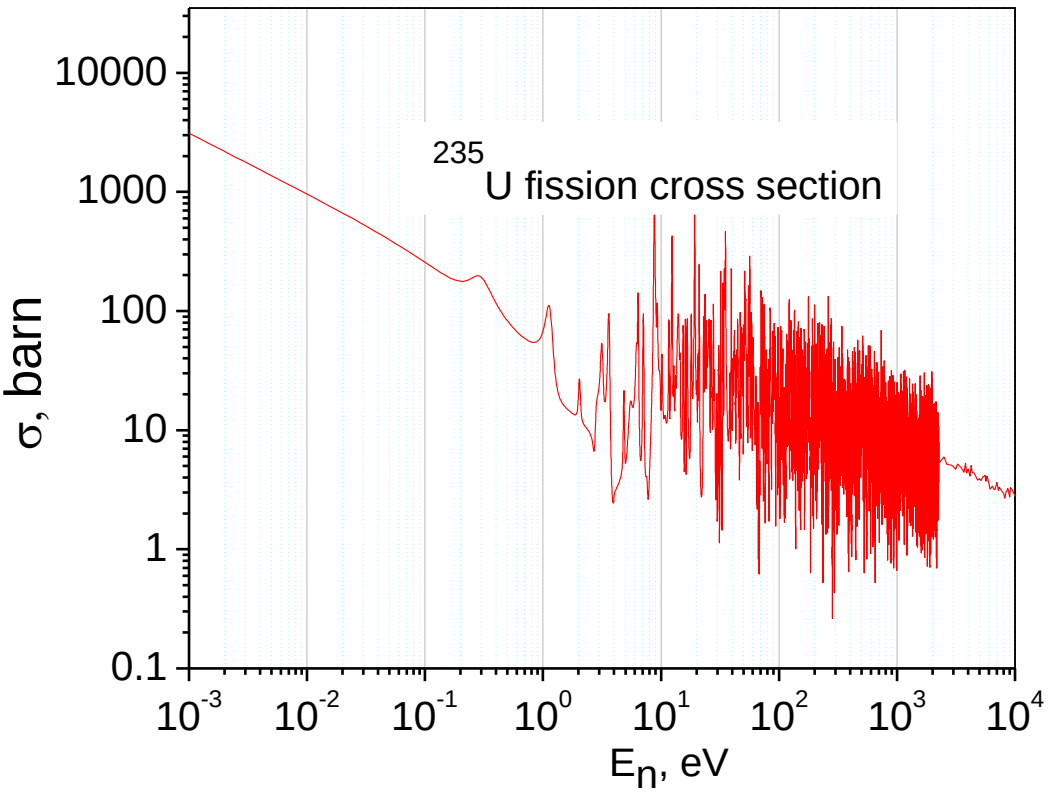

Figure 10: Fission neutron cross section of ^{235}U

Resonance peaks occur when there is an enhanced probability for the approaching nuclei to interact with the nucleus. The approaching neutron that strikes the target nucleus, transfers approximately the amount of energy which matches an energy level in the target nucleus. Therefore, a neutron with an appropriate energy which matches a resonance energy of the target, will have a highly enhance probability for interaction with the target. Due to the strong dependence of neutron interaction with their energies, it is common to classify neutrons by their energies. At low level energies, where E= 1/40 eV, they are considered slow, or thermal. Between 0.1 eV and 10 *keV*, where resonance peaks are observed, neutrons are known as epithermal. At

100 *keV* to tens of *MeV* neutrons are known as fast, and higher than 100 *MeV* they are known as high energy neutrons.

Neutron interactions are divided into two types, scattering and absorption. When an interaction takes place, the neutron will strike the target nucleus, and may disrupt the system of the target. In scattering interactions the number of the protons and neutrons in the target material do not change, whereas in absorption interactions the neutron is absorbed, giving the target nucleus an opportunity for a wide range of emissions. The interaction is written by using symbols to represent the reaction, such as, *X(n,a)Y*, where *X*, and *Y* are target and recoil nucleus, respectively. The symbols within the parentheses reflect the type of incoming radiation, and emission of the particle, respectively. Such as ^{6}Li *(n,α)* ^{3}H represents a neutron collision onto a Lithium and the release of tritium and an α-particle thereafter. A chart of various interactions induced by neutrons is represented below in Figure 11.

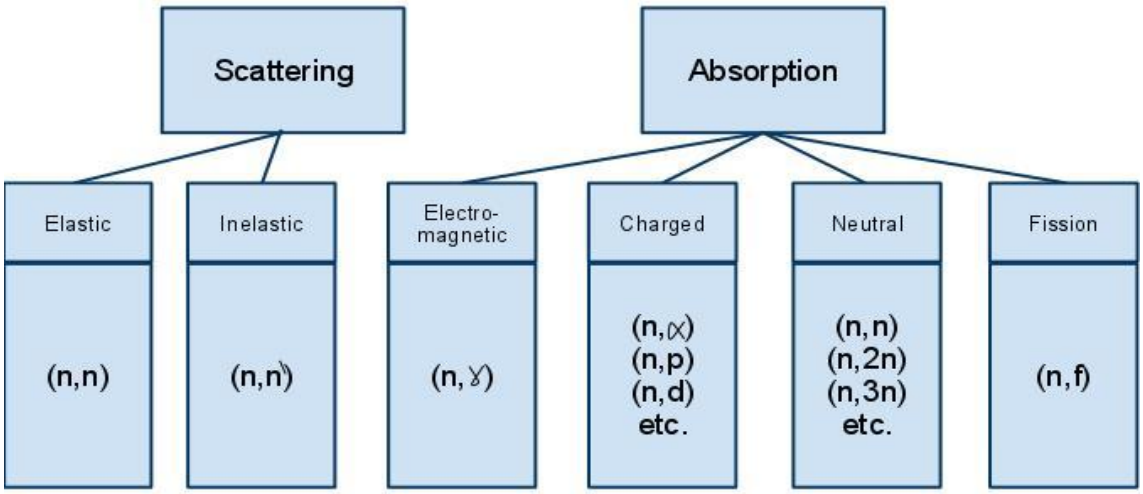

Figure 11: Neutron interaction modes

For neutron interactions to occur, the neutron must have the appropriate energy and must be sufficiently close to the nuclei of the target. An oncoming neutron may transfer some of its initial kinetic energy to the target, leaving the nucleus of the target with some recoil energy. In inelastic neutron scattering the neutron has sufficient energy to cause the target nucleus to undergo an internal rearrangement causing the nuclear particles to jump from their ground levels to a higher level. When the nuclear particles rearrange themselves the transition from excited nuclear state to ground state will emit γ radiation (Figure 12). The energy emitted in radiation is equal to the loss of kinetic energy minus the nuclear binding energy. Each nucleus has different energy levels and therefore the loss of kinetic energy is particular to the nuclear energy levels of the target material.

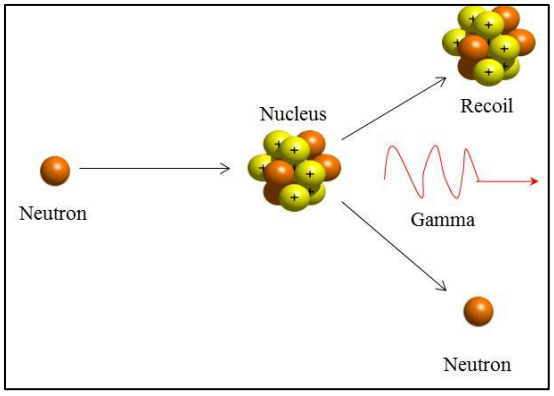

Figure 12: Inelastic neutron scattering

Neutrons below 1 *MeV* threshold do not have sufficient energy to excite the nucleus. If the energy levels in the nucleus are higher compared to the incident neutron then the neutron will interact only by elastic scattering. In this case there is no excitation of the nucleus. Elastic scattering causes the neutron to retain most of its original energy subsequent to the interaction and the nucleus with some recoil energy (Figure 13).

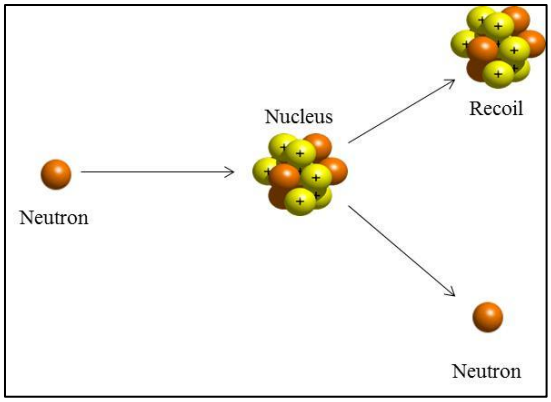

Figure 13: Elastic neutron scattering

The second major neutron interaction is neutron absorption. When the neutron is absorbed, the resulting nucleus will increase in mass and become excited. In order to de-excite from the excess energy the atom may result in radiation of various kinds such as fission fragments, neutrons, and charged particles such as α, protons, deuteron etc…

If a neutron is absorbed by the nucleus causing an emission of another neutron, it is referred to as single neutron emission but would appear to be similar to scattering, in terms of oncoming and outgoing particles. On the other hand multiple neutron emissions which follow neutron absorption gives rise to greater number of free neutrons within the material compared to the number of free neutrons prior to interaction.

Fission occurs when a heavy element captures a neutron to form a highly energetic element. Due to the unstable nature of the formed compound, it may split into two smaller fragments known as fission fragments thereby releasing other particles such as neutrons (Figure 14). Nuclear fission is different from other nuclear reactions in that neutrons and other particles are also released and can

interact with neighboring atoms to produce a chain reaction. In addition to fission fragments particles such as γ-rays may also release following neutron absorption.

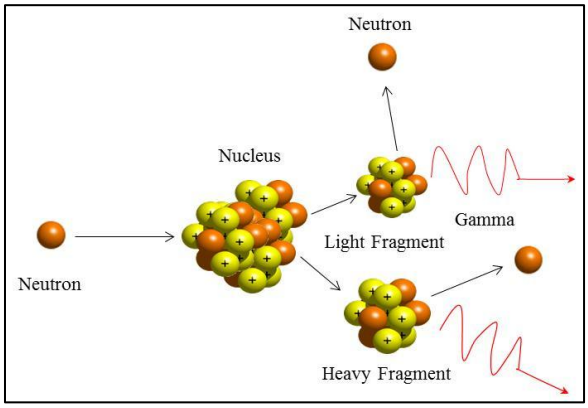

Figure 14: Neutron induced fission

A reaction which involves the formation of an isotope of the target following absorption of the neutron, and release of electromagnetic radiation is called radiative capture (Figure 15). Electromagnetic particles such as γ-rays are released after a transition from an excited nuclear state to ground state. Therefore the energy released is equal to the difference between the nuclear states minus the nuclear binding energy due to the law of conservation of energy.

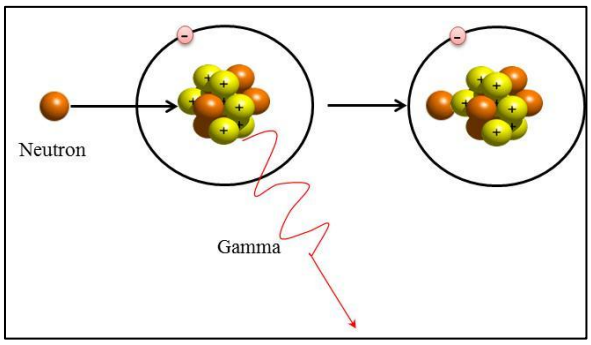

Figure 15: Radiative capture

Neutron absorption may cause the compound that is formed to de-excite in the form of proton emission or α emission. This process which causes the formation of a new element is known as transmutation. For example in the reactions $^{16}O\ (n,p)\ ^{16}O$, and $^{6}Li\ (n,\alpha)\ ^{3}H$, two new elements are formed (Figure 16, Figure 17).

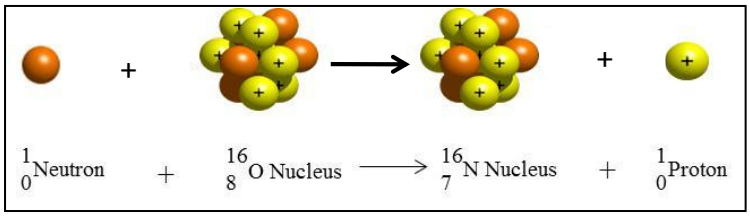

Figure 16: Proton release followed by neutron absorption

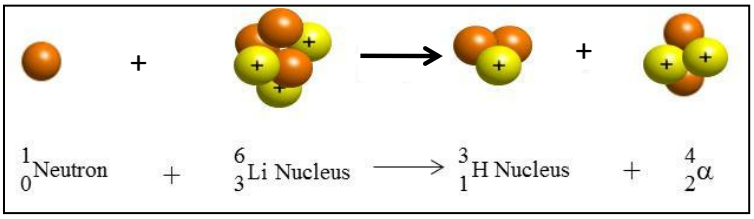

Figure 17: Alpha release followed by neutron absorption

The energy released is shared amongst the products of the reaction. In general, the energy released (*Q*-value) following a nuclear reaction is the difference in energy-mass equivalence between reactant and product. If the *Q*-value is negative it is an endothermic reaction, and conversely a positive *Q*-value is an exothermic reaction. In an exothermic reaction, the released energy is in the form of kinetic energy to products of the reaction. For example, the reaction $^{6}Li\ (n,\alpha)\ ^{3}H$ occurring in the LiI(Eu) crystal has a *Q*-value is 4.78 *MeV* and it is shared amongst the tritium and α-

particles, and may be calculated using equation 9, assuming the target is at rest and incoming neutron is thermal and has 1/40 eV ≈ 0, and 1amu is equal to 931*MeV*:

$$\boldsymbol{Q = E_R - E_P}$$

$$\boldsymbol{Q = E_n + [(M_n M_{Li}) - (M_{He} M_T)]931\ MeV} \tag{9}$$

$$\boldsymbol{Q = [(6.015122\mu + 1.00866\mu) - (4.002603\mu + 3.016049\mu)]931\ MeV}$$

$$\boldsymbol{Q \cong 4.78\ MeV}$$

Also in the reaction ^{6}Li *(n,α)* ^{3}H, the kinetic energy of the out coming particles is essentially the *Q*-value that is shared between the reaction products. Their energies can be calculated using conservation of momentum as shown in equation 10.

$$\boldsymbol{E = \frac{1}{2}mv^2}$$

$$\boldsymbol{\frac{2E}{v} = mv}$$

$$\text{but } \boldsymbol{v = \frac{\sqrt{2E}}{m}}$$

$$\boldsymbol{mv = \frac{4E^2 m}{2E} = 2Em}$$

$$\text{so } \boldsymbol{2E_t m_t = 2E_{He} m_{He}}$$

$$\boldsymbol{and\ E_t + E_{He} = 4.78\ MeV}$$

Solving simultaniously gives:

$$\boldsymbol{E_T = 2.73\ MeV \rightarrow E_{He} = 2.05\ MeV} \tag{10}$$

As can be seen by all the examples which show neutron interaction, it requires a medium to interact with. For example, for detector design, the appropriate medium must be selected according to its ability to interact with neutron (high cross section). Due to the neutron lacking any charge, detection of the neutron directly would be very difficult because a pulse cannot be created via ionization or excitation in the detector sensitive volume. Therefore neutrons are detected indirectly through an emitted secondary charged particle. This was the basis for neutron detection and it is discussed in greater detail in section 1.5.

1.4. Neutron Sources

Neutron emission may occur when the excitation energy of the nucleus is above the neutron binding energy. Natural neutron emitters which can be utilized in a laboratory do not exist, therefore practical neutron sources use reactions induced by γ-rays, α–particles and spontaneous fission. These sources have several disadvantages which limit their usage. In order to produce a large neutron yield, the activities of the isotopes must be very high. Even when higher activities are used, the relative neutron yield compared to competing sources will be less by several orders of magnitude. Secondly, the neutron spectrum is quite broad, and is also accompanied with γ-ray emission. Despite these drawbacks, the sources have several advantages. Their neutron intensity is predictable, and reliability is relatively high. Matched with low manufacturing cost, low maintenance, the small size and ease in portability these sources have found wide range of practical uses within research laboratories.

Spontaneous fission occurs in heavy nuclei, from which neutrons are emitted. All heavy nuclei in theory are unstable against spontaneous fission. It occurs predominantly in heavy transuranic elements. The mode of decay in most these transuranic elements generally occur in the form of α-particle decay, and in some less probable events spontaneous fission. Along with the fission fragments, several fast neutrons, β's and γ's are also emitted. In some elements the probability of spontaneous fission is reasonably high enough so that it can be considered to be used as a neutron source. If the element is intended to be used as a neutron source, it must be encapsulated with sufficient thickness to prevent β's and γ's from emerging from the source.

A very commonly used spontaneous fission source is ^{252}Cf produced in reactors with a neutron flux of about 10^{15}n/cm^{2}s (Cierjacks, 1983). The isotope that is irradiated can be ^{242}Pu, until there are 10 neutron captures and 4 beta decays until it is converted into ^{252}Cf. Alternatively berkelium-249 ($^{249}_{97}Bk$) is also commonly irradiated convert into berkelium-250 ($^{250}_{97}Bk$) by neutron caputure, and followed by β^- decay to produce ($^{250}_{98}Cf$). ^{252}Cf is finally produced via neutron capture (Heiserman, 1992). The following represents the two step reactions that take place:

$$\mathbf{^{249}_{97}Bk(n,\gamma)^{250}_{97}Bk \rightarrow {}^{250}_{98}Cf + \beta^- \rightarrow {}^{250}_{98}Cf(n,\gamma)^{252}_{98}Cf} \quad (11)$$

The californium isotopes are collected though a solvent extraction and purified by exchange chromatography (Cierjacks, 1983). Various methods for production are available. A common procedure is to precipitate californium and iron as the hydroxide, which is converted to an oxide by heating and finally compressed into a small pellet (Cierjacks, 1983). Further detail on the fabrication procedure is available in the reference above. Californium neutron sources are usually produced in sealed sources which range between few micrograms to 5 milligrams and can provide a rate of neutrons of 10^{10}*n/s*. ^{252}Cf sources would require less mass by 1-2 orders of magnitude when compared to other sources available in order to achieve similar neutron output.

Neutrons induced by α-particle interaction are possible if the correct α-particle emitter and target are chosen. There are a number of α-emitting isotopes which are widely available because highly energetic α-particles are decay products from many radionuclide sources. The target material is typically a light isotope. α's travel a short distance due to coulomb forces, therefore the target and the α-emitter is kept as close as possible by fabrication of the neutron source into self-contained mixtures of α emitting isotope into the target isotope. Historically naturally occurring α emitters

were chosen, such as polonium or radium, however contemporary sources generally utilize artificially produced transuranic isotopes due to their favorable decay properties and lack of secondary radiations. The half-life and emission energies of the α source are important properties to be considered. The number of neutrons per α interaction (neutron yield) is proportional to the energy of the α-particle. The specific activity of the neutron is inversely proportional to the half-life of the α-emitter. The half-life of the α-emitter would dictate the practical use of the neutron source. To achieve a reasonably high neutron output within a small volume, a suitable α-emitter would have reasonable α-particle energies, and half-life.

Based on the application, various forms of neutron sources are available. Plutonium (^{239}Pu) has been used as an α-emitter due to lower specific activities, and high neutron yields

Table 3: Characteristics of Be(α,n) Neutron Sources (Cierjacks, 1983)

		E_{α}	Neutron Yield per 10^6 Primary Alpha Particles		Percent Yield With E_n < 1.5	
Source	Half-Life	(*MeV*)	Calculated	Experimental	Calculated	Experimental
^{239}Pu/Be	24000 y	5.14	65	57	11	9-33
^{210}Po/Be	138 d	5.30	73	69	13	12
^{238}Pu/Be	87.4 y	5.48	79[a]	--	--	--
^{241}Am/Be	433 y	5.48	82	70	14	15-23
^{244}Cm/Be	18 y	5.79	100[b]	--	18	29
^{242}Cm/Be	162 d	6.10	118	106	22	26
^{226}Ra/Be + daughters	1602 y	Multiple	502	--	26	33-38
^{227}Ac/Be + daughters	21.6 y	Multiple	702	--	28	38

Some neutron sources can use mixtures of ^{239}Pu as the primary α-source and 0.7% ^{241}Pu. Overtime the ^{241}Pu will β^- decay to form ^{241}Am which will contribute initially to the neutron yield of approximately 2% annually (Cierjacks, 1983). It is also possible to increase neutron yield by fissioning ^{239}Pu because the isotope also has a high cross section for thermal neutrons. If the source is placed in a neutron moderating material, the α-induced neutrons emerge from the source, become thermalized, and may return to cause neutron induced fission, which will increase the neutron yield by as much as 2% (Cierjacks, 1983). ^{241}Am is another widely used α-emitter which we will discuss in detail in section 2.1.

The most common target isotope for α induced neutron sources is Beryllium (^{9}Be):

$$^{9}_{4}Be + ^{4}_{2}He \rightarrow ^{12}_{6}C + n$$

The neutron yield as mentioned above is dependent on the incident α-particle. If a beam of α-particles of typical energies bombard a thick beryllium target, approximately 10^4 neutrons (Cierjacks, 1983). A convenient method to produce free neutrons is by mixing a suitable target material with a strong γ-ray emitter (Equation 12).

$$\begin{aligned} &^{2}_{1}H + \gamma \rightarrow {}^{1}_{1}H + n && \text{Q=-2.226 } MeV \\ &^{9}_{4}Be + \gamma \rightarrow {}^{8}_{4}Be + n && \text{Q=-1.666 } MeV \end{aligned} \qquad (12)$$

The target Beryllium and deuterium material are usually chosen because their binding energies are reasonably low. The minimum required photon energy to liberate a neutron from the target material, is equal to the absolute value of the *Q*-value therefore, other target materials are not suitable because of their higher binding energies. Many radio nuclides are available which emit the required energies in order to liberate photo neutrons from targets mentioned above. If the γ-ray

energy has a higher value than the *Q*-value, the neutron caries away the excess energy by the formula: excess photo-neutron

$$\boldsymbol{E_{(n)}(\theta) \cong \frac{M(E_\gamma + Q)}{m + M} + \frac{E_\gamma[(2mM)(m + M)(E_\gamma + Q)]^{1/2}}{(m + M)^2} cos\theta} \tag{13}$$

Where:

E_γ: gamma energy (<<931 MeV)

θ: angle between gamma photon and neutron

M: mass of recoil nucleus times c^2

m: mass of neutron times c^2

The second term introduces only slight changes of a few percent to the neutron energy as the angle between the γ-ray photon and neutron varies between 0-π. In case where the isotope produces a single γ-ray photon above the *Q*-value, the neutron spectrum has a single narrow peak. Therefore the emitted neutrons are considered to be nearly mono energetic, and advantageous for many applications.

Table 4: Photo neutron Source Characteristics (Knoll, 1989)

Gamma Ray Emitter	Half-Life	Gamma Energy*	Target	Neutron Energy(keV)	Neutron Yield (n/s) for 10^{10} Bq Activity#
^{24}Na	15.0 h	2.7541	Be	967	340,000
			D		330,000
^{28}Al	2.24 min	1.7787	Be	101	32,600
^{38}Cl	37.3 min	2.1676	Be	446	43,100
^{56}Mn	2.58 h	1.8107		129	91,500
		2.1131		398	91,500
		2.9598		1.149	91,500
		2.9598	D	365	162
^{72}Ga	14.1 h	1.8611	Be	174	64,900
		2.2016		476	64,900
		2.5077		748	64,900
		2.5077	D	140	25,100
^{76}As	26.3 h	1.7877	Be	109	3,050
		2.0963		383	3,050
^{88}Y	107 d	1.8361	Be	152	229,000
		2.7340		949	229,000
		2.7340	D	253	160
^{116m}In	54.1 min	2.1121	Be	397	15,600
^{124}Sb	60.2 d	1.6910	Be	23	210,000
^{140}La	40.3 h	2.5217	Be	760	10,200
		2.5217	D	147	6,600
^{144}Pr	17.3 min	2.1856	Be	462	690

Photo neutron sources require special handling techniques due to the high γ-ray activities that are present. For a neutron yield of 10^6 a γ-ray activity of approximately 10^{12} Bq is required. Secondly, photo neutron sources are relatively short lived, and thus would usually require the operating facility to be close a reactor where the sources are produced. Lastly, in experiments where it is essential to have only neutrons, the high γ radiation background will interfere with measurements.

γ-ray emitting sources are produced by thermal neutron activation. The target and source mixtures may be fabricated into spherical or cylindrical dimensions. Below shows a photo neutron source design where the γ-ray emitting core is surrounded by the neutron emitting target. Other photo neutron source designs allow the γ-ray emitting source to separate from the target material, thus shutting off the photo-neutron source like an on/off switch.

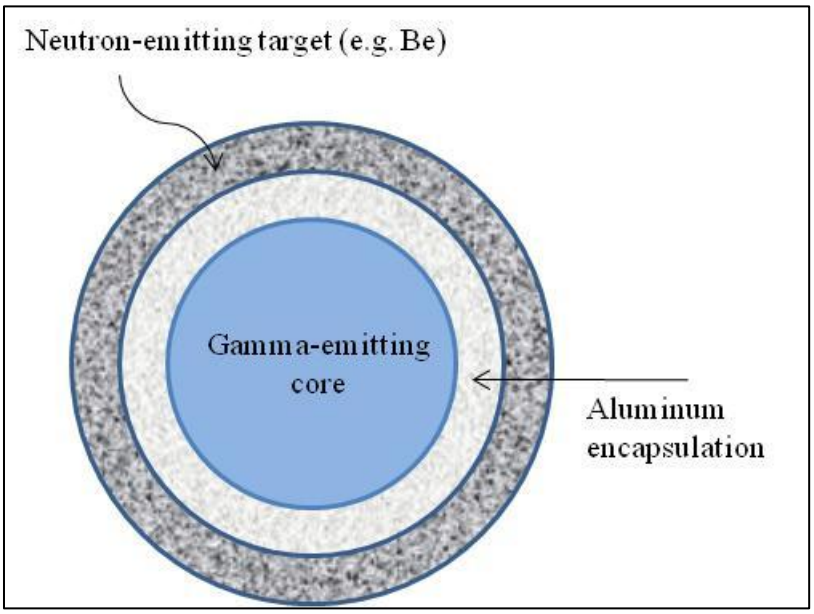

Figure 18: Construction of a simple photoneutron source

1.5. Neutron Detectors

Commonly used thermal neutron detectors use solid, liquid or gas-filled detection material. Thermal detectors take advantage of high probability of reaction at low energies by moderating oncoming neutrons. It is essential therefore, to accommodate the detector with material to thermalize oncoming neutrons. Due to the loss of information of the original neutron energy after moderation, thermal neutron detectors are limited. Therefore the information that is collected refers to the number of neutrons detected and not the energy of the incident neutrons. Neutron detection is based on indirect methods. In order to detect neutrons, the neutral particle must interact with various nuclei first. For this reason the cross section of the target material should be as large as possible. Moreover the element should be of high natural abundance, or be economic to produce artificially. In the following section, gas filled tube and scintillation detectors are discussed.

In a generic radiation detector, an electric charge is observed within a detection volume subsequent to any radiation interaction. The common detector is designed to record the quantities of charge. Commonly used detectors use gas filled tubes as the active volume for the neutron detection. The neutron interaction creates an opposite charged particles (electrons and ions). An electric field is applied to the detector and an anode and cathode is created within the detector. The negative charges flow to the anode end of the detector, while the positive charges flow to the opposite end of the cathode. The collection time of these charges depend on the type of detector. The charges cause a burst of current to be observed by the detector system. The time integral of the total charge is proportional to the energy deposited in the detector. This detector operation is

known as a pulse mode, in contrast to current mode operation, and is often used for neutron detectors.

Neutron detectors are based on two principle modes of interaction. Firstly, the neutron may scatter leaving the target nucleus with recoil energy. The recoil nucleus ionizes the surrounding material. The secondary electrons produce a signal, which are collected and processed by the detector system. The second mode of detection is based on absorption of neutrons which may release protons, α–particle, γ-rays, and fission fragments. The distance that is travelled by the reaction products is dependent on detector geometry. If the aim is to capture the full kinetic energy of the products, a sufficient active volume for absorption reaction is a requirement for the detector. The requirement is easily fulfilled with the use of a solid medium capable of neutron detection because reaction products may only travel a fraction of a millimeter within a solid medium. On the other hand, if gas is used the reaction products may travel several centimeters. If the detector is sufficiently sized, then the loss of deposited charge (Q) will be minimized and the detector would be able to discriminate between lower energy deposits such as γ and high energy deposits such as neutrons (secondary charged particles such as alpha, proton or electron).

A typical gas filled detector system is shown in Figure 19. It has a detector casing which is usually constructed of a cylindrical metal case, with electrical connectors on one end. Various metals may be chosen depending on the desired efficiency. A wire that runs along the center of the tube is which could be a few millimeters thick and made of material that offers good conductivity and tensile strength.

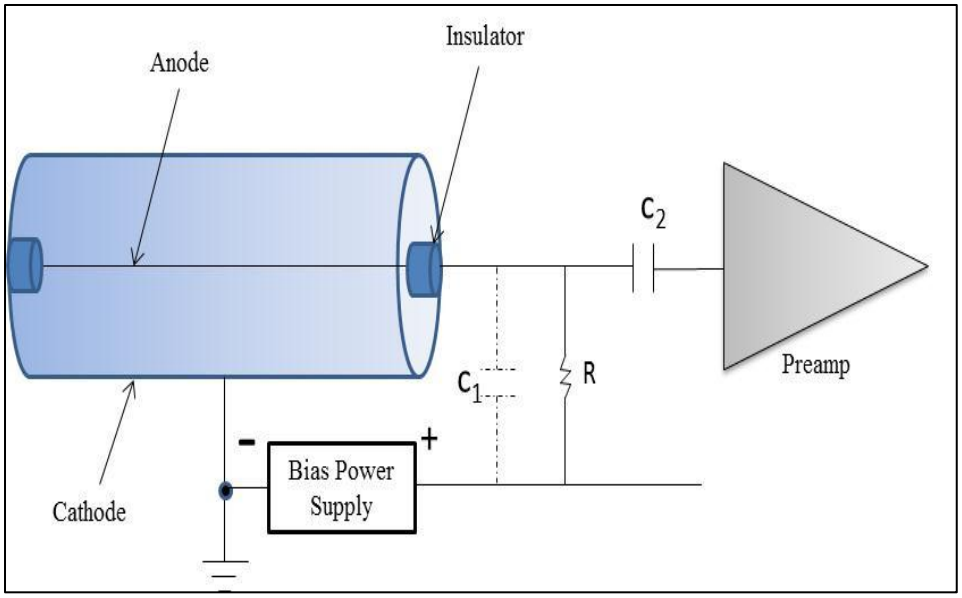

Figure 19: Typical gas filled neutron detector

Neutron interactions within the active gas volume create secondary particles as shown below:

$$_{5}^{10}B + _{0}^{1}n \rightarrow _{3}^{7}L + _{2}^{4}\alpha + Q$$

The secondary charged α-particle will travel across the volume exciting atoms of the gas along its path and separating the gas into their ion pairs. A voltage applied to the central wire causes the electrons to move to the anode (wire) and the positively charged ions to drift to the cathode (wall) of the detector. The distance that is travelled by the reaction products is dependent on detector design. The electrons will be collected to produce a signal, whose amplitude depends on the applied voltage, the dimensions of the detector, and the gas within the detector. Variations of these parameters will determine if the detector will operate in ionization region, proportional region, or Geiger Mueller region.

In the ionization region, there is low voltage applied in order to collect the ion pairs before they can recombine. The ion pairs produce a charge which is collected by the detector system. The

charge is proportional to the energy that is deposited in the gas. This operation of the detector is known as an ion chamber.

If increased voltage is applied to the central wire it may create an electric field sufficiently large to cause primary electrons which ionize the gas molecules to create further ionizations in the volume of the detector. If the electric field is increased the secondary electrons will induce further ionization of the gas molecules. The amplification is the number of induced ion pairs from a primary single ion pair. The total amplification is proportional to the electric field that an electron travels. Since the detector is cylindrical, the electric field becomes stronger closer to the anode wire. Therefore most of the amplification occurs near the anode allowing the collection of the electrons to be relatively short compared to the positive ion's drift time due to its traversed distance to the cathode wall. The pulse that is generated has a fast initial rise time because of the distances traversed by the electrons and a subsequent slower rise time because of the positive ions relatively long drift towards the cathode wall. The pulse can only reach full amplitude when all the positive ions are collected. A detector that operates in this region is known as a proportional counter, whose charge collected is proportional to the energy deposited within the gas. Gas filled neutron detectors which operate in proportional region usually contain BF_3 gas ^{3}He gas (Crane, Accessed 2011)

BF_3 neutron proportional counters operate based on the reactions shown in equation 14.

$$\begin{aligned} {}^{10}_{5}\boldsymbol{B} + \boldsymbol{n} &\rightarrow {}^{7}_{3}\boldsymbol{Li} + {}^{4}_{2}\boldsymbol{\alpha} \quad (\mathbf{1}) \\ {}^{10}_{5}\boldsymbol{B} + \boldsymbol{n} &\rightarrow {}^{7}_{3}\boldsymbol{Li}^{*} + {}^{4}_{2}\boldsymbol{\alpha} \quad (\mathbf{2}) \end{aligned} \tag{14}$$

$$\mathbf{E_{Li} = 0.84\ MeV} \qquad \mathbf{E_{\alpha} = 1.47\ MeV}$$

7% of the reactions follow channel 1 leading ^{7}Li to a ground state and product energy of Q=2.79 *MeV*. From the reactions above, 93% of the reactions follow channel 2 leading to ^{7}Li to an excited state and product energies of Q= 2.31 *MeV*, where the Q energy is shared amongst the product.

^{3}He neutron detectors are also used for detection of thermal neutrons, and are coupled with a neutron moderator to thermalize fast neutrons. Ease of use, non-toxicity, and higher sensitivity to neutrons when compared to BF_3 detectors are the reasons ^{3}He have found its use across various applications such as portal monitors, medicine, and cryogenics.

^{3}He proportional counters are based on reactions shown in equation 15.

$$\begin{gathered} {}^{3}_{2}He + n \rightarrow {}^{1}_{1}H + {}^{3}_{1}H + Q \\ \mathbf{E_p = 0.573\ MeV \text{ and } E_T = 0.191\ MeV} \end{gathered} \tag{15}$$

The products of the reaction carry a kinetic energy of Q = 0.764 *MeV*. The physics of the two proportional detectors are similar. However due to the properties mentioned above, the ^{3}He detectors have historically been the preferred choice of neutron detectors.

Currently, within the United States of America Helium-3 is mainly produced by the U.S. federal government who manufactures and produces tritium which decays into ^{3}He. Historically the supply for ^{3}He has outweighed the demand. In 1990 the helium stockpile grew from 140000 liters to 235000 liters in 2001(D.A Shea, 2010). After the terrorist attacks of September 11, 2001, the U.S. federal government began to deploy neutron detectors across the nation's borders in order to

help prevent the smuggling of radiological material. The demand of helium has since sharply increased (Figure 20). Higher demand of the ^{3}He isotope quickly resulted in annual demand exceeding the annual production of helium supply. By 2010, the stockpile of helium supply within the United States had decreased to 50,000 liters (D.A Shea, 2010).

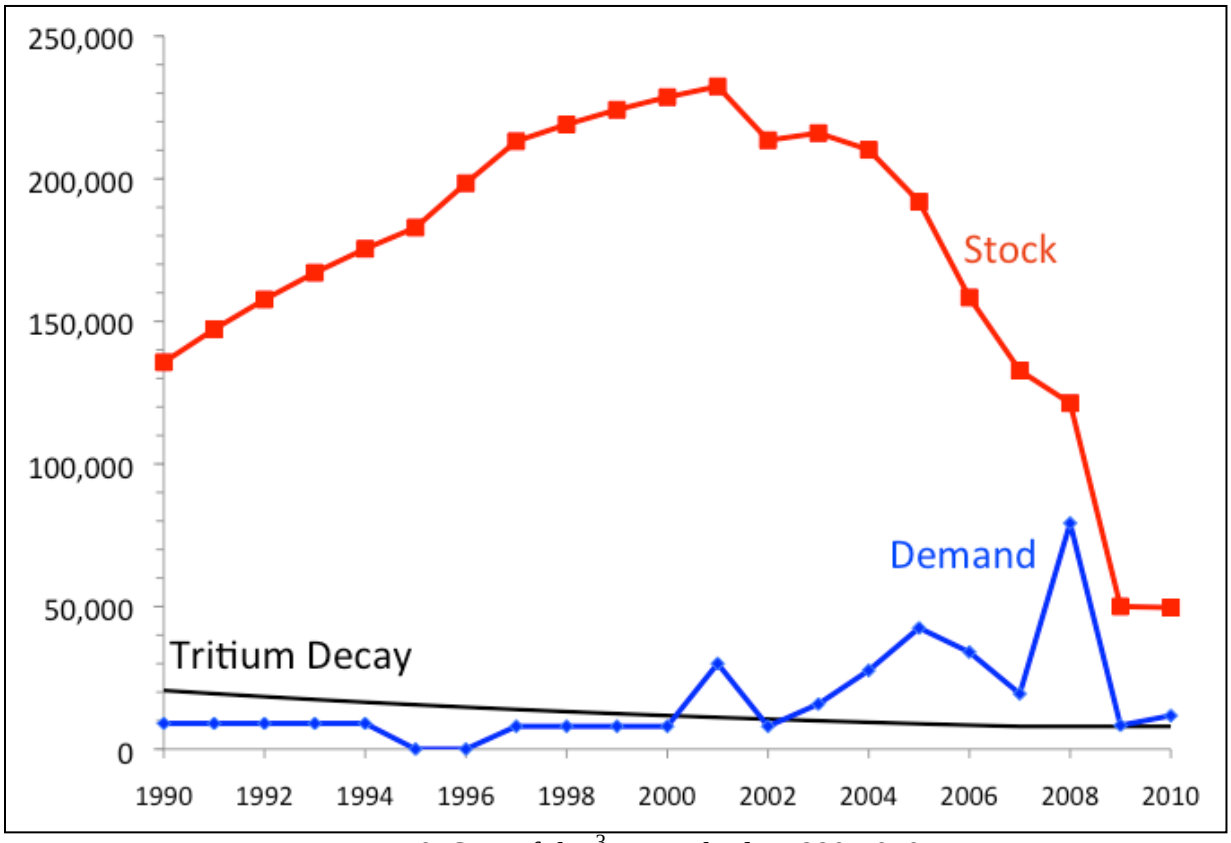

Figure 20: Size of the ^{3}He stockpile, 1990-2010

Source: Adapted from Steve Fetter, Office of Science and Technology Policy, "Overview of Helium-3 Supply and Demand," presentation at the American Association for the Advancement of Science Workshop on Helium-3, April 6, 2010.

Neutron detectors based on using crystal scintillators are currently being investigated as an alternative to the traditional gas filled ^{3}He neutron detectors. Neutron detection in a scintillator is based on indirect methods which use a crystal as a sensor to produce light pulses. Scintillation is based on the energy levels which depend on the crystal lattice of the material. The low,

intermediate, and high energy bands in the lattice are called valence, forbidden and conduction bands respectively. Forbidden layers are energy states in pure crystals in which electrons are never found. Valence bands cause the electron to become essentially bound to the lattice of the crystal.

A nuclear reaction is required between an incident neutron and the crystal target thereby releasing a charged particle. A charged particle with sufficient energy may excite an electron and elevate it into the conduction band. The electron leaves a hole in the valence band and is free to migrate within the conduction band (Figure 21). In a pure crystal the de-excitation of the electron from the conduction band to the valence band, which causes an emission a photon, is of low probability. Also this emission of photon would not be visible due to the typical high energy differences between the bands' gap. Therefore small amounts of impurity are added during the growth of the crystals in order to create special sites in the lattice called activators. As a result the excited electron can migrate into the special sites which are situated in the forbidden gap, from which the electron can de-excite and causing a visible photon to be released.

An ideal scintillation material should possess the following properties (Knoll, 1989):

1. It should convert the kinetic energy of charged particles into detectable light with high scintillation efficiency.
2. This conversion should be linear-the light yield should be proportional to deposited energy over as wide a range as possible.
3. The medium should be transparent to the wavelength of its own emission for good light collection.
4. The decay time of the induced luminescence should be short so that fast signal pulses can be generated.
5. The material should be of good optical quality and subject to manufacture in sizes large enough to be of interest as a practical detector.

6. Its index of refraction should be near that of glass (- 1.5) which is matched to the index of refraction of the PMT glass to permit efficient coupling of the scintillation light to a PMT.

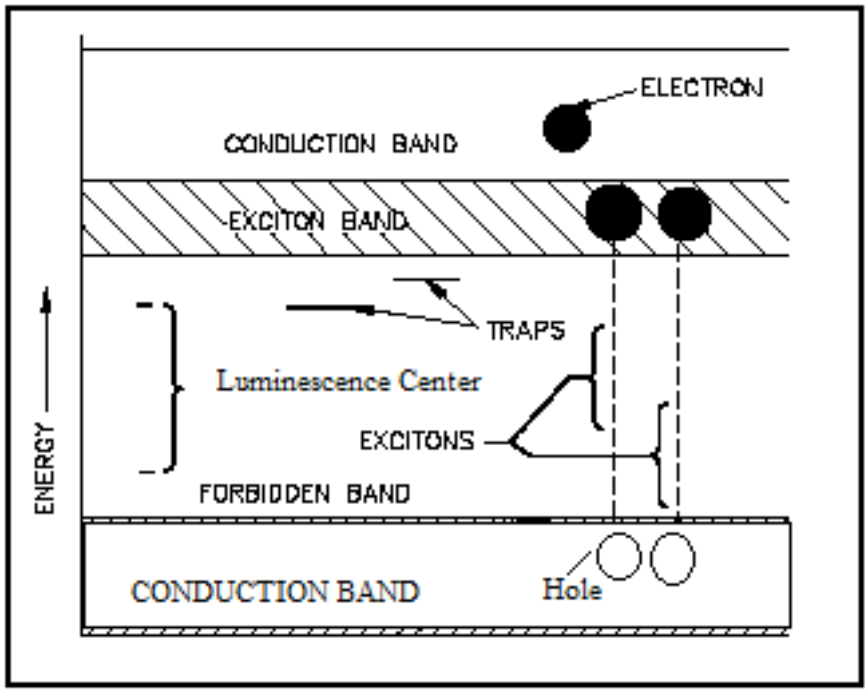

Figure 21: Scintillation mechanism in activated crystals

The visible light is converted into a current using a PMT. The PMT is a vacuum tube with an electron rich entrance known as a photocathode, and a series of dynodes. The visible light which is released due to scintillation strikes the surface of the photocathode and subsequently liberating electrons in the rear side. An applied voltage across the dynodes causes electron attraction towards the first dynode. The collisions with the first dynode result in more produced electrons. The second generation of electrons is attracted towards the second dynode. This process continues with approximately 10 dynodes in a typical PMT. Subsequent to the electron amplification in the final dynode, sufficient electrons are present to form a voltage pulse which is proportional to the deposited energy in the detector medium.

Some of the standard thermal neutron scintillators used in industry are shown in Table 5. They provide good neutron sensitivity and good resolution to thermal neutrons. The crystals can be enriched to various degrees in the purity. The cost of the crystal increases as the enrichment is increased. Their sizes can also be varied, and the cost of the crystal increases for larger crystals. They can easily be assembled with a hydrogenous material such as paraffin to detect fast neutrons after moderation. Their ease of production, operation and portability make it an ideal choice for thermal neutrons.

Table 5: Thermal neutron scintillators most commonly used and under test combinations (van Eijk et al., 2004)

Host	Dopant (conc. mol %)	Light yield photons per Neutron	*MeV* gamma
^{6}Li glass	Ce	~6000	~4000
^{6}LiI	Eu	50000	12000
^{6}LiF/ZnS	Ag	160000	75000
$LiBaF_3$	Ce,K	3500	5000
$^{6}Li^{dep}Gd(^{11}BO_3)_3$	Ce	40000	25000
$Cs^{6}LiYCl_6$	Ce (0.1)	70000	22000
$Cs^{6}LiYBr_6$	Ce (1)	88000	23000

Chapter 2

Methodology Description

2.1 General Description of Methodology

As mentioned in the introduction this work aims to investigate the feasibility of a dual neutron and gamma detector based on a single crystal and to evaluate its ability to detect thermal neutrons and gamma-rays from natural sources of radiation which generally range between 0-3 *MeV*, having thorium being the highest energy at 2.6 *MeV*. This was achieved utilizing LiI (Eu) scintillating crystals. The rationale for the selection of the crystal is described below in section 2.2. To build the system, a photomultiplier (PMT) was requested from Hamamatsu Company to match the optical proprieties of the LiI (Eu) crystal in term of emission spectra. Further information on the PMT selection is described in Chapter 3. The crystal was manufactured by Kharkov Institute of Physics and Technology in Ukraine while the data acquisition system has been assembled by Bridgeport Company. All parts of the DAQ system along with the crystal were put together and taken to the UOIT neutron facility in order to perform different experiments with neutron as well as with gamma sources. Before carrying out the experiment and to optimize the crystal size to cover the above mentioned gamma energy range, a Monte Carlo calculation has been performed. However, the need of the experimental value of the detector resolution was required as an input parameter to the Monte Carlo code. Without a resolution input parameter, the simulation would only give a delta peak. Therefore, we have measured the pulse height spectra with crystal of ϕ11x6 mm to get the resolution of the detector (See section 4.1.). However, due to the small crystal size, we were unable to distinguish gamma ray energies higher than 1 *MeV* (very low resolution). Thus, after consulting with the manufacturer the largest LiI(Eu) crystal available was

ϕ 25x10 mm and it has been used further in the simulation as well as in the rest of the experiments.

2.2 Detector and Mixed Neutron Gamma Field

Neutron and γ radiation detection is basically dependent on the signal responses generated after the interaction between the sensor medium and incoming particle. Neutron and γ-rays are unable to produce any response directly because they are uncharged particles. If the primary interaction between the uncharged radiation and the detector does not occur, the radiation will pass through the detector without any indication that the radiation was present. Therefore secondary particles generated from interactions between the sensor and incident particles are necessary in order to achieve detection for the latter.

The LiI crystal has a high thermal neutron cross section, and a low cross section for epithermal to high energy neutrons. Therefore a moderating material was utilized in order to bring the neutrons into a thermal energy range. Further discussion about the moderator selection can be found in Chapter 3: Experimental Setup.

Table 6: Secondary Charged Particles Relased in LiI(Eu) Crystal

Uncharged Radiations Interaction with LiI	Emitted Charged Particulate Radiations
Neutron	Alpha Particle (and ^{3}H)
Gamma Ray	Fast Electrons

In contrast to the neutron interaction with matter, fast electrons and α-particles are charged with a

negative and positive charge, respectively, therefore they interact with the electrons of the LiI crystal as they pass through the crystal. Due to their coulomb force they will partially or completely transfer their energies to the orbital electrons. The response will be unique to each charged particle due to the mechanism in which they transfer energy. Below will be a discussion on major mechanisms which cause the loss of energy of α-particles, and fast electrons as they interact with LiI(Eu) detector.

The following reaction is likely to occur assuming that neutrons have already been thermalized, and are incident upon the LiI crystal:

$$\boldsymbol{n + {}^{6}_{3}Li \rightarrow {}^{4}_{2}\alpha + {}^{3}_{1}H + 4.78\ MeV}$$

Where the Q -value is shared amongst the products of the reaction: tritium (T) and alpha particle with the energy E_T = 2.73 *MeV* and E_α=2.05 *MeV*, respectively. The α-particle is considered heavy particle due to the mass of its nucleus. It has two neutrons and two protons tightly bounded together in the nucleus and resembles a helium atom but has a charge of +2 due to the lack of valence electrons. The positive charge makes the interactions possible with the electrons within the crystal. The α-particle will simultaneously interact with all the electrons in the vicinity of its path. These electrons will feel an attraction due to coulomb forces. The amount of force applied will depend on the distance between the interacting particles and the time of the interaction. The interaction between the charged α-particle, and an electron of the sensor molecules, will cause the electrons of the crystal to become excited or ionized. The excitation of the electrons will cause the electrons to elevate into the conduction band of the crystal. The excited electrons leave holes in

the valence band and are free to migrate within the conduction band. During the growth of the LiI crystals small amount of europium impurity is added in order to create activator sites between the valence band and conduction band. As a result the excited electron can migrate into the activator site which is situated in the forbidden gap, from which the electron can de-excite subsequently causing scintillation or visible photon to be released.

As α-particle passes through the LiI (Eu) crystal, it will gradually lose energy in small steps. Therefore the energy that is gained by the electrons is compensated by the loss of energy of the α-particle. The definition of stopping power (S) is the average energy loss of the particle per unit path length and usually measured in *MeV*/cm or *MeV*cm^2/g. The stopping power is dependent on composition of the LiI (Eu) crystal and the mass, energy and charge of the incident particle. It is proportional to the number of interaction that occurs within the volume and is written as follows:

$$\mathbf{S} = -\frac{\boldsymbol{dE}}{\boldsymbol{dx}} \tag{16}$$

Where E = Energy (eV)

x= traversed distance traversed along particle path (mm)

The stopping power can be generally regarded to follow $\frac{\mathbf{1}}{\boldsymbol{v^2}}$ trend, where *v* is the velocity of the particle. Therefore, as the α-particle loses energy while moving along its path, the rate of energy loss will increase. This trend can be explained because as the α-particle slows down, it will spend a longer time within the vicinity of the electrons, and therefore the rate of interactions will increase. It is important to note that as the α-particle nears its end of track it will lose its kinetic

energy at a high rate while absorbing free electrons into its electron shell subsequently becoming a neutral particle. At this moment the stopping power is at the highest value and is known as the Bragg peak. The plot of energy loss of the α-particle along its track path can be described by the Bragg curve.

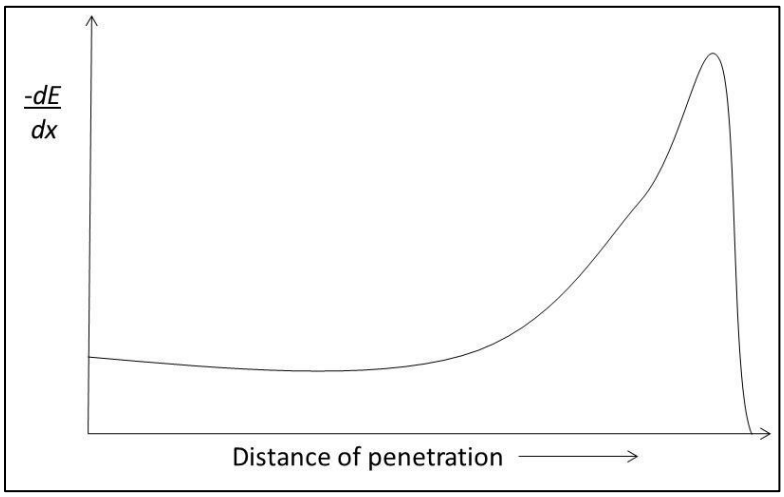

Figure 22: Bragg Curve along an alpha track

Gamma ray detection on the other hand is based on γ-ray energy transfer to electrons or to the nucleus. This reaction is described by Compton effect, photoelectric effect and pair production as discussed in Chapter 1. The fast electron will encounter the electrons of the LiI (Eu) crystal and cause a force of repulsion with the electrons in its vicinity. Due to the relative smaller mass, charge and velocity of the electron with respect to alpha particle, fewer electrons will be in the vicinity of the interaction. Due to the lower number of interaction occurring per electron, electrons are able to travel further into the crystal before coming to a stop. Each interaction with sufficient energy will initiate the scintillation process similar to that found in α-particle interaction with the crystal.

In the past, a number of models to explain the luminescent process in crystals have been put forward. Murray and Meyers have suggested a model which says the energy transfer from the beginning of the track of the ionizing radiation is due to the formation of excitons (bound electron-hole pairs). It says the number of recombination of n_e pairs of particles (per unit path length) in the wake of an incident particle produces a number of energy carriers n_o, (Meyer et al., 1961).

$$\boldsymbol{n_o = \frac{\alpha {n_e}^2}{1 + \alpha n_e}}$$

Where α is a recombination parameter.

Eaton et al. show that the total light output from the particle E can be written as follows (Eaton et al., 1964):

$$\boldsymbol{\varepsilon E = \int_0^E \frac{dL}{dE}(E)dE = KP \int_0^E aK \frac{dE}{dx}(E)\left[1 + aK \frac{dE}{dx}(E)\right]^{-1} S(aK, E)dE} \quad (17)$$

Where, ε is the luminescent efficiency for the particle of energy E.

K is a constant relating the ion pairs produced per unit length to the crystal

$\boldsymbol{\frac{dE}{dx}}$ is the stopping power and

a is parameter that is inversely proportional to the probability of electron trapping.

$\boldsymbol{\frac{dL}{dE}}$ is the light output per unit energy loss

$\boldsymbol{S}$ is the probability of an exciton being captured by a luminescent center

P is the probability of radiative transition at the luminescent center.

Typical excitation energy required for scintillation in a generic material are between 20 – 500 eV

(Spieler, 2002). Experiments show that LiI doped with approximately 1% Eu shows a light output of $14x10^3$ photons/*MeV* with a decay of 300 ns (Tavernier, 2010). The decay parameter is dependent on the half-life of the electron while in the luminescence region. These findings are comparable to other experiments which show light output for gamma rays and neutron to be, $12x10^3$/*MeV* and $50x10^3$/neutron. Using the total light output ratio, the number of photons can be determined, given the energy of the gamma of interest. i.e. light output for gammas are shown in the following calculation.

$$For\ gamma: \frac{\boldsymbol{Mev}}{\boldsymbol{\gamma}}\ \boldsymbol{x}\ \frac{\boldsymbol{12000\ photons}}{\boldsymbol{Mev}} = \frac{\boldsymbol{12000\ photons}}{\boldsymbol{\gamma}}$$

$$For\ neutron: \frac{\boldsymbol{50000\ photons}}{\boldsymbol{neutron}}$$

These photons mainly fall onto a photosensitive screen called the photocathode. The photocathode is an electron rich material that releases negatively charged photoelectrons as a result of the interactions with the attenuated photons. Electrons are attracted to a positively charged electrode, thereby causing a release of more electrons i.e. multiplication of electrons is observed. These electrons continue towards the next electrode, and a similar reaction takes place causing even more electron release. The photomultiper tube consists of many electrodes where electron amplification takes place in order to create an electrical pulse also called the signal. The magnitude of the signal is the ratio of excitation energy to absorbed energy as shown below:

$$\boldsymbol{Magnitude\ of\ signal} = \frac{\boldsymbol{absorbed\ energy}}{\boldsymbol{excitation\ energy\ for\ scintillation}} \quad (18)$$

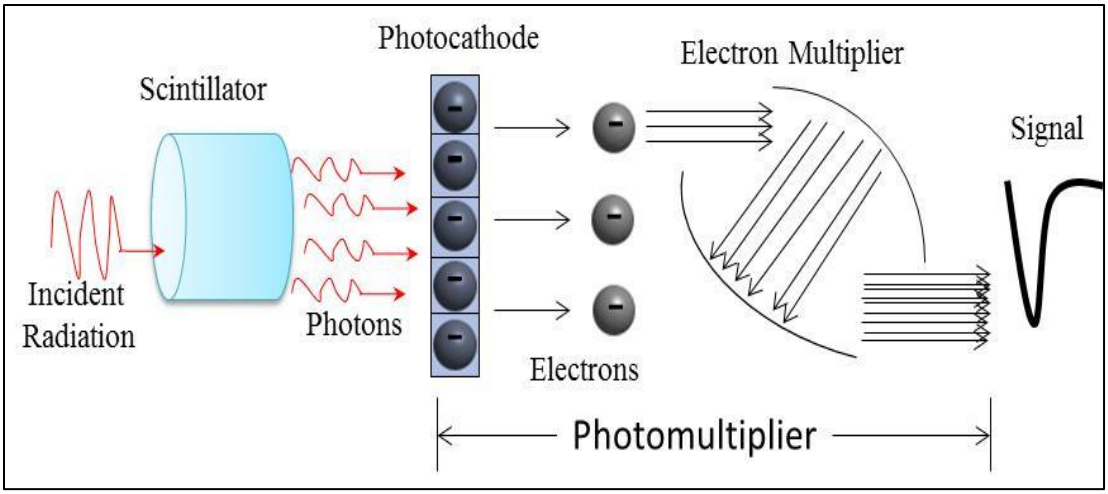

Figure 23: Simplified process of signal generation in scintillating radiation detectors

The amplitude and shape distribution (i.e. photo peak, Compton distribution, and backscattering) of the signal carries with it the information about the incident radiation. Therefore a unique signal is expected from γ-ray and neutron sources due to the interactions which emit secondary particles of different energies, sizes, and charge. A description of the detector system as well as the necessary components required to process the signal that is acquired from the scintillation process will be described in section 3.2.

2.3 Monte Carlo Simulation

The Monte Carlo method was developed at Los Alamos National Laboratory during the Manhattan Project in the early 1940s. This method is often used to perform radiation transport calculations. MCNP (Monte Carlo N-Particles) is a general-purpose Monte Carlo radiation transport code for modeling the interaction of radiation with different materials. The code can perform coupled neutron-photon-electron transport calculations. In our case it has been used to model the LiI(Eu) detector and to simulate its response function to gamma radiation.

2.3.1. Detector Model

To write a proper code in MCNP it requires the specific parameters and data to be written into the input file. The input file contains information about the problem, including the geometry specification; the description of materials and selection of cross-section data used in the calculation; the location and characteristics of the source; the type of output data or "tallies" desired; and any variance-reduction which is a technique to increase precision given a certain amount of iterations.

The setup of the detector is presented in Figure 24.

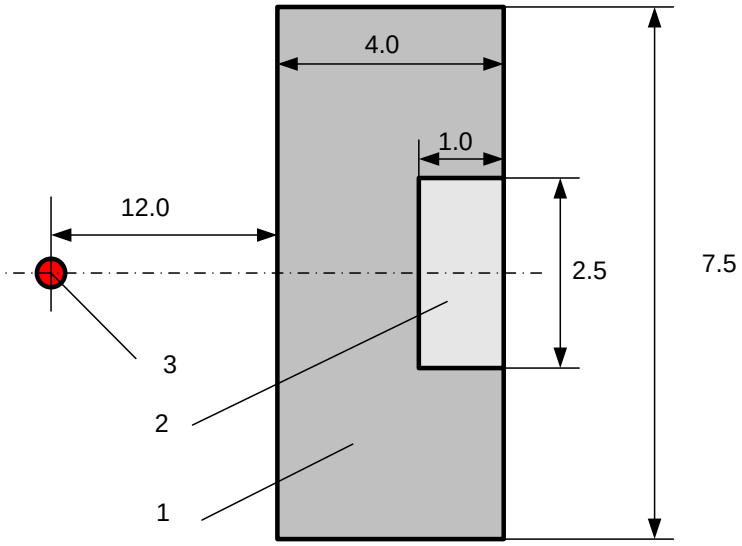

Figure 24: Monte Carlo model of the LiI(Eu) detector with polyethylene moderator
(1-polyethylene cap; 2 -LiI(Eu) crystal; 3-Cobalt- 60 source)
All dimensions are presented in cm

The structure of the input file is shown below:

Data	Description
Geometry specification	The geometry specified for the crystal is cylindrical with a concentric moderator surrounding it. The dimensions can be seen in Figure 24 above.
Materials selection and properties	The model has three material components. First being air gap between the source and detector. The moderator is encasing the detector. And Lastly the Lithium Iodide crystal. The material and composition is shown the tables below. Something worth noting is that we require the materials to have importance for photons as indicated by the suffix (p).
The location and characteristics of the source	The source location is relative to the detector. The source is a cobalt source therefore ERG= d1 and S1= 1.33, 1.17 (in *MeV*). Location of the source was 12 cm away axially. Therefore POS= 12 0 0.
Output desired (tallies)	The tally type required for a pulse height distribution in the cell of the crystal is type F8. A special tally is required for resolution.

Table 7 Input Data for Lithium Iodide Crystal

Material : Lithium Iodide Crystal Density: 4.06 g/cm3	Constituent Element	Cross sectional Data Library	Weight Fraction (%)
	Lithium Iodine Europium	3000.04 p 53000.04 p 63000.04 p	5.1 94.4 0.5

Table 8 Input Data for Moderator

Material : Paraffin Wax Density: 0.9 g/cm3	Constituent Element	Cross sectional Data Library	Weight Fraction (%)
	Carbon Hydrogen	6000.04 p 1000.04 p	74.1 25.9

Table 9: Input Data for Air

Material : Air Density:1.24×10^{-3} $g\cdot cm^{-3}$	Constituent Element	Cross sectional Data Library	Weight Fraction (%)
	Nitrogen Hydrogen Oxygen Argon	7000.04 p 1000.04 p 8000.04 p 18000.04 p	77.08 1.18 21.28 0.46

Along with the executive code, the MCNP Visual Editor is a graphical user interface for the MCNP computer code; it allows the user to create the geometry directly from the plot window. It also provides different views of the geometry including 3D. Figure 25 shows the detector model in the visual editor.

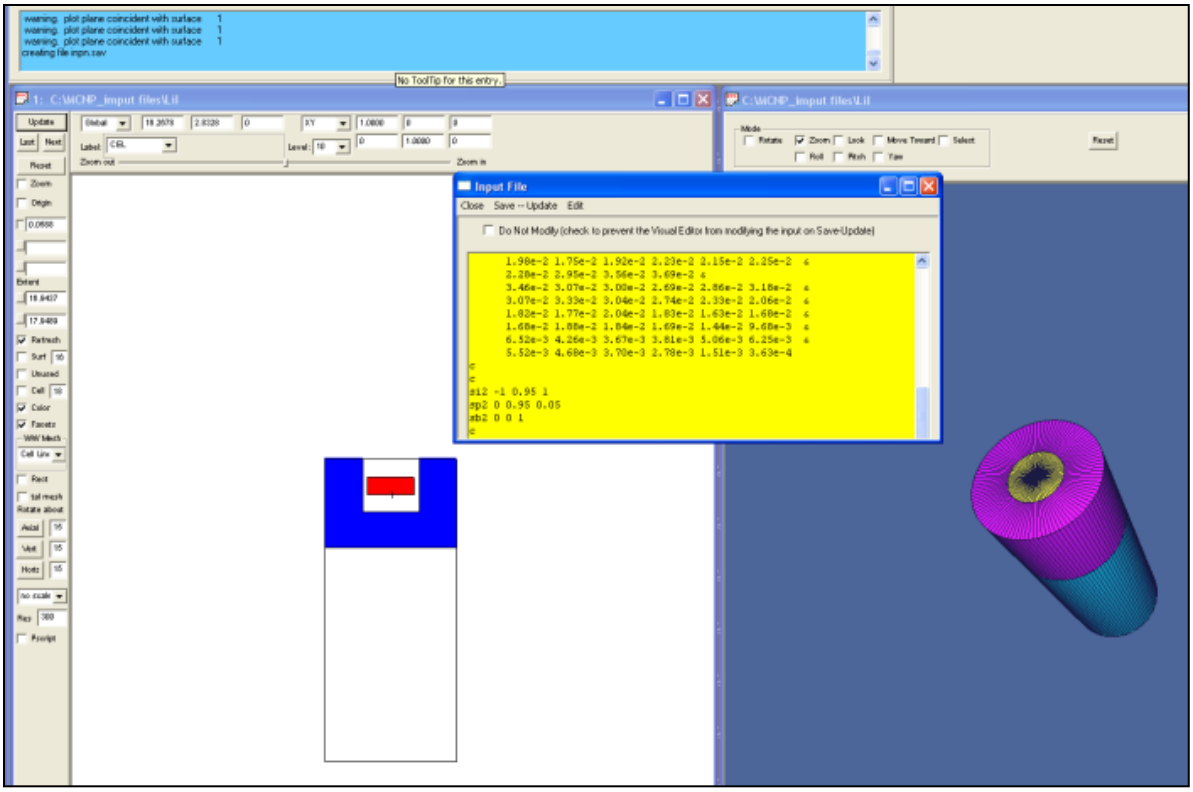

Figure 25: Screen shot of the detector from MCNP visual editor

2.3.2. Detector response function

In the simulation the detector whose dimensions have been described in section 2.3.1, has been placed at 12 cm from the ^{60}Co source and the code has been run for 10^7 particles. The geometry and parameters of the input file were described in the tables 7, 8 and 9. The result of the simulation is shown in Figure 26.

Since the input of the Monte Carlo code required the resolution of the detector as one of its parameters, an experiment has been conducted to measure the resolution of the detector see later in chapter 4. This resolution of 11% has been used in the input file.

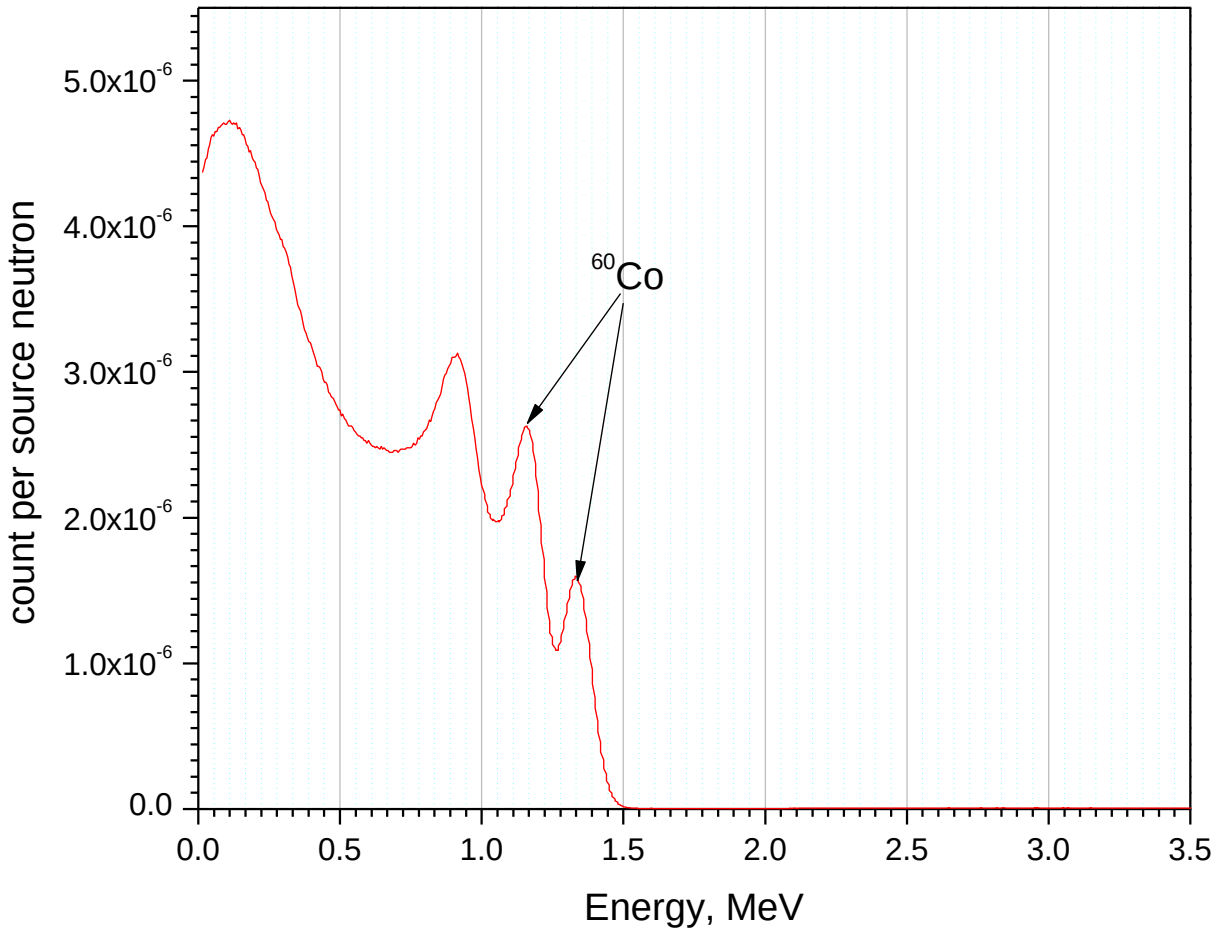

Figure 26: Simulated response function to ^{60}Co of the developed detector

Chapter 3

Experimental Setup

This chapter describes the neutron facility, equipment setup including the assembly procedures are all components required for the detector, and provides the detection principle of the developed detector.

The developed detector consists of an assembly of ^{6}LiI(Eu) scintillation crystal constructed into a cylinder casing and coupled with a photomultiplier (PMT). The PMT serves as an interface between the sensor and the pulse processing electronics. The dual detection process uses the advantage of unique interaction of neutron and γ-ray with the sensor media. When γ-rays and neutron interact with the crystal they generate electron and α-particles, respectively. The latter excites molecules of the media that emit photons of light the number of which are proportional to energy of the energy deposited in the crystal.

The neutron facility described in this chapter is located in the University of Ontario Institute of Technology (UOIT) engineering building basement. The room is adequately designed to house a neutron source in a special shielding. The source is housed within a single room that is caged for safety and security purposes. The neutron facility has an Am-Be neutron source stored in light water tank and can be used when mechanically raised up to a desired level above the water level. The experiments were conducted by placing the detector on a conveyor stand which was operated by the user from outside the cage boundaries.

Since neutrons emitted by the Am-Be source are fast, they need to be slowed down to a thermal energy. A paraffin moderator was designed. The moderator surrounded the detector in order to thermalize fast neutrons prior to contact with the detector face. Various gamma sources were introduced along with the neutron source in order to have mixed gamma and neutron fields.

The following sections of this chapter will review some concepts regarding the interaction between the sources and matter, but more specifically it will discuss the interactions that occur within the detector.

3.1. Description of UOIT Neutron Facility

The UOIT neutron facility has been designed and set up in early 2010. It was utilized to carry out all the experimental work. It is located in UOIT's engineering building in the basement. The basement location serves as an ideal location for research purpose because it is below ground and the concrete walls plus the earth surrounding the facility will provide more than sufficient shielding for neutron and γ-ray radiation. A general view of the facility id shown in Figure 27.

Figure 27: UOIT Neutron Facility

The operation of the neutron source is protected within a locked up secure perimeter within the UOIT neutron facility. The facility is equipped with an automatic controlling system and alarm interlock for safe and secure operation.

The facility consists of radioisotope based neutron sources housed inside a water tank. Water is an excellent source of shielding for the neutrons due to its composition of high concentrations of

hydrogen. The tank can be refilled without changing the shielding integrity using an in/out water circulation system.

The neutron source is based on α-particle induced reactions that occur between ^{241}Am and ^{9}Be. ^{241}Am releases is an alpha emitter and when in close proximity to a suitable target such as beryllium, the interaction occurs and a release a neutron as shown below, where reaction 1 is most dominant.

$$\mathbf{^{4}_{2}\alpha + ^{9}_{4}Be \rightarrow ^{12}_{6}C + n} \quad (\mathbf{1})$$

$$\mathbf{^{4}_{2}\alpha + ^{9}_{4}Be \rightarrow ^{8}_{3}Be + ^{4}_{2}\alpha + n} \quad (\mathbf{2})$$

$$\mathbf{^{4}_{2}\alpha + ^{9}_{4}Be \rightarrow 3^{4}_{2}\alpha + n} \quad (\mathbf{3})$$

For Am-Be source, a neutron yield of approximately 70 neutrons for 10^6 alpha's can be achieved with ^{241}Am as an α-source (K.W. Geiger, 1975). The yield of neutrons is 1 to 2 orders of magnitude greater with α-source, than with a γ-source. Due to the loss of energy of non-interacting alpha's, the problem of background radiation from α-particles does not exist. In the reaction above low energy γ-rays are emitted, and are negligible source of background radiation, although they pose a challenge when discriminating their interactions with the detector from those of the α-particles. Conversely if a γ-ray induced neutron source were used, the high energy large γ-ray background would exist, and pose greater radiation protection concerns. Currently in the UOIT Neutron Facility there are three individual Am-Be sources 40 mCi each. The flux is at a given distance from the source is given as shown in the equation and figure below:

$$\boldsymbol{\phi\left(\frac{n}{cm^2 s}\right) = \frac{120mCi}{\frac{4}{3}\pi r^2} = \frac{120x10^{-3}\frac{\alpha}{s}}{\frac{4}{3}\pi(r)^2}\, x\, 70\frac{n}{10^6\alpha}}$$

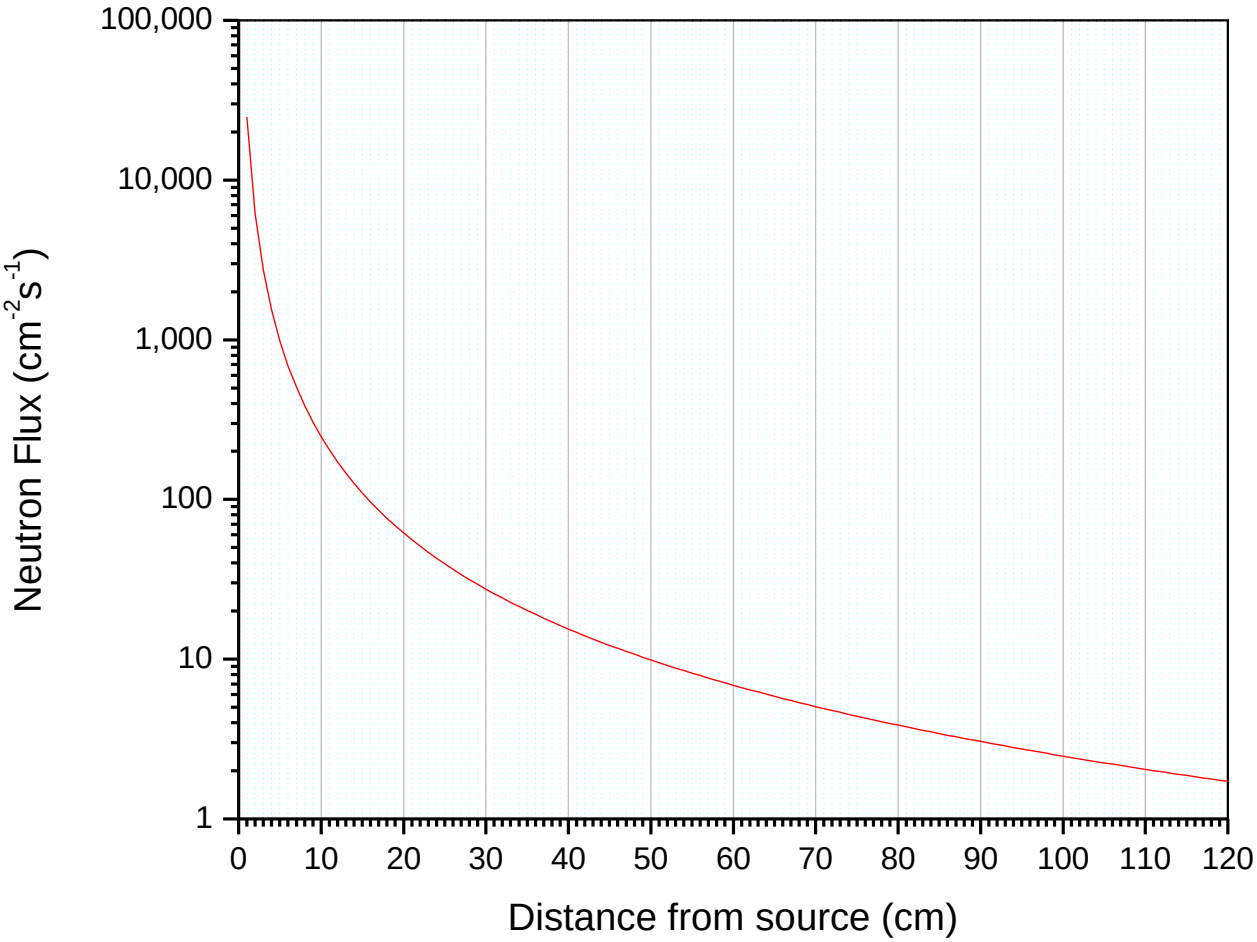

Figure 28: Calculated Am-Be neutron flux at varying distances from the source

A rectangular grid cage provides adequate distance between the operator and source location in order to sufficiently decrease the flux to acceptable levels as per $\frac{1}{r^2}$ law. The tank is located in the

center neutron facility and within its center there are nine vertical aluminum cylindrical rods in a 3x3 configuration (Figure 29). A pulley system which is concentric to each of the rods allows the neutron sources to be raised above the water level when measurements are taken or dropped within the water shielding when necessary (Figure 30). The remainder six of the tubes can accommodate insertion of other sources, small sized detectors, samples or they are used for teaching purposes.

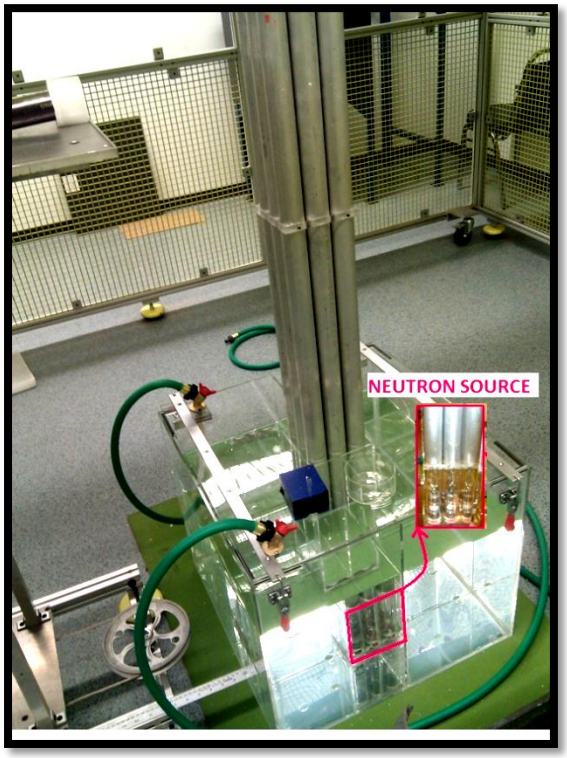

Figure 29: Neutron sources in hollow aluminum cylindrical tubes

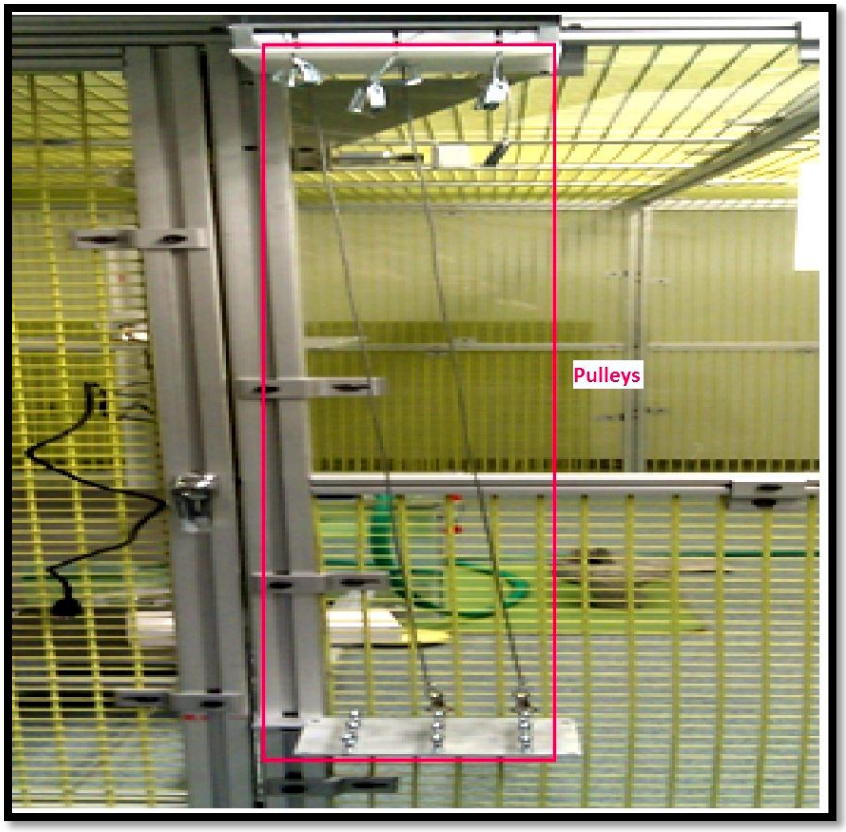

Figure 30: UOIT Neutron Facility source pulley

In order to record measurements, the detector is placed on a manually operated conveyor stand. The conveyor is operated from outside the cage and serves to bring the detectors to desired distance from the neutron source (Figure 31). The detector is placed on top of the conveyor stand (Figure 32) which is connected to a computer via USB to log data in the duration of the experiments.

Figure 31: UOIT Neutron Facility conveyor

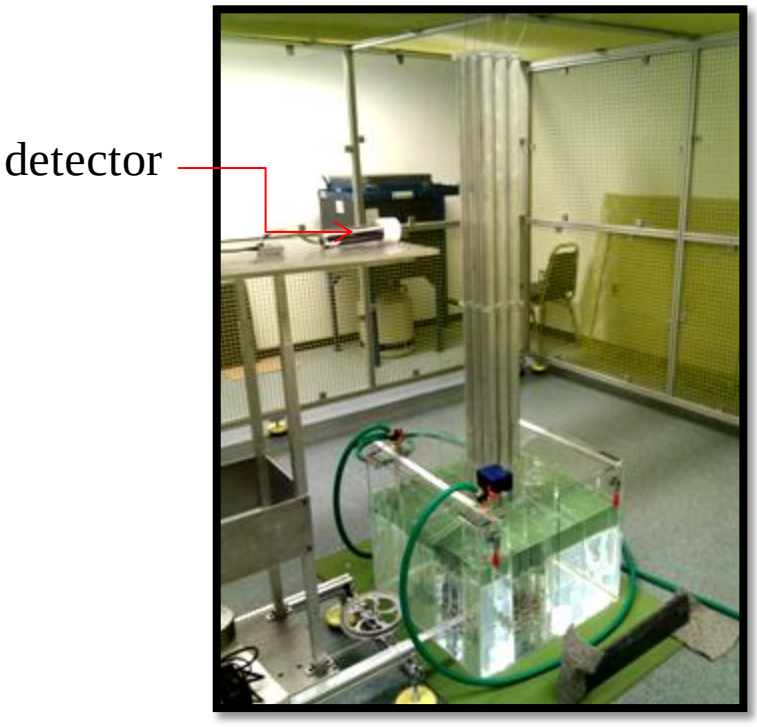

Figure 32: Position of neutron-gamma detector during measurements

3.2. Detector Description and Characteristics

3.2.1. Crystal Description

Europium activated lithium iodide scintillator was used for γ-ray and neutron detection. Neutrons are detected through interaction with ^{6}Li isotope presented in the scintillator, via the following reaction:

$$\boldsymbol{n + {}^{6}_{3}Li \rightarrow {}^{4}_{2}\alpha + {}^{3}_{1}H + 4.78\ MeV}$$

The large cross section for thermal neutron capture (940 barns) gives a high detection efficiency of thermal neutrons on high γ-radiation background. The reaction is exothermic and releases 4.78 *MeV* of energy. The energy of the reaction is distributed between ^{4}He and ^{3}H (Tritium) ions. The scintillation light has a maximum luminescent emission at 470 nm wavelength, and a decay time of scintillation process is 1.4 μs. The density of LiI (Eu) scintillator was 4.06 g/cm^{3}.

The LiI (Eu) scintillator is a very hygroscopic material and has to be used in hermetically sealed assembly. In our case, the LiI (Eu) crystal with 99% of ^{6}Li isotope enrichment had a cylindrical shape with 2.5 cm in diameter and 1 cm length and was packed in an aluminum case.

3.2.2. Photomultiplier (PMT)

The PMT is a 2.5 cm tube in diameter and 6 cm length. The tube has been chosen so that its specifications were to match the emission spectra of the crystal. The Hamamatsu PMT model R3998-02 covers the necessary spectral response in the range between 300 to 650 nm which meets

the range required for the luminescent emission from the crystal. The figure below shows the spectral response as a function of wavelength.

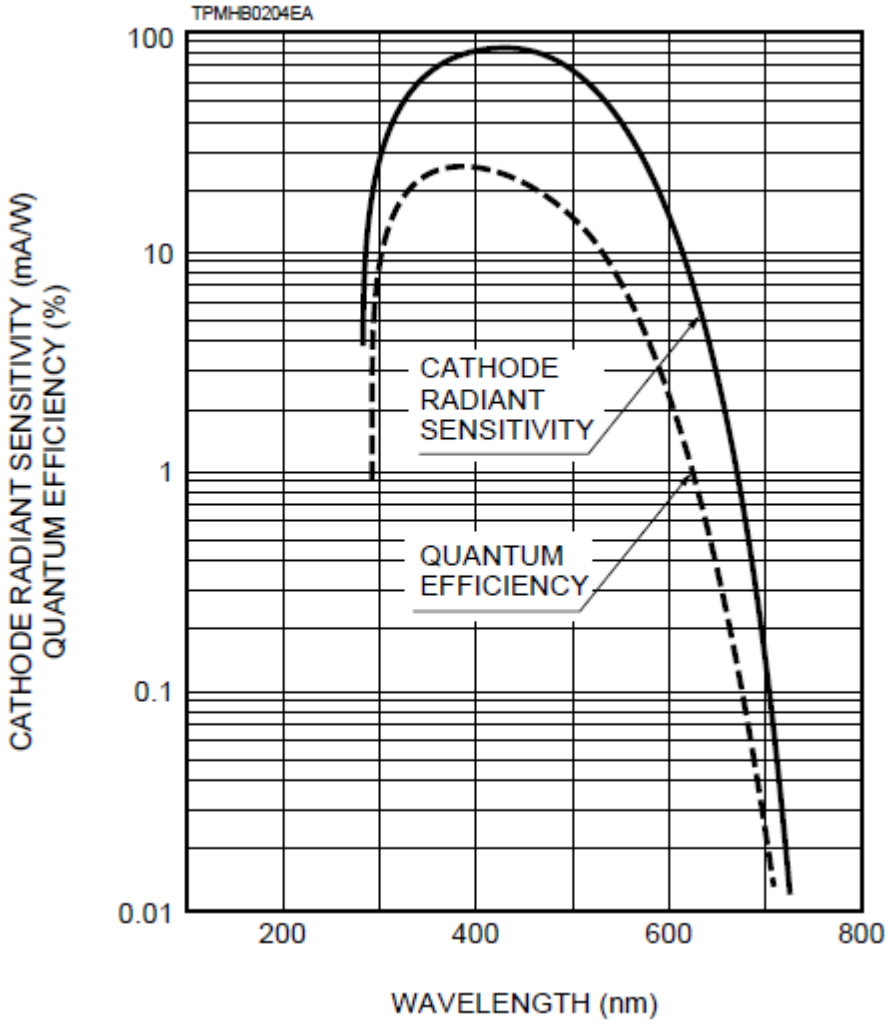

Figure 33: Typical spectral response of PMT

Additional properties of the PMT such as operating voltage, operating temperature etc… are shown below:

Table 10: General Parameters of PMT

Parameter		Description / Value	Unit
Spectral Response		300 to 650	nm
Wavelength of Maximum Response		420	nm
Photocathode Material	Material	Bialkali	–
	Minimum Effective Area	25	mm dia.
Window Material		Borosilicate glass	–
Dynode	Structure	Box(3) and Line(6)	–
	Number of Stages	9	–
Base		14–pin glass base	–
Suitable Socket		E678–14C (Supplied)	–

Table 11: Maximum Ratings of PMT

Parameter		Value	Unit
Supply Voltage	Between Anode and Cathode	1500	Vdc
	Between Anode and Last Dynode	250	Vdc
Avarage Anode Current		0.1	mA
Ambient Temperature		–80 to +50	℃

The PMT has a 14 pin socket which connects to the electronics of the preamplifier. The dimensions in millimeters of the PMT are shown in the figure below:

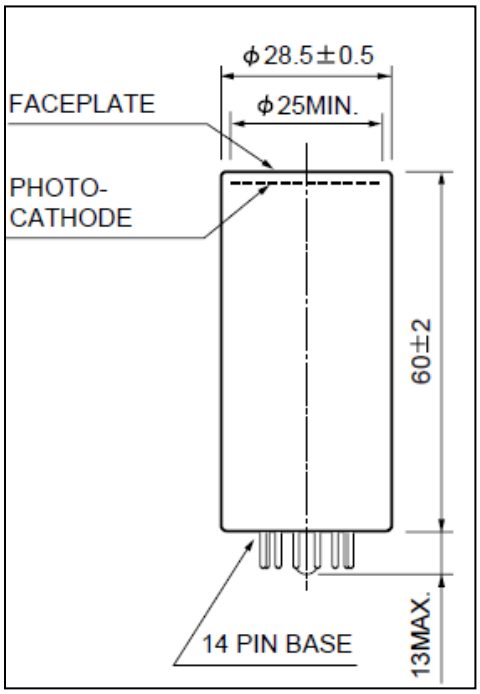

Figure 34: Dimensions of the PMT

3.2.3. Detection Chain

In order to assemble the components of the detector, Eljen optical grade silicone grease was applied to couple the PMT to the scintillating crystal. The grease is a clear colorless optical compound with moderate viscosity but provides excellent transmission of light as shown below in Figure 35:

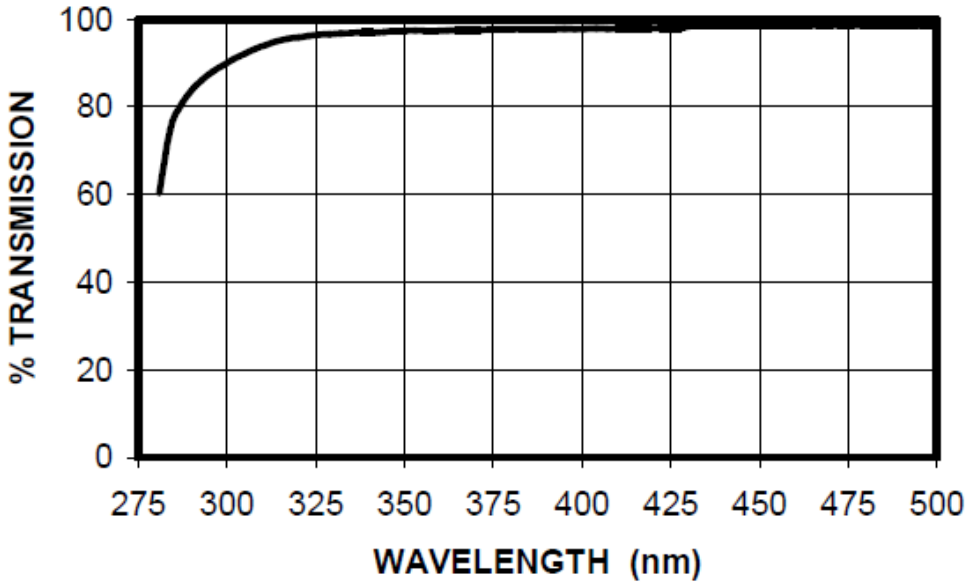

Figure 35: EJ-550 Optical Transmission of 0.1 mm Thickness grease

The detector chain was assembled and connected to data acquisition system. A quality assurance experiment has been carried out with a ^{137}Cs prior to further measurements. The components of the assembly are shown in figure 36 and details of the assembly with the crystal are described in section 4.1.1. and 4.1.2.

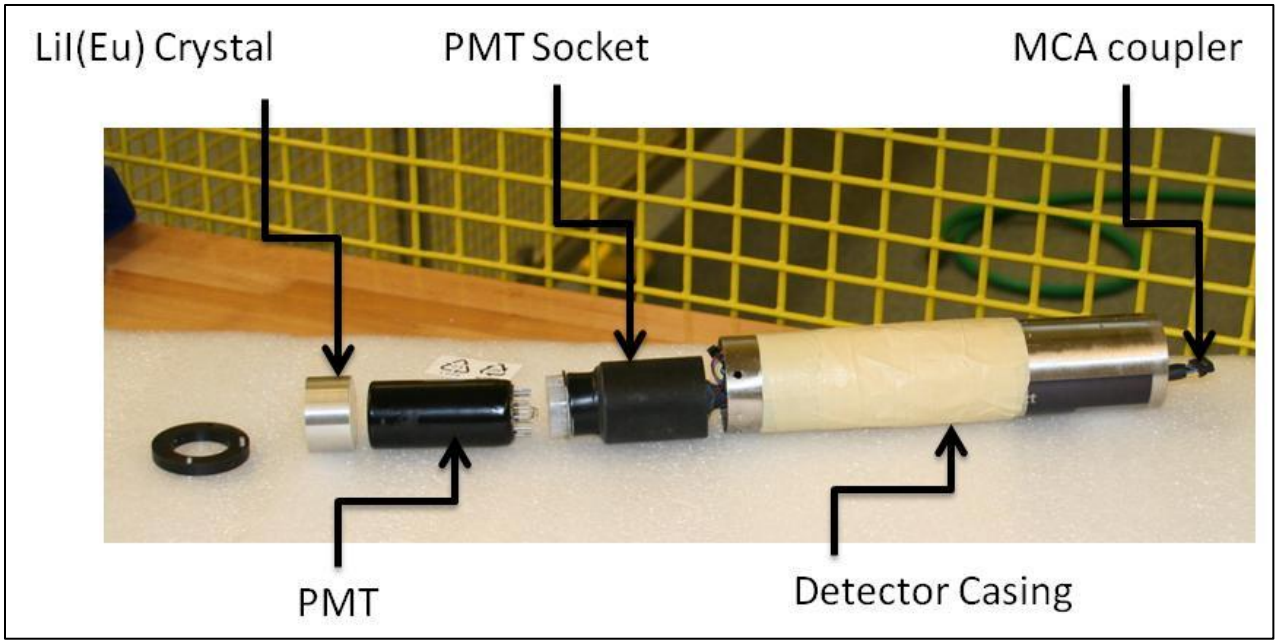

Figure 36: Detector chain

3.3. Moderator Design

The Am-Be neutron source has a hard spectra with an average energy around 5 *MeV*. At this energy the neutron cross section of ^{6}Li is negligible. However the thermal neutron cross section is considerable at 940 barns. Therefore to test the detector, a material was required to moderate the Am-Be neutrons in order to increase the detection efficiency.

In a moderator Neutrons will strike the nucleus and lose energy on an average $\boldsymbol{E_{loss}}$ calculated by the equation below (Rinard, 1991):

$$E_{loss} = \frac{2E_o A}{(A+1)^2} \tag{19}$$

Where A is the atomic weight of the target nucleus,

E_o is the initial energy of the neutron.

The most efficient energy loss of a neutron would be to a very low atomic weight material such as hydrogen, A=1. For example, the Am-Be (5.18 *MeV*) neutrons will lose approximately half (2.59 *MeV*) of its energy, after the first interaction with hydrogen in a front collision. After approximately 33 interactions the neutron comes to a thermal energy of 0.0025 eV (see figure below). Below are some common materials which are used for moderation.

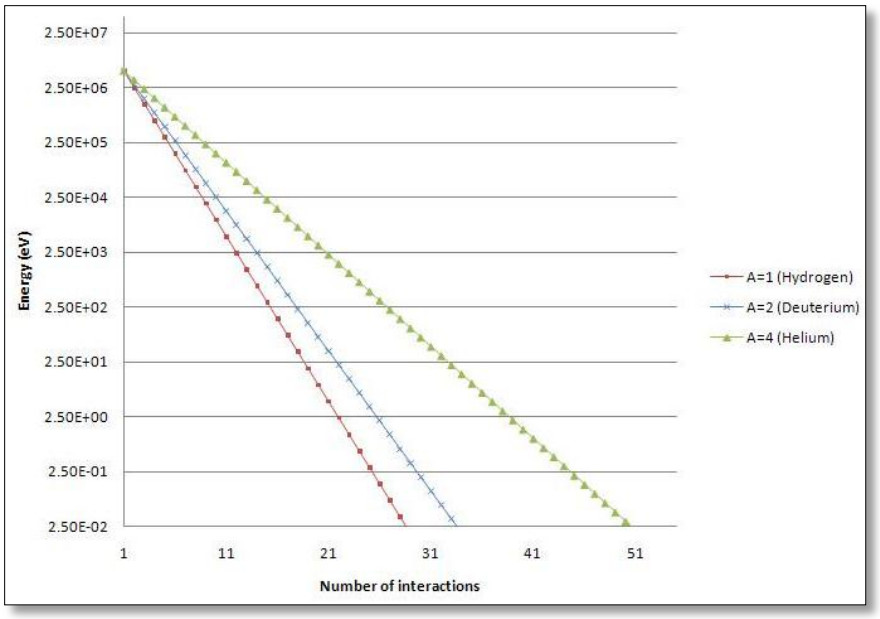

Figure 37: Calculated loss of neutron energy after colliding with various materials

Based on the above calculation, it was recognized that a hydrogenous material would be ideal for the moderation material. A suitable material was determined to be paraffin wax for its high concentration of hydrogen, and its ability to conform into various shapes and sizes.

The appropriate thickness for the moderator requires an assessment of the distance travelled by a neutron from its initial energy to thermal energy.

The spatial distribution of neutrons of energy E_2 which have slowed down from a point source of energy E_1 is of the form $\exp(-r2/4\tau)2$ where τ is referred to as the Fermi Age and is the mean square distance a neutron migrates in slowing down from E_1 to E_2 (M.G. Sowerby). It is given by:

$$\boldsymbol{\tau = \int_{E_2}^{E_1} \frac{DdE}{E\xi\sum_{nn}}}$$

where D is the diffusion coefficient.

The table refers to the age of fast neutron with energy E_1 slowing down to energy E_2 of 1.46 *eV*, which is just above energies of thermal neutrons. It is noteworthy that ^6Li has considerable cross section at this energy, and with approximately 8 collisions, the neutron with E_2 will be thermalized.

Properties of Paraffin:

Material	*Density* 10^3 kg m^{-3}	$\tau/(10^3\ mm^2)$
Paraffin Wax ($C_{30}H_{62}$)	0.89	1.8*

* M.G. Sowerby, R.A. Forrest (Accessed online 2011)

Furthermore, the mean square distance which corresponds to the Fermi age is calculated as follows (Jevremovic, 2009):

$$\overline{r^2} = 6\tau$$

Based on the value of r, a thickness of around 4 cm has been used to moderate neutrons emitted by the source. Since the objective of the moderator was to simply thermalize a sufficient number of neutrons to test the detector, the above dimensions were sufficient for such task.

In order to produce a cylindrical shape to cover the detector, a paraffin block was melted on a stove top and the liquid poured into a cylindrical container. Furthermore a cylindrical hole was drilled into the center of the moderator for detector insertion. The following figure shows a schematic of the moderator:

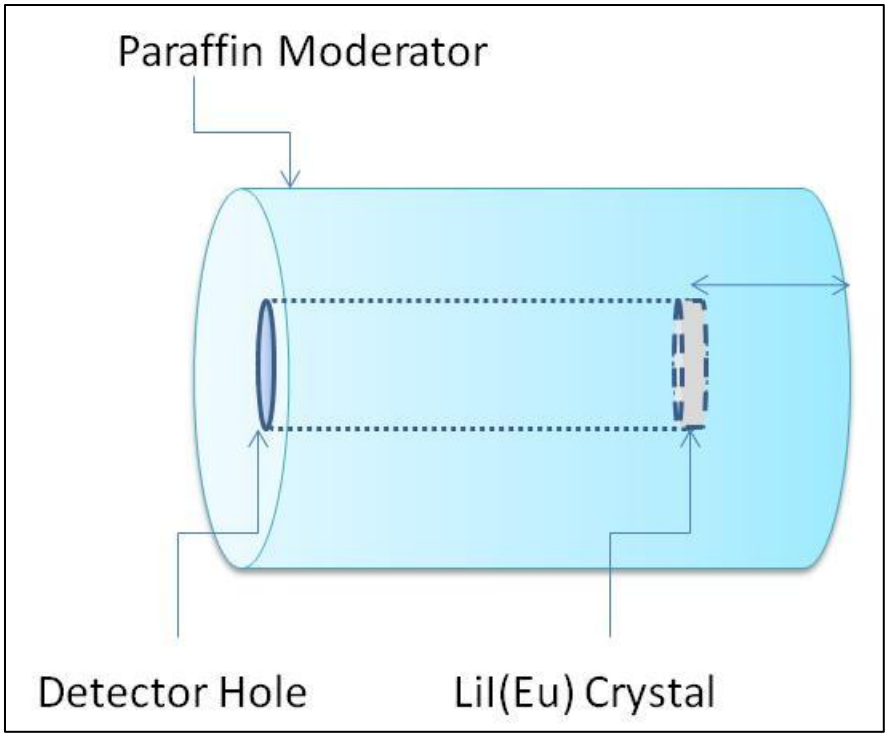

Figure 38: Schematic of the moderator

The detection of γ-rays were not affected by the paraffin moderator, as the effect on γ-radiation has low interaction with material of low atomic number. γ-ray interaction in the LiI crystal cause partial or full energy transfer to the electrons of the LiI crystal.

3.3. Data Acquisition System

The signal from the anode of a PMT is fed to a digital multichannel analyzer (MCA). The MCA model eMorpho from Bridgeport Instrument LLC (BridgePort Instruments, 2009. has been used as a data acquisition system. The eMorpho is a member of a product line that includes digitally controlled plug-on high-voltage generators and multichannel analyzers that employ digital signal processing. The signals from the PMT are fed into a pre-amp which is already built in the eMorpho line of MCA. Furthermore the MCA will count the number pulses. The MCA digitizes the amplitude (height) of each pulse. The height of the pulse is related to the energy of the radiation. The analysis of both pulse counts and pulse height allows the spectral analysis. In the following section we will describe the processes involved for signal extraction and processing.

Along with the Am-Be neutron source, the γ-ray sources that were used included ^{137}Cs, ^{60}Co, ^{22}Na.

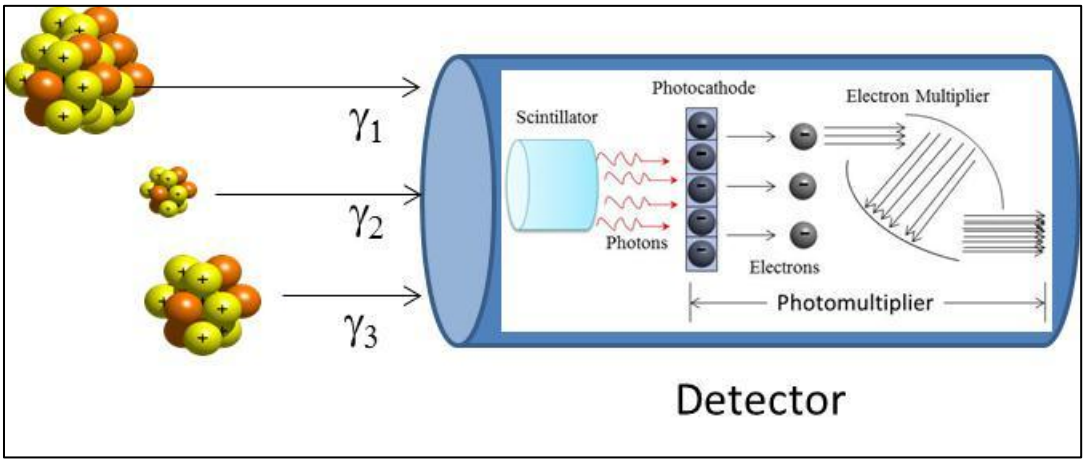

Figure 39: Experiment gamma sources and detector arrangement

When γ-rays with different energies interact with the scintillator, different pulses are generated at the output of the detector. A preamplifier is the first component used for signal processing. It borrows its name from the fact that it is a component that is situated just before the amplifier and pulse processing electronics which follow (hence the name pre- "before" amplifier). The preamplifier can provide the detector bias voltage required by the PMT and provide signal extraction from the detector (Figure 40).

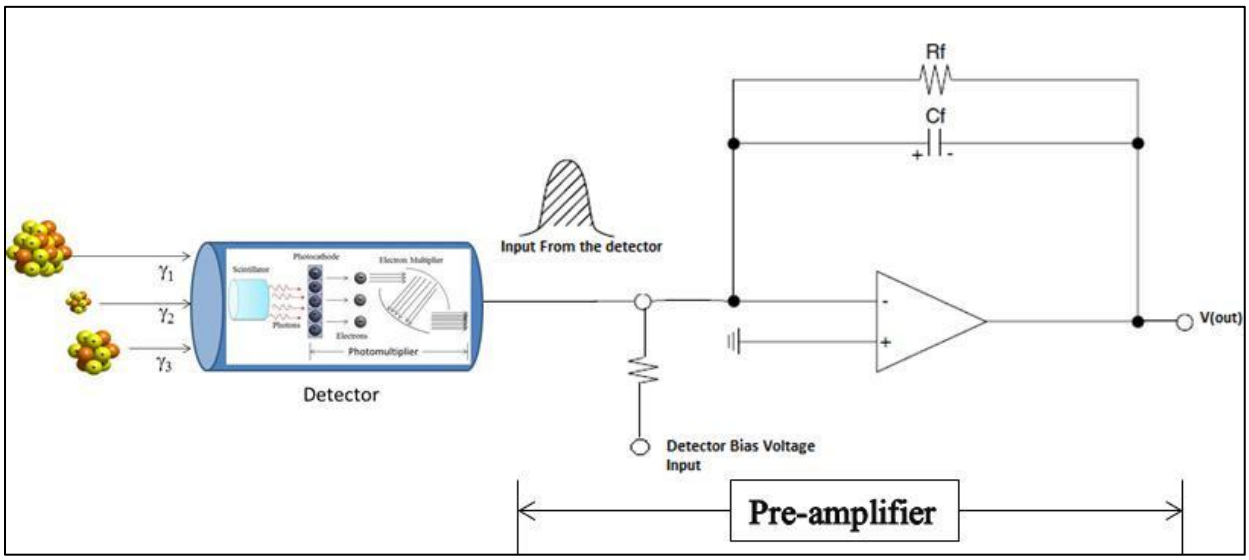

Figure 40: Typical RC feedback charge sensitive preamplifier

In the charge sensitive preamp, the charge input from the detector is integrated by the feedback capacitor (C_f). As the charge is collected on the C_f, it produces a step change in voltage. At this point the C_f is connected to a feedback resistor (R_f) in parallel which causes the voltage pulse to be discharged slowly with the time constant equal to R_fC_f. The time constant is a delay which is set to be longer than the duration of the time required to collect the charge in C_f. If this is the case, the

step voltages will reflect the entire pulse collected, which is proportional to the energy deposited in the detector.

At high count rates it may become necessary to make sure that new pulses do not ride on the tail end of a previous pulse as shown in Figure 41. The Trigger Dead Time setting instructs the eMorpho to wait that time after a trigger before it will allow new triggers. The Trigger Dead Time was 1.2 μsec. After the shaping of the pulse, it becomes nearly a Gaussian shape. The eMorpho MCA board uses numerical integration to compute the pulse energy. In practice the integration time is chosen to cover 90% of the emitted scintillator light. The integration time for the current experiment was 8 μsec.

The eMorpho uses pattern recognition to identify piled up pulses. A single parameter governs this process which is called the pile up time. The pile up time should be somewhat larger than the full width at half maximum (FWHM) of the signal pulse (see Section 4.1.3). During the experiment, the pile-up rejection was turned off due to the lower count rate of detecting events. It was done by setting the pile up time to be equal to the integration time.

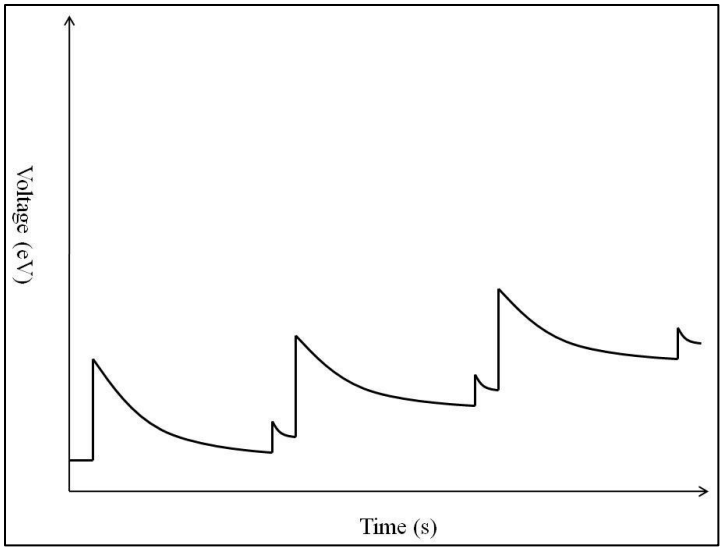

Figure 41: Signal pattern of a resistive feedback charge sensitive preamplifier

After the pulse has left the preamplifier, the pulses enter an amplifier whose purpose is to shape apply a gain and increase the amplitude of the original pulse. For example, a gain of 100 increases the amplitude of the original signal by a factor of 100. This makes it easy to distinguish similar pulses. For example a pulse of 2 mV and 3 mV with a gain of 100, has a difference in pulse size of 100 mv (300 mV-200 mV), which is much easier to distinguish from the original difference of 1 mV.

eMorpho has five resistors in series (100, 330, 1000, 3300 and 10,000 Ω) to determine the overall current gain. Computer-controlled switches are used to selectively short circuit any of the four biggest resistors, in order to achieve trans-impedances from as small as 100 Ω to more than 14 kΩ (BridgePort Instruments, 2009)

Following the amplification, the pulse is presented to a waveform digitizing analog-to-digital converter (ADC) where the conversion from analog pulse to digital data is performed. A peak sensing ADC measures the peak of the pulse and then converts the magnitude into a digital value.

The units for the ADC are channels. The digital image of the incoming pulse train is sent to a programmable logic gate array (FPGA), which performs the entire digital signal processing in real time. A USB cable connects the eMorpho to the computer where this data is stored. The computer software sorts out the data and places them into a histogram relative to the channel number and counts. In reality the energies will reflect all energy deposits that are due to photoelectric, Compton, and pair production effects and could be in the range of thousands and upwards to millions depending on the activity of the source. A sufficient number of counts will then produce what is called energy spectra.

3.4. Data Analysis Software

In this work commercial software has been used: IGOR PRO. It is a graphics data-analysis and data presentation environment that allows the user to use predefined data acquisition and display code such as this eMorpho graphics user interface (GUI) (BridgePort instrumetns,2009). At the same time it provides a very simple C-like programming language to create custom applications. The wealth of built-in functionality for graphics display, controls and data analysis tools allows the user to create fairly complex applications with a minimum of coding effort. IGOR PRO uses some unusual terms for some of its components and makes use of object oriented programming resulting in some unexpected behavior. For the benefit of an IGOR novice here are some explanations.

All code written under the IGOR PRO development system, as well as any data and settings created are stored together in a single file. That file is referred to as an "experiment". In fact, the extension "pxp" of the file name is an abbreviation of "packed experiment".

IGOR PRO knows local and global variables just as any other programming language. All variables are the equivalent of double in C. Except for complex double and string there are no other variable types.

IGOR PRO does not have a simple linear array of numbers but employs an object called a wave. It acts similar to an array in others programming languages but is more powerful and quite similar to the array object now seen in MS C#.net.

It includes automatic boundary checks, linear interpolation between entries and scaling factors for the abscissa. If a new user to IGOR wants to program under IGOR, it is required to spend a moment to read the help files concerning wave functions and familiarize with expressions such as data[2], data[2.5], data(0.01) and the built-in operators p and x (which do not act as variables). The spectra of the measurements are displayed in the GUI on the computer screen (Figure 42). Detailed instructions may be found in the eMorpho user manual in reference (Bridgeport Instruments, 2009).

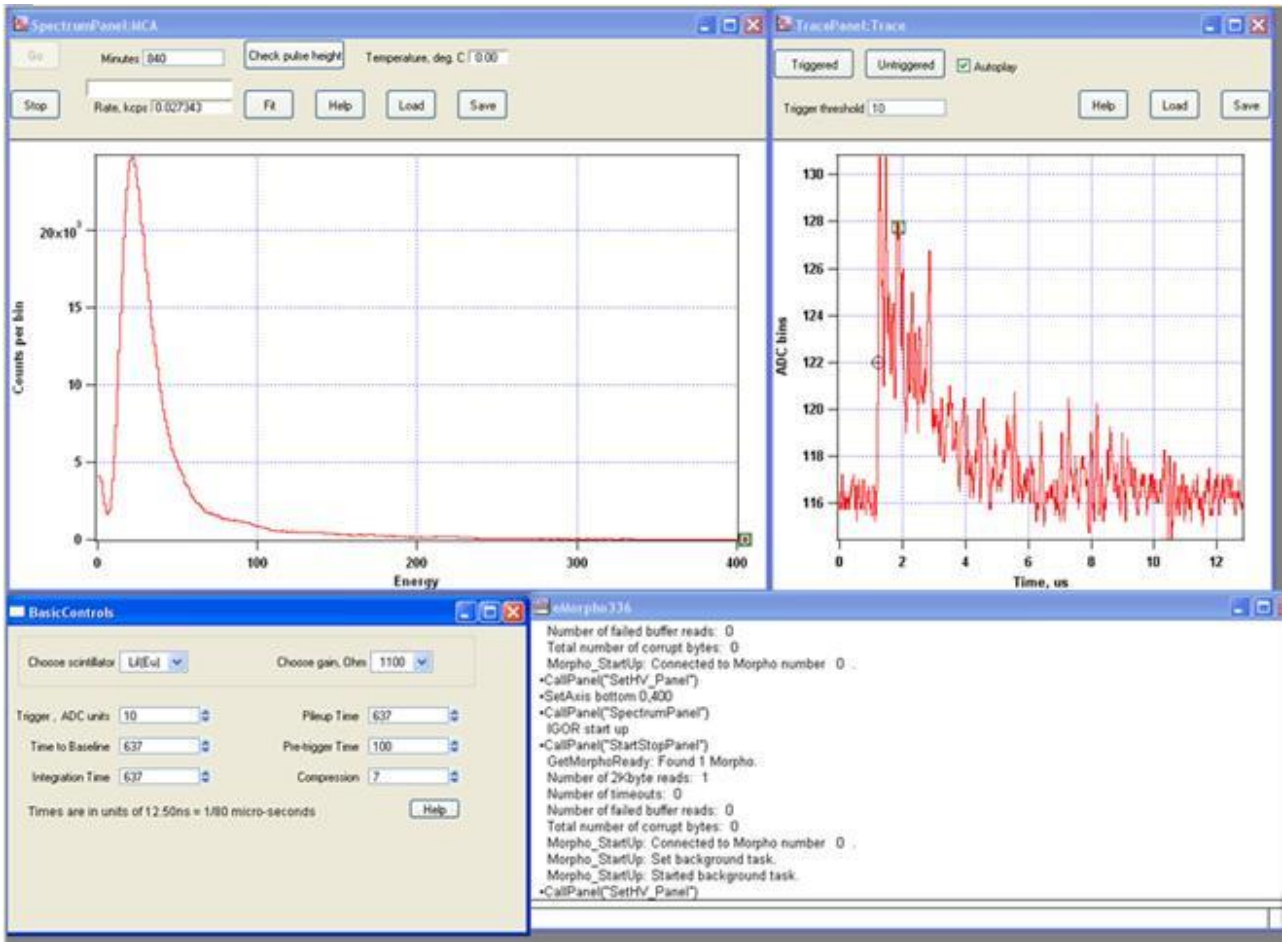

Figure 42: Graphical user interface (GUI) of IGOR PRO

3.5. Apparatus Setup

The experiment schematic is shown in Figure 43. As can be seen the detector is placed 12 cm away from the radiation source. The DAQ is connected by the coupling wires to the detector. And finally the DAQ communicates to IGOR PRO where the spectra analysis is achieved via a USB cable.

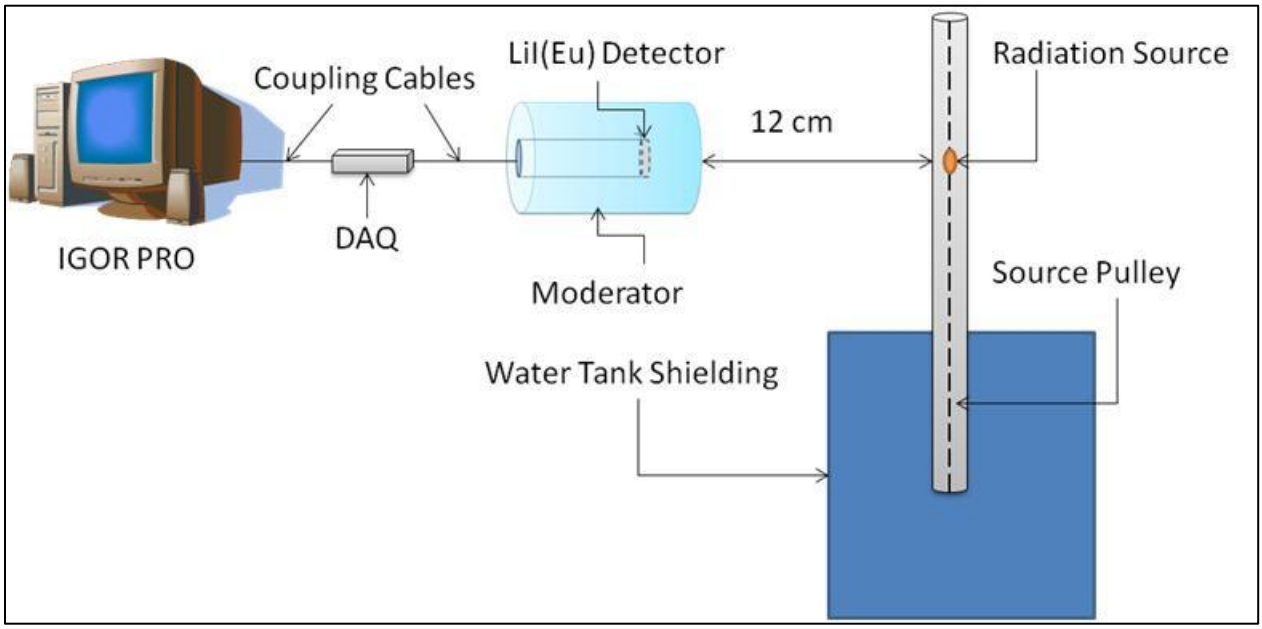

Figure 43: Schematic of apparatus setup

Chapter 4

Results and Discussion

4.1. Experimental Data with Gamma Radiation

A spectrometer requires the measurement of gammas from 0 to 3 *MeV*. A Large crystal is required to cover this energy range to allow secondary electrons to deposit its entire energy into the sensitive volume of the detector. Therefore measurements utilizing different crystal sizes were taken at UOIT neutron facility with various gamma energies. Below are the sections pertaining to the data obtained with measurements from gamma sources, using crystal sizes, ϕ6x11 mm and ϕ10x25mm.

4.1.1. Measurement with ϕ6x11 mm size crystal

In the first experiment, a ϕ6x11 mm crystal was coupled to the photomultiplier tube. In order to ensure that the coupling was in fact intact without air gaps, optical grade silicone grease was applied in between the PMT and crystal. The PMT was connected to the 14 pin socket, which provides the high voltage to the PMT. The components were assembled together, and the casing of the detector was screwed on tightly in order to prevent moisture ingress and escape of light. The detector was connected to the MCA via the MCA coupling wire, and finally the MCA was connected to the computer via USB for further analysis.

To carry out the experiment, the detector was placed 12 cm away from a radiation sources. The first experiment carried out with the system has used Cobalt-60 and Cesium-137 source. The

discrimination level has been set up to minimize the background contribution directly from the graphical user interface utilizing the controls of the DAQ. A pulse height spectra was obtained as shown in Figure 44.

Pulses at channel 190 refer to the photoelectric peak of Cesium-137 which has energy of 662 *keV*. For further assessment, the detector has been irradiated with a 1 μCi ^{60}Co gamma source. The peaks in channels near 340 and 375 refer to the energies of gamma rays which are 1173 *keV* and 1332 *keV* respectively. However, it is clear from the spectra that the two peaks of cobalt cannot be resolved due to the low resolution of the detector.

Due to the small size of the crystal, high energy electrons produced by high energy gamma which are born near the periphery of the crystal therefore are unable to deposit their full energy. Moreover the statistical character of events gives rise to fluctuating energy deposition, thereby causing a low resolution of the detector. More specifically some photoelectrons from 1332 *keV* gammas are partially depositing their energies and generate pulses that fall into lower energy channels. Moreover, some photoelectrons related to both gamma lines (1173 and 1332 *keV*) are partially depositing their energies which are mixed with the Compton electrons, and cause a continuum of energy deposits in between. The two peaks become difficult to resolve, and therefore, the smaller crystal was not appropriate for high energy gamma detection. Thus a larger crystal was required in order to overcome the shortcomings of the smaller crystal.

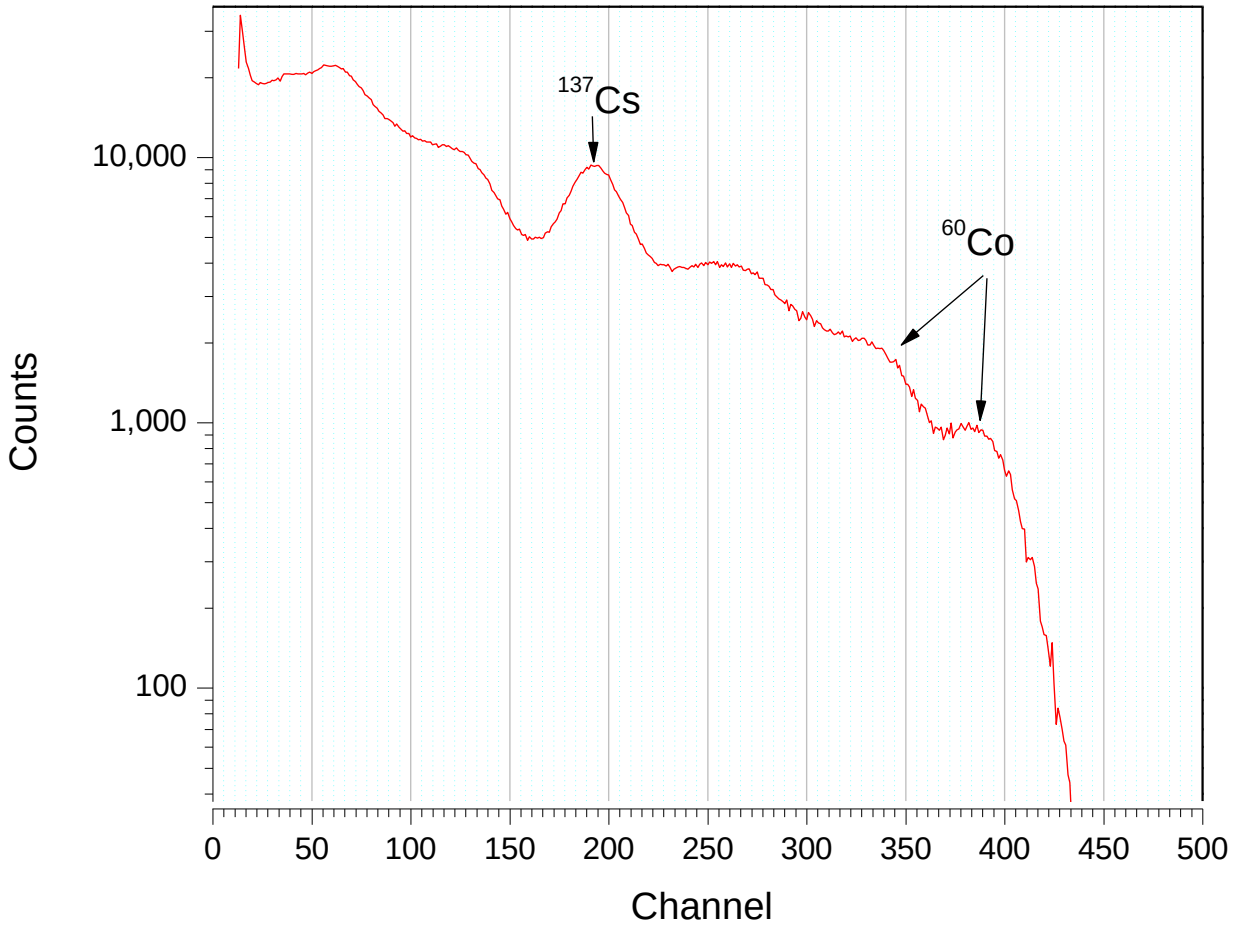

Figure 44:^{60}Co spectra measured with ϕ6 mm x ϕ11 mm LiI Crystal

4.1.2. Measurement with ϕ25x10 mm Size Crystal

The detector assembly was disconnected from the DAQ, and the detector cover was unscrewed which revealed the internal components namely PMT, PMT socket, and crystal. The PMT was disconnected from the socket, and the small crystal was decoupled from the PMT.

For the new ϕ25x10 mm crystal to be coupled, the previously used optical grease was cleaned off and new optical grease was applied between the new crystal and PMT making sure there are no air bubbles in the region between PMT and the crystal. The detector was assembled in the manner described in section 4.1.1. The detector was connected again to the DAQ via the MCA coupling wire, and finally connected to the computer via USB in order to perform further measurements. In the same way as before, a ^{60}Co gamma source was placed at the same distance from the front face of the detector i.e. 12 cm away from the detector and the energy spectra was recorded as shown below in Figure 45.

From this figure, the peaks in channels near 170 and 190 refer to the energies of gamma rays which are 1173 *keV* and 1332 *keV*, respectively. It is clear that the detector with this new larger crystal is able to resolve the two cobalt peaks and therefore, this crystal was adopted for further measurements and use such as calibration, linearity, and resolution as discussed in later sections below. At this point the resolution of the detector was measured in order to feed the input file of the Monte Carlo simulation.

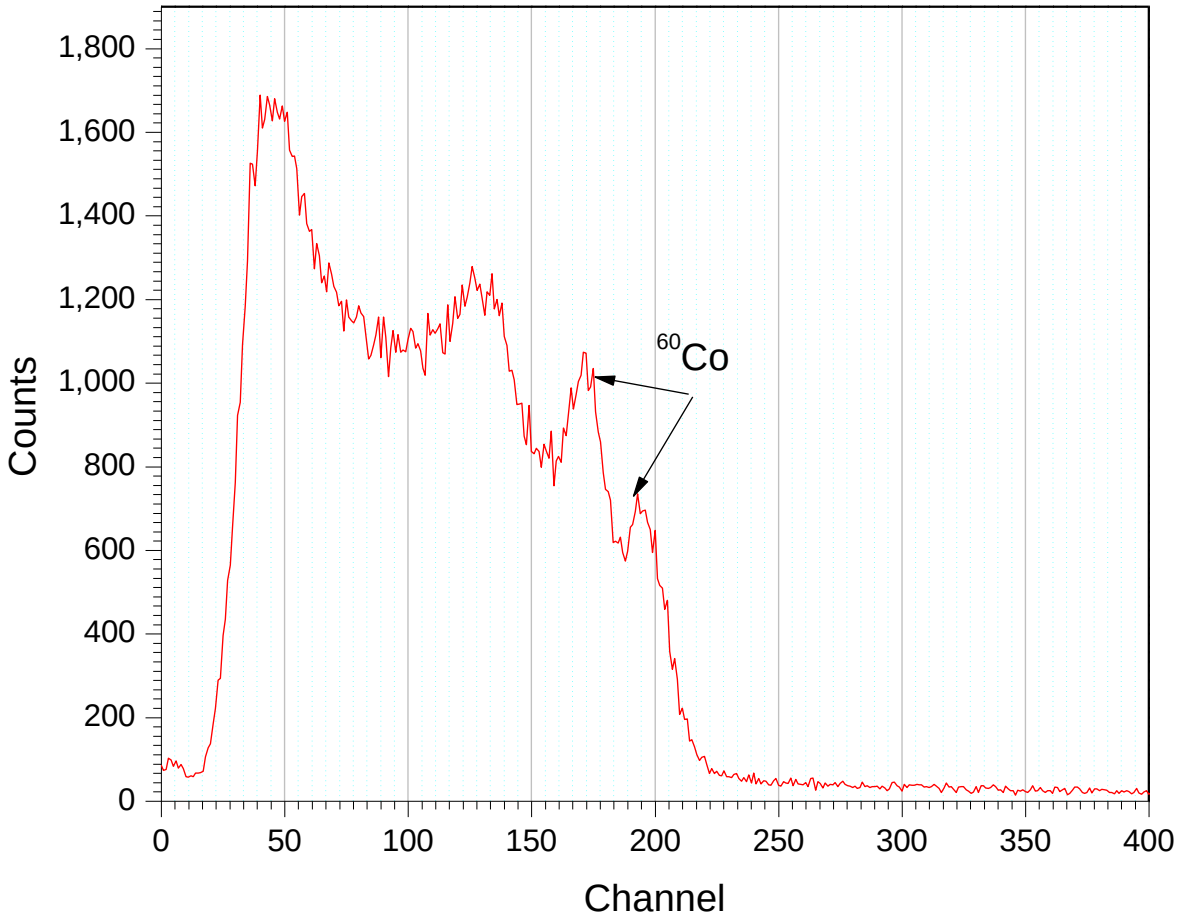

Figure 45: ^{60}Co spectra measured with ϕ10 mm x ϕ25 mm LiI Crystal

It noteworthy to compare the response of the two crystals and a brief comparison from Figure 44 and Figure 45 shows the inability of the small crystal to resolve ^{60}Co gamma peaks.

4.2. Measurement With the Selected Crystal

The ϕ25x10 mm crystal was selected in all further experiments to investigate the resolution of the detector, measurements with a broad energy range of gamma energies, and simulated response function of the detector.

4.2.2. Linearity of the system

In order to check the linearity of the built system (crystal, PMT and electronics) the unit has been irradiated with different γ -sources listed below in Table 12.

Table 12: Characteristics of the Calibration γ Sources

Isotope	Date of Production	Activity on Date of Production	*Present Activity	Reason for use
^{60}Co	Nov. 2004	37 kBq	15.7 kBq	Calibration Validity
^{22}Na	Nov. 2004	37 kBq	6.6 kBq	Calibration
^{137}Cs	Nov. 2004	37 kBq	32 kBq	Calibration

*Note the calculated activities are based dates referring to May 1 2011.

The experiment has been carried out with the above calibration sources and the spectra is shown in Figure 46.

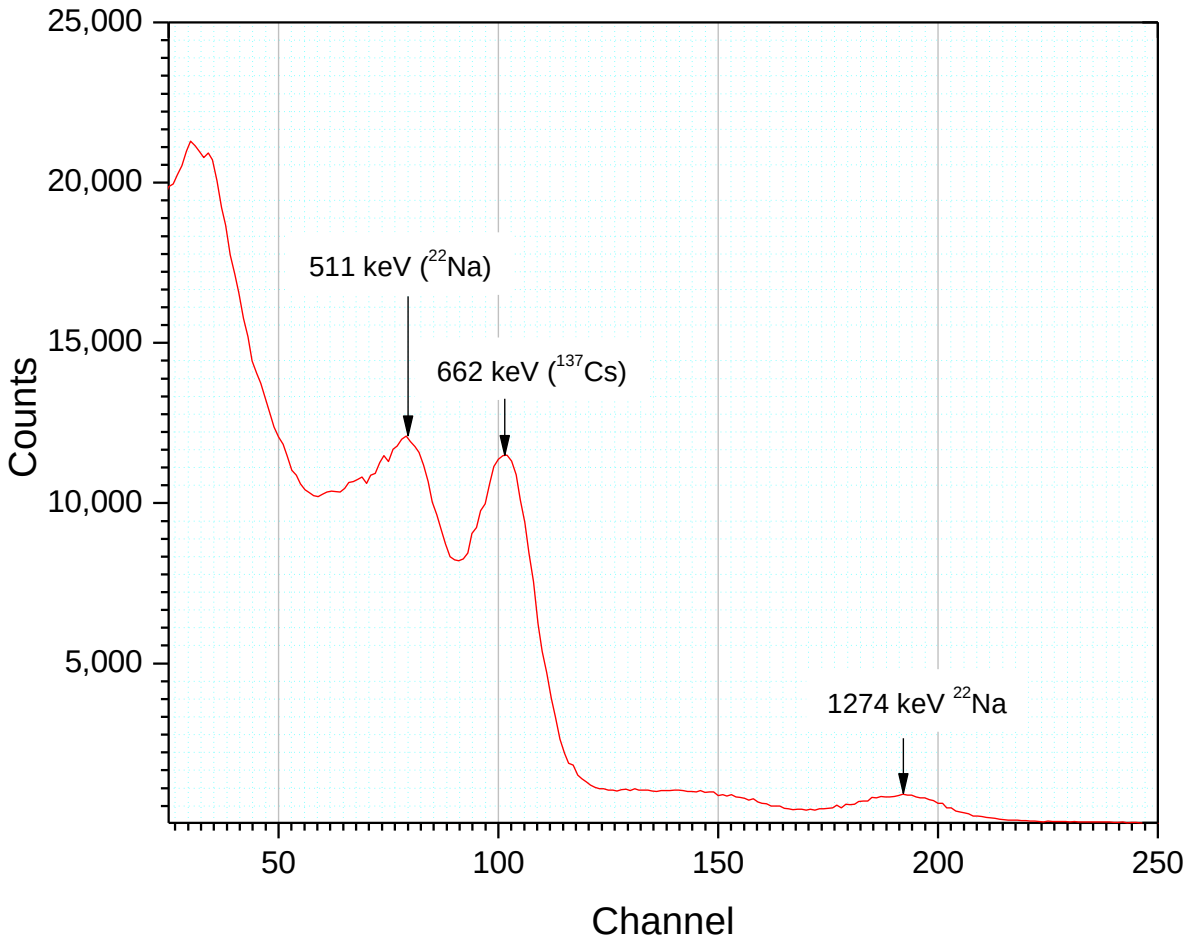

Figure 46: Measured Energy spectrum of ^{22}Na and ^{137}Cs

In the spectra above, the peaks 511 *keV*, 662 *keV*, and 1274 *keV* are shown. The peaks do not occur at one single channel, and are distributed along the channels due to the variations in energy deposits and variations in the fluctuating detector response which are inherent characteristics of the detector. Therefore the peaks which are observed in the spectra are distributed in the shape of a Gaussian curve, where the centroid of the peak represents the largest number of counts recorded. Thus, each peak was analyzed and a Gaussian curve fitting was applied. Figure 47 represents an example of fitting the experimental data to find the centroid of the peak. The area under the curve

which is shaded represents the number of counts integrated over the energy distribution. The centroid of each peak has been defined and the data are listed in Table 13.

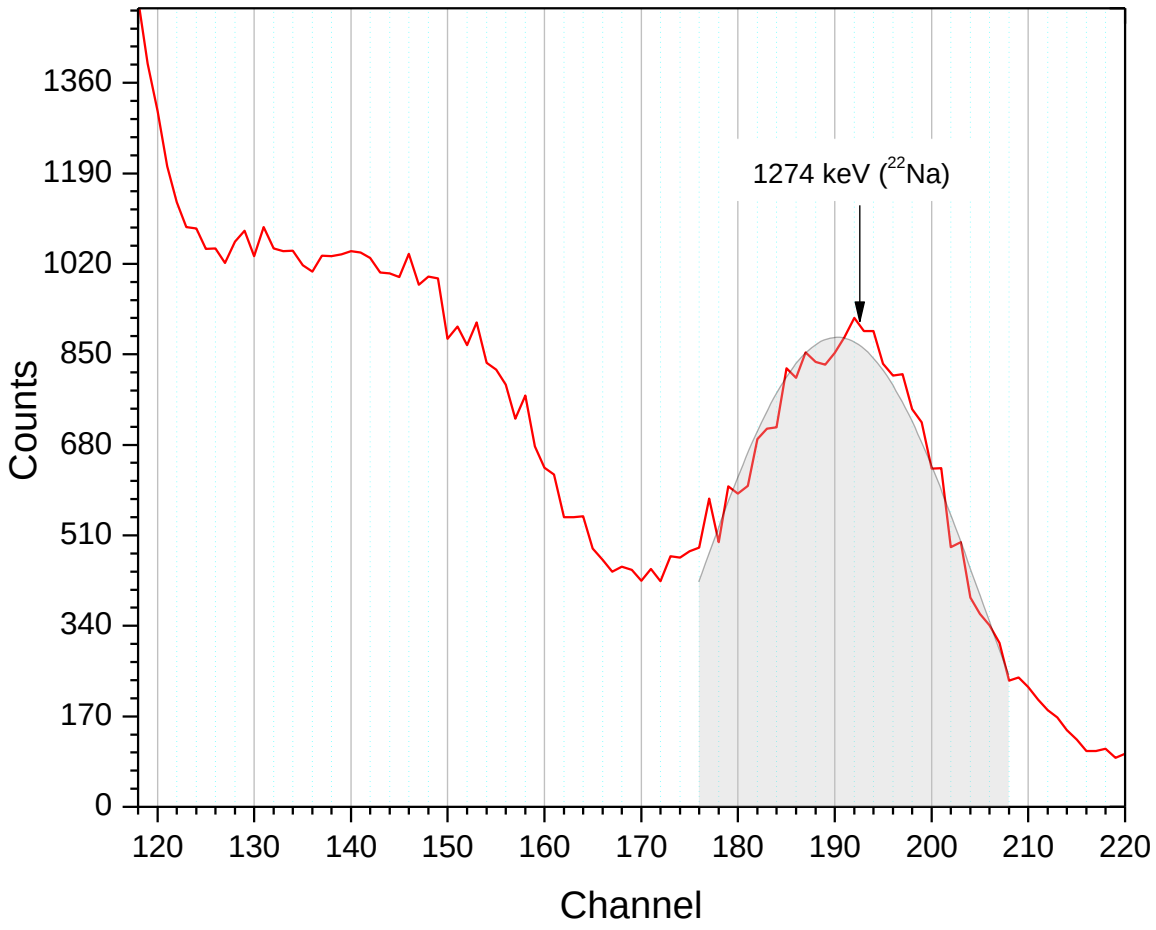

Figure 47: Gaussian fitting to 1274 *keV* peak

Table 13: Centroid of ^{137}Cs, ^{22}Na peaks

Energy, *keV*	Centroid (Channel)
511	77
662	100
1274	190

Based on table 13, the data has been plotted in Figure 48. One can see the good linearity of the built system.

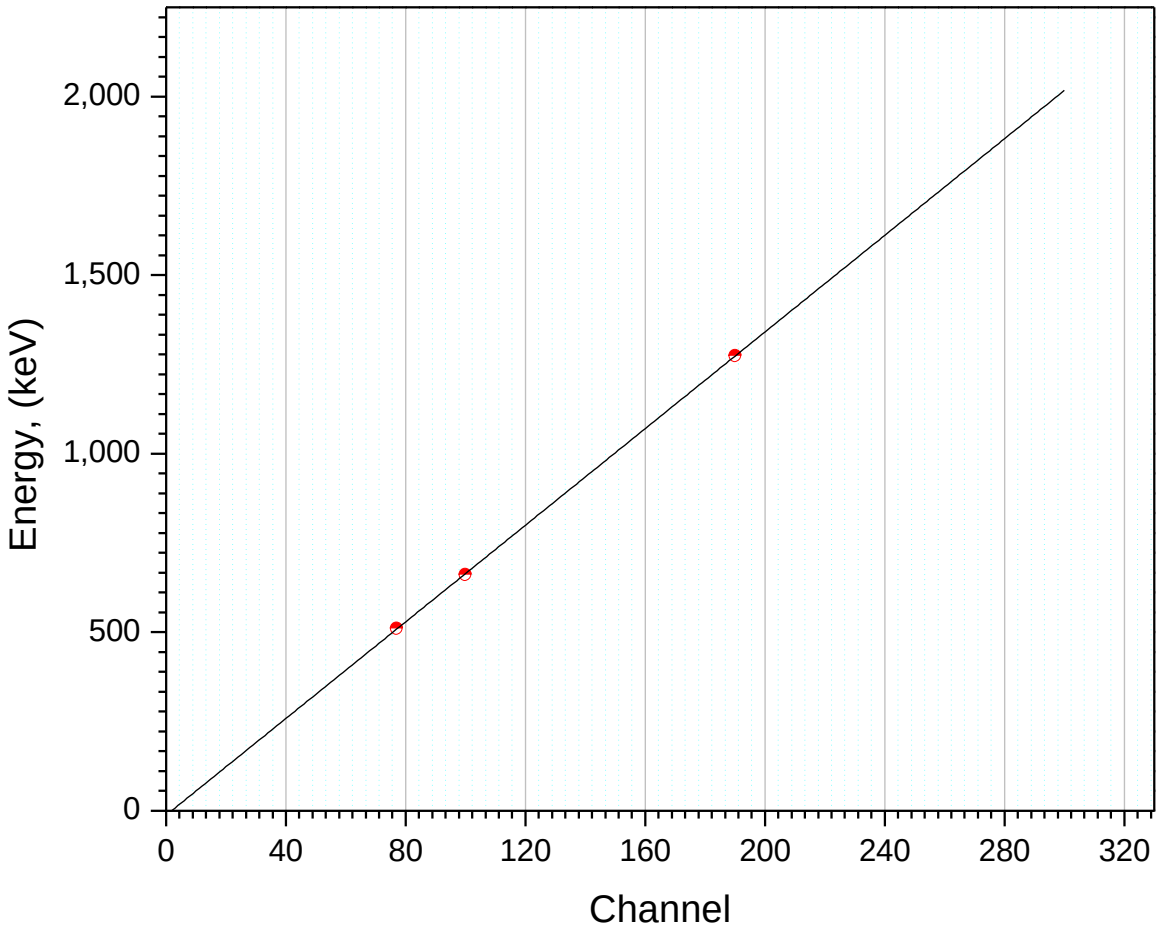

Figure 48: Linearity of the detector

Since the detector has been built to cover a large range of gamma radiation (up to ~3 *MeV*) and at the same time to have the ability to detect thermal neutrons, one have to check the channel location of the highest energy gamma (2614 *keV* of thorium) relative to the position of thermal neutron peak which will be discussed after the measurement with neutrons in later section.

4.2.1. Resolution of the detector

The intent of the detector is to be used as a spectrometer with the capability to perform gamma spectroscopy of natural radioisotopes. Some of the gamma emitters have energy lines that are very close in value, and therefore produce pulses in nearby channels. In order for the detector to be useful it must have the ability to respond to different energies with acceptable resolution. An experiment was conducted to measure the resolution. For such purpose, a mono energetic ^{137}Cs which emits 662 *keV* γ-rays has been placed in front the detector and the spectra has been recorded. If the detector records energy pulses across a wide range of channels, it would be considered "poor" resolution. On the other hand, if the detector stores the same number of counts, and has the same centroid, but within a narrow range of channels, it would be considered "good" resolution. The obtained data from the experiment described above are shown below in Figure 49.

.

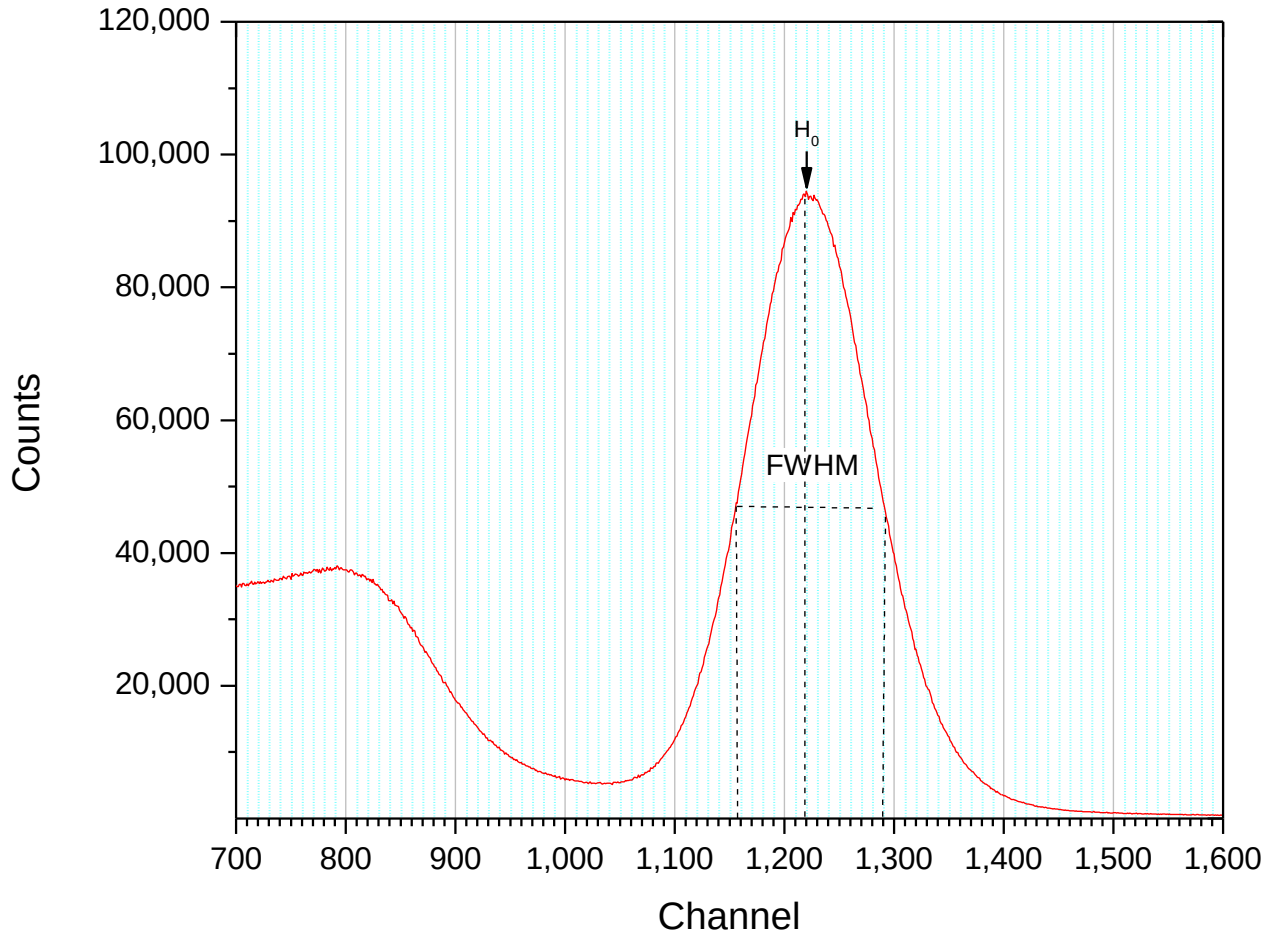

Figure 49: Resolution of the detector for gamma radiation at 662 *keV*

The full width at half maximum (FWHM) is illustrated in the figure above and is defined as the width of the distribution at a level that is just half the maximum ordinate of the peak. The resolution of the detector which is defined as the FWHM divided by the location of the peak's centroid H_o. The units for resolution are dimensionless and are usually represented in percentage. It follows that the resolution of the detector for gamma radiation is:

$$R_\gamma = \frac{\mathrm{FWHM}}{\mathrm{H_o}} = \frac{\mathrm{n_2 - n_1}}{\mathrm{H_0}} = \frac{1291 - 1158}{1219} \cong 11\%$$

The built unit offers a resolution of 11% at Cs peak this means that in order for the energy peaks to be resolved with nearby peaks in the range of ±72 *keV*. Notice that the detector based on NaI crystal has a comparable resolution of 8%.

4.3. Comparison between experimental and simulation data

Once the resolution parameter was fed to the simulation code, a simulated response function was generated and compared with the experimental data as shown in Figure 50. The dominant regions in the pulse height distribution due to the ^{60}Co source are as follows:

Background energy: Background energies are shown in the lower channels and appear to have a discrepancy between the experimental and MCNP data. This is explained because the surrounding environment causes the low energy photons to be absorbed whereas, in the code, the objects in the environment were not modeled.

Compton electrons: The Compton curve is clear in both spectra and its range is from low energy to approximately the Compton edge which falls around 1 *MeV*. With this regard, the two comparisons are in good agreement.

Photoelectron: The photoelectrons produce photoelectric peaks which are 1173*keV* and 1332*keV*. These peaks can be seen in both MCNP data and Experimental data. In this regard, the simulation and experimental data are in agreement.

Overall the comparison of the experimental data and MCNP data shows good agreement, and therefore the simulated response function can be used for other energies up to 3 *MeV*. Since the MCNP model is in a good agreement with the experiment, the simulated response function of the detector can be used to overcome difficulties encountered in experimental investigation. For instance close to an accelerator, the Bremsstrahlung radiation can have different energies, and

therefore the only way to get the response of the detector to such energy is through to the simulation.

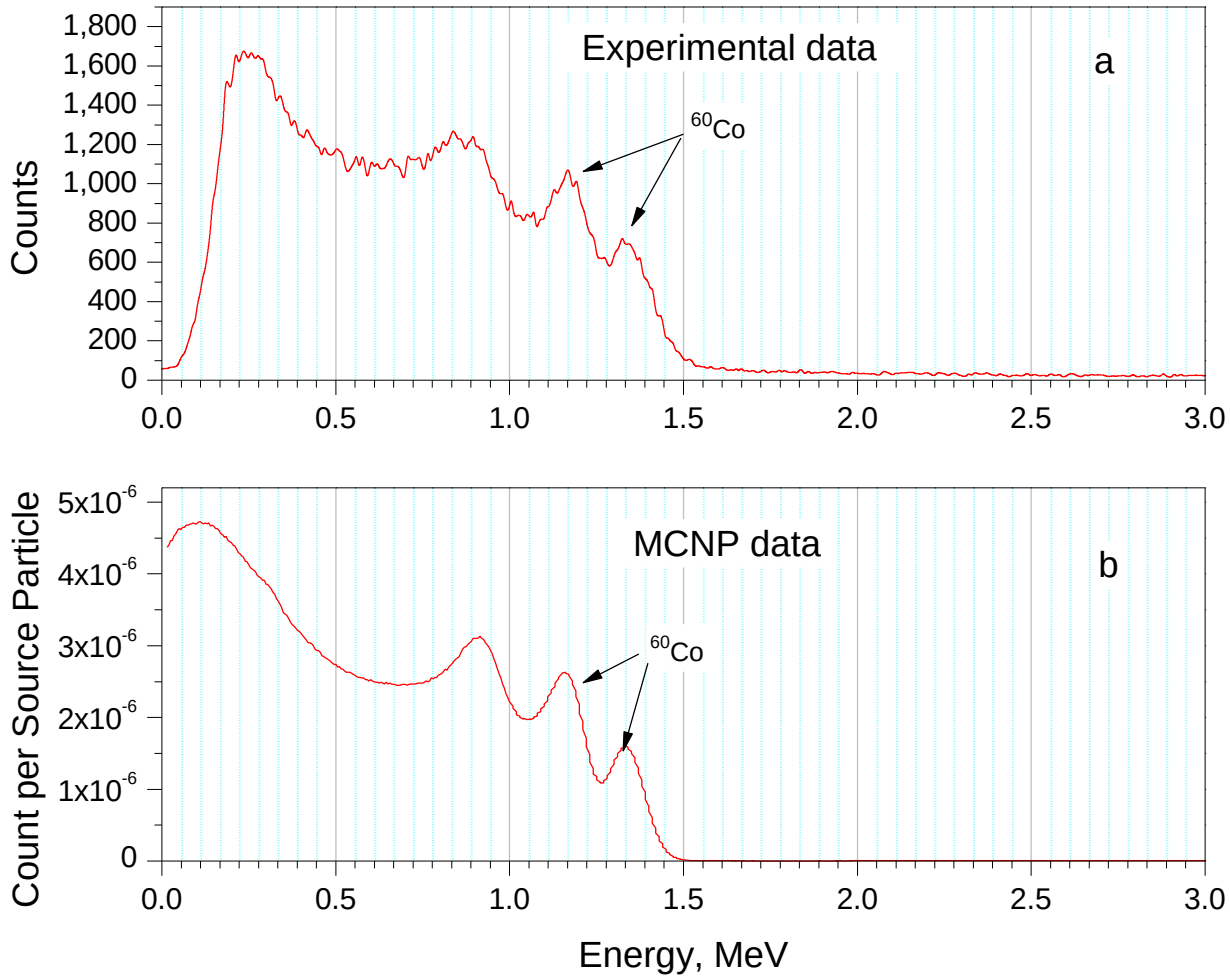

Figure 50: Comparison of ^{60}Co spectra between experimental and simulation (MCNP)

4.4. Measurement With Neutron Sources (Am-Be)

The developed detector was designed not only to detect γ radiation but also thermal neutrons. The detector was utilized in a series of experiments which were conducted at UOIT neutron facility. The experiment used an Am-Be source of 120 mCi described in the methodology section. The Am-Be source has a hard spectra with an average energy around 5 *MeV*. To thermalize neutrons, the designed moderator has been used and the pulse height spectra have been recorded. The spectrum is shown in Figure 51. On the spectra one can see clearly the contribution of thermal neutron peak at channel 600. Also there is a bump at the left side of the peak referred to as region R1 on the spectra. This region shows a continuum of energy that is extended from the total deposit energy of 4.78 *MeV* to 0 and it is due to the contribution of those reactions that take place at the border of the detector and the products of whose deposit only a part of their energy in the sensitive volume of the detector. This effect is known as wall effect, and is especially significant in gas filled detector due to the long range of the reaction products. In our case, this contribution is minimal due the small range of tritons and alpha particle in LiI medium. It should be noticed that this effect lower the resolution of the detector.

Another feature which can be seen on the spectra is related to the contribution of γ-rays in low energy range. This contribution firstly comes from background radiation and secondly from γ-radiation emitted from Am-Be source after de-excitation. These low energy γ-rays interact with the crystal and their secondary electrons deposit their energy in low channels.

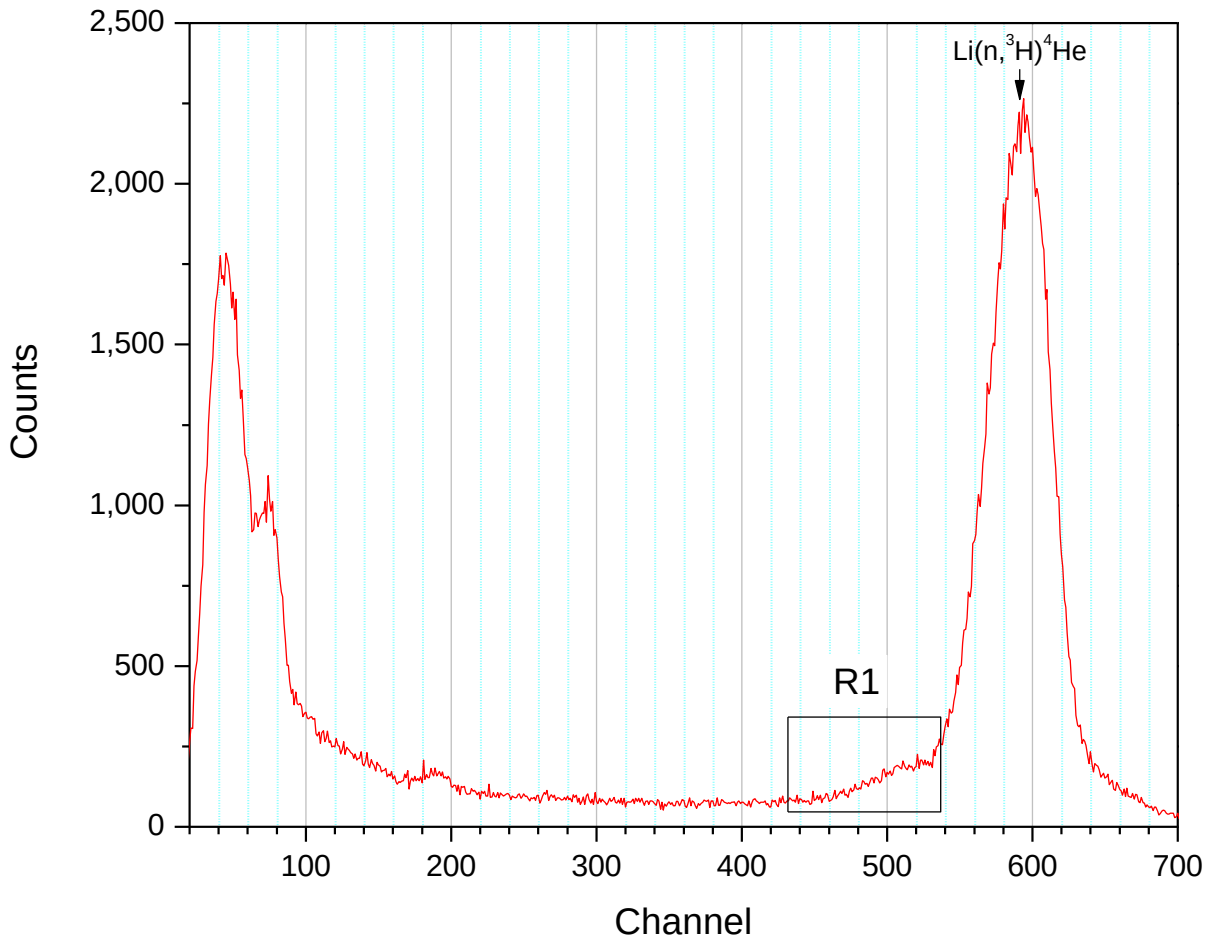

Figure 51: Am-Be neutron source energy spectra

Furthermore, and to have an estimation of the contribution of fast neutrons, it was necessary to measure the detector resolution for neutron radiation. It follows that the resolution for the detector for neutron radiation is as follows:

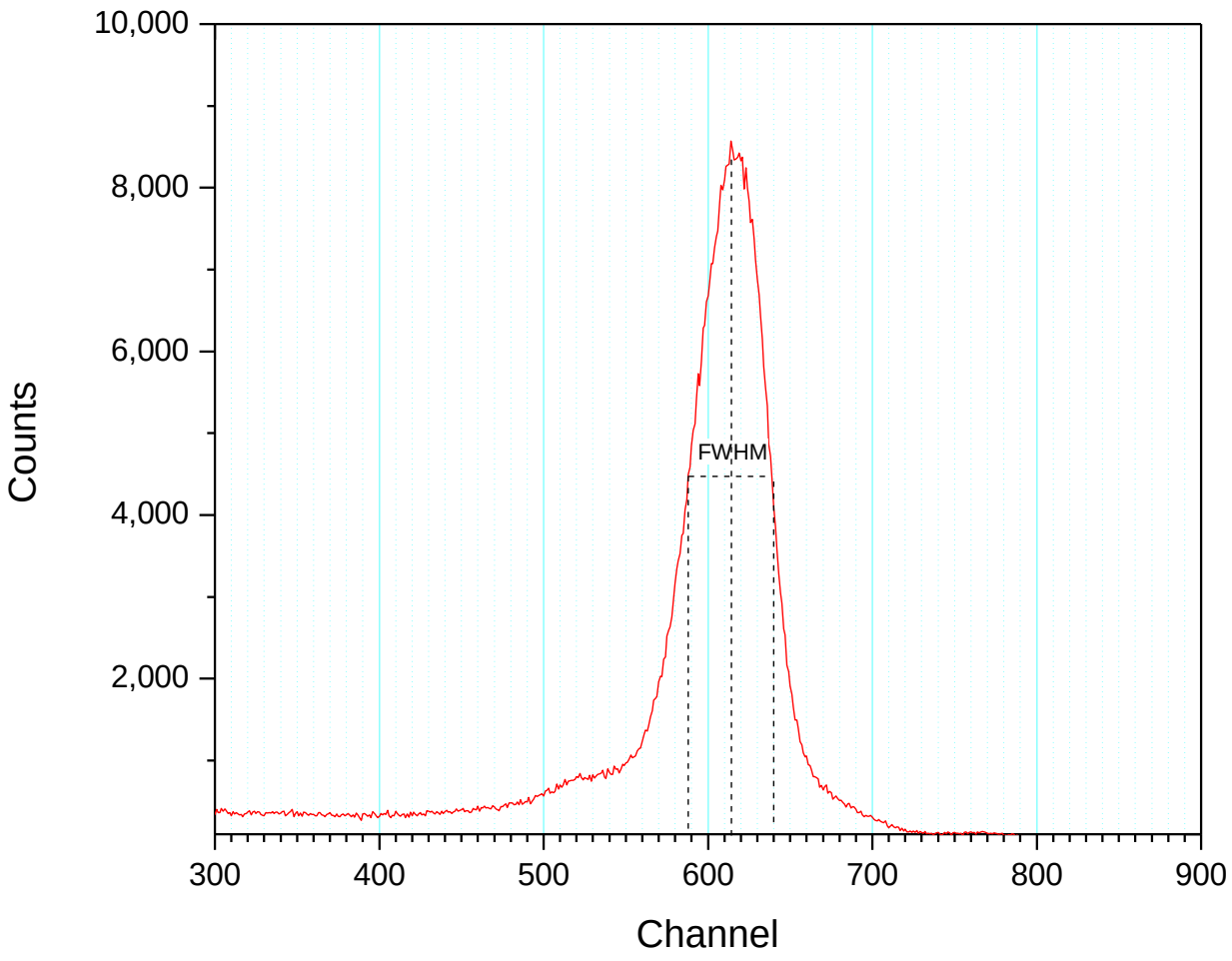

$$R_n = 8\%$$

Figure 52: Resolution of detector for thermal neutrons

4.5. Measurement With Neutron and Gamma Mixed Field

To carry out this experiment, the neutron source of Am-Be described above has been used along with a γ-source of ^{60}Co. Both sources have been placed in front of the detector and the pulse height spectra which resulted from a mixed neutron and γ field has been measured. The data obtained in this experiment are shown in Figure 53.

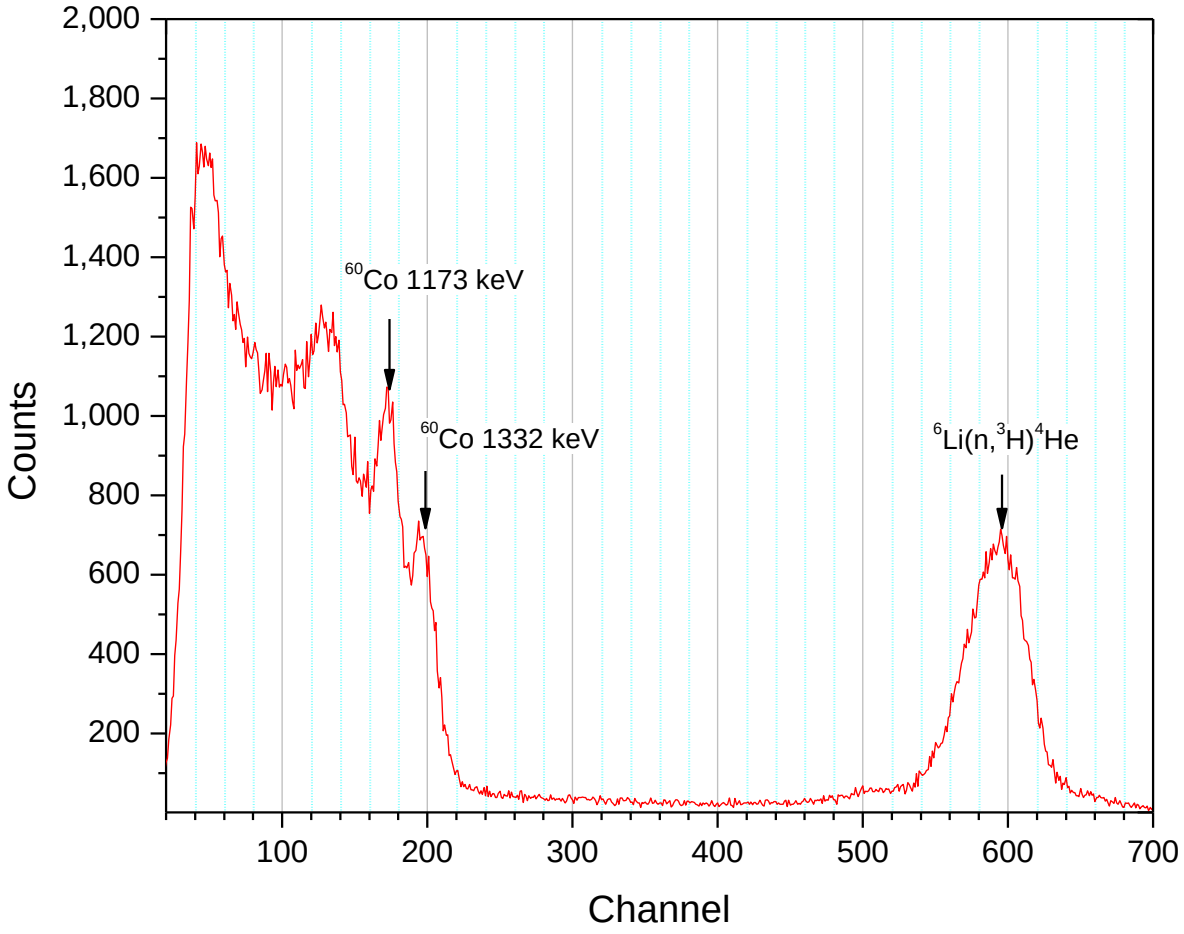

Figure 53: Mixed field energy spectra for ^{60}Co and Am-Be source

The spectrum exhibits the two photo peaks corresponding to ^{60}Co at 1173 keV, and 1332 keV. Also in the figure above, background radiation are dominating is low channels. The Compton edge of the first ^{60}Co peak can be also seen. In addition to the ^{60}Co peaks, we observe the contribution of thermal neutron from the Am-Be source resulting from ^{6}Li(n,^{3}H)^{4}He interactions lies in higher channel (around 600). In order to show the versatility and the spectroscopy features that the detector possesses, the ^{60}Co source was replaced by a ^{22}Na source and the pulsed height spectrum has been measured. The obtained data in this experiment are shown are shown below in Figure 54.

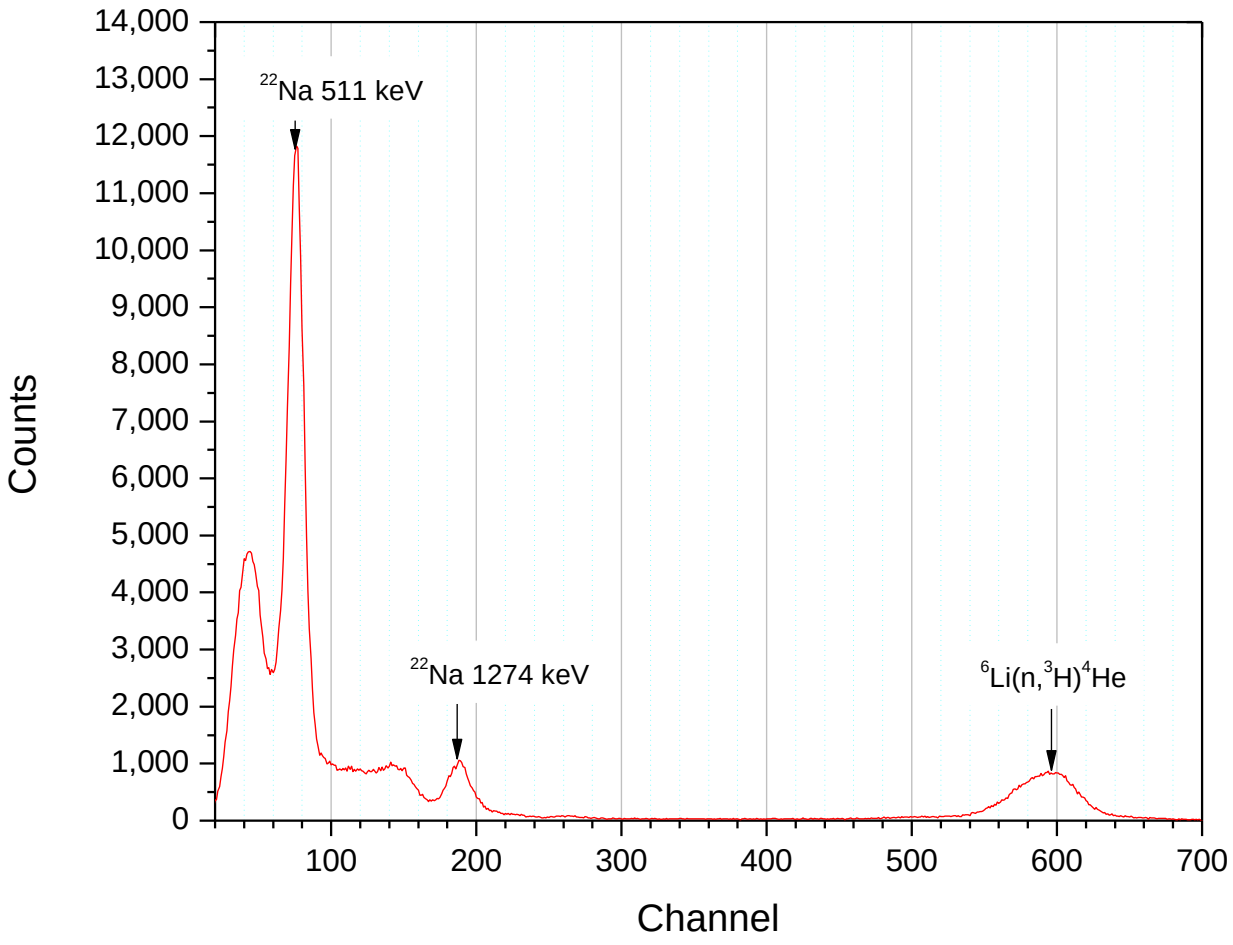

Figure 54: Mixed field measured energy spectra of ^{22}Na and Am-Be Source

The figure above shows a measured energy spectrum of ^{22}Na γ-ray source and Am-Be neutron source. The spectra exhibit peaks corresponding to ^{22}Na at 511 *keV*, and 1274 *keV*. In Figure 54, background radiation, the Compton effects can be clearly observed. In addition to the ^{22}Na peaks, the contribution of neutron peak due to $^{6}\mathrm{Li}(n,{}^{4}\mathrm{He})^{3}H$ interactions is present.

We have to notice that any γ-detector dedicated to serve as spectrometer should have an energy range up to 3 *MeV* to cover the spectroscopy of all natural occurring isotopes since the highest γ-

ray energy corresponds to ^{232}Th isotope and its value is 2614 *keV*. From the calibration experiment in section 4.1.2., the corresponding channel for such energy is around 400 and energy of 3000 *keV* should be around 500. Both these energy can be seen by the developed detector and therefore the unit can serve as a good spectrometer and spectrometer with a medium energy resolution and at the same time as a device for neutron signature.

Conclusion

A detector for dual neutron and γ-rays detection has been developed using a single europium activated lithium iodide crystal. The system consists of a single crystal mounted on a PMT to detect γ-radiation as well as thermal neutrons, simultaneously.

To build the system 2 different crystals size has been tested, mainly, ϕ6x11 and ϕ25x10 mm and the latter was adopted.

A miniature compact data acquisition system has been used for neutron-γ radiation discrimination. The system has been tested with different γ-ray energies and with an Am-Be neutron source at the University of Ontario Institute of Technology (UOIT) neutron facility. More specifically, γ-ray sources ^{137}Cs, ^{60}Co, and ^{22}Na were used individually and then coupled with the Am-Be neutron source.

The energy spectra from different γ sources were used to investigate the characteristics such resolution and linearity of the detector. the resolution measurement used a standard source of ^{137}Cs, 662 *keV* and it was proved to be close to medium resolution commonly measured with NaI crystal.

The pulse height spectra measured in separated field and in mixed field have been investigated to evaluate the performance of the detector in term of dual neutron gamma detection and discrimination.

The detector has shown its ability to identify the major common naturally occurring isotopes from low energy γ-ray to around 3 *MeV*. Therefore, γ-spectroscopy has been achieved with a

medium resolution. Moreover in addition to the γ-ray spectrum, a peak corresponding to the induced thermal neutron energy deposits was clearly identified and the unit is able to detect neutrons signature in mixed neutron γ-ray field.

Based on the analysis, the detector has proven to detect neutrons and γ-rays simultaneously by discriminating the pulses generated at its output.

A MCNP model was built to simulate the response function of the detector to gamma radiations. A comparison between the simulated data and the experiment has been evaluated and a good agreement between the two sets of data has been achieved.

Future Work

The developed detector is a part of neutron γ-ray spectrometer under development and it presents a fundamental corner for future development of a neutron/γ spectrometer to detect neutron from thermal to about 20 *MeV* and gamma radiation from low energy to 3 *MeV*.

References

1. A. Bessiere, P. D. (2003). Luminescence and scintillation properties of Cs2LiYCl6:Ce3+ for gamma and neutron detection. *Presented at SCINT 2003* .
2. Boland, J. (1970). *Nuclear Reactor Instrumentation (In-Core).* Amer Nuclear Society.
3. BridgePortInstruments. (2009). *eMorpho User Manual.* Austin, Texas: Bridgeport Instruments.
4. Brookheaven National Lab. (1998). Internation Workshop on thermal neutron detectors for Spallation Sources.
5. van Eijk, C. W. E., Bessière, A., & Dorenbos, P. (2004). Inorganic thermal-neutron scintillators. *Nuclear Instruments and Methods in Physics Research Section A: Accelerators, Spectrometers, Detectors and Associated Equipment, 529*(1-3), 260-267. doi:10.1016/j.nima.2004.04.163
6. Cierjacks, I. (1983). *Neutron Sources.* Pergamon Press.
7. Crane, T. (Accessed 2011). Neutron Detectors. In E. T. Physics, *available onine at www.fas.org/sgp/othergov/doe/lanl/libwww/* (p. Chapter 13). Los Alamos Scientific Laboratory.
8. Czirr, J. (1998). Proceedings of European workshop on Thermal Neutron Detectors for the Eutropean Spallation Source. *Deft University of Technology* .
9. D.A Shea, D. M. (2010). The Helium-3 Shortage: Supply, Demand, and Other Options for Congress. *Congressional Research Service* .
10. Evans, R. D. (1955). *THe Atomic Nucleus.* New York: Mcgraw-Hill Pubblishiing Company LTD.
11. Fano, U. (1953). 11(8): 8 ; 11(9): 55 . *Nucleonics, ,* Chapter 23.
12. G. Nelson, D. R. (Accessed 2011). Gamma-Ray Interactions with matter. In *Available online at www.fas.org/sgp/othergov/doe/lanl/libwww/* (p. Chapter 2).
13. Heiserman, D. L. (1992). Element 98: Californium: Exploring Chemical Elements and their Compounds.
14. Knoll, G. F. (1989). *Radiation Detection and Measurement 2nd Edition.* Toronto, Canada: John Wiley & Sons.

15. Leo, W. (1994). *Techniques for Nuclear and Particle Physics Experiments 2nd Edition.* Berlin, Germany: Springer-Verlag.
16. Malmskog, I. O. (1962). Investigation of the Pulse Height Distribution of Boron Trifluoride Proportional Counters. AE , 84.
17. Recent developments in neutron detection , Nuclear Instruments and Methods in Physics Research Section A: Accelerators, Spectrometers, Detectors and Associated Equipment, Volume 443, Issues 2-3, 1 April 2000, Pages 400-415
    A. J. Peurrung.
18. Rinard, P. (1991). *Neutron Interactions with Matter.* Los Alamos Technical Report NUREG/CR-5550.
19. Spieler, H. (2002). Pulse Processing and Analysis. *IEEE NPSS Short Course* .
20. Tavernier, S. (2010). Experimental Techniques in Nuclear and Particle Physics.
21. W.R. Mills, J. R. (1969). Volume 71 issue 3. *Nuclear Instruments and Methods* , 292.
22. Radioactive neutron source spectra from 9Be(α, n) cross section data Original Research Article Nuclear Instruments and Methods, Volume 131, Issue 2, 24 December 1975, Pages 315-321
    K.W. Geiger, L. Van Der Zwan.
23. Meyer, R. M. (1961). Volume 122, Pages 815-826. Scintillation Response of Activated Inorganic Crystals to Various Charged Particles Proc. Phys. Soc.
24. Tatjana Jevremovic. (2009). Migration Length. Nuclear principles in engineering (Second Edition ed., pp. 445). New York: Springer Science Media.

Appendices

A-1: Sample of MCNP Model

```
c     Created on: Monday, July 18, 2011 at 19:01
c    ------------------------------------------------
c     UOIT: LiI(Eu) detector.
c    Geometry: D 2.5cm * 1 cm LiI(Eu) + wax.
c    Detector response function simulation.
cc ---------------------------------------------------------------
c cell cards
    1  11 -4.06 -1      $ D 2.5cm *1 cm LiI
    2  0  1 -2          $ space between detector and wax
    3  22 -0.94 2 -3  $ wax
    4  0  -4            $ space for source
    5  0  5             $ outside my interest
 c ---------------------------------------------------------------
c surface cards
    1  RCC 0 0 0    0 1 0    1.25
    2  RCC 0 -1 0   0 3 0    1.5
    3  RCC 0 -3 0   0 5 0    3.75
    4  RCC 0 -15 0  0 12 0   3.75
    5  RCC 0 -15 0  0 17 0   3.75
C ---------------------------------------------------------------
c     Source Card
c     ---------------------------------------------------------------
sdef pos 12 0 0 erg D1
SI 1.173 1.332
SD 0.5 0.5
c     ---------------------------------------------------------------
c     Tally Cards
c     ---------------------------------------------------------------
……
……
……
ctme 20 $run time in minutes
print
c     ---------------------------------------------------------------
c                    END OF PROGRAM
c ---------------------------------------------------------------
```

A-2: Publications

1. A. Fariad, R. Machrafi, V. Kovaltchouk, Sharman Perera, Development of a Dual Neutron and Gamma Detector for Online Measurement, Canadian Radiation Protection Association, Ottawa (Canada), May 2011.

2. R. Machrafi, A. Fariad, V. Kovaltchouk, The Second Conference on Physics and Technology of Reactors and Applications, Fez (Morocco), September 2011.

3. R. Machrafi, A. Fariad, V. Kovaltchouk, Proceedings of Radiation Measurements, 2011 (Submitted).